Modification of magnetic properties in granite during hydrothermal alteration (EPS-1 borehole, Upper Rhine Graben)

Inaugural-Dissertation
zur Erlangung der Doktorwürde
der Naturwissenschaftlich-Mathematischen Gesamtfakultät
der Ruprecht-Karls-Universität Heidelberg

vorgelegt von Diplom-Geologin Jana Just

Heidelberg, Dezember 2004

Gutachter:
HD Dr. Agnes Kontny
Prof. Dr. Helga de Wall

Ich erkläre hiermit,

a.) dass ich die vorgelegte Dissertation selbst verfasst und mich dabei keiner anderen als der von mir ausdrücklich bezeichneten Quellen und Hilfen bedient habe und,

b.) dass ich keiner anderen Stelle ein Prüfungsverfahren beantragt bzw. die Dissertation in dieser oder anderen Form bereits anderweitig als Prüfungsarbeit verwendet oder einer anderen Fakultät als Dissertation vorgelegt habe.

Heidelberg, den 07. Dezember 2004

"Well, I'm beginning to see the light.
Well, I'm beginning to see the light.
Some people work very hard,
but still they never get it right.
Well, I'm beginning to see the light"

The Velvet Underground

Acknowledgements

First of all I want to thank with all my heart my supervisors Agnes Kontny and Helga de Wall for their excellent support. I have never felt alone with my problems.

Many thanks to all the people, who supported me during my dissertation time. Without you I would *"work very hard but still never get it right"*:

Axel Emmerich, Birgit Dietrich, Carlo Dietl, my roommate Carsten Vahle, Carsten Laukamp, Fabio Lapponi, Francis Cueto, Gesine Lorenz, Guy Spence, Hartwig Schröder, Heiko Hoffmann, Isabelle Fahimi, Jens Grimmer, Jochen Schneider, Johanna Kontny, Luca Nano, Marta, Margot Isenbeck-Schröter, Michael Seeling, Rike Bauer, Roswitha Marioth, Thomas Angerer, Zbynek Veselovsky, and Prof. Greiling, Prof Bechstädt, as well as, all the colleagues at the GPI in Heidelberg.

Very special thanks go to the Soultz-group at Heidelberg: Laurence Warr (!) and my friend Anja Schleicher, Bernd Kober, Emmanuelle Laverret, Dominique Aubert and Sven Traxel, for their cooperation and constructive discussions.

I want to thank gratefully to Jörg Baumgärtner from Socomine at Soultz for enabling sampling of the EPS-1 cores, Christian Rolf und Katrin Worm from the Magnetiklabor in Grubenhagen for their support during NRM measurements. A great thank to Ann Hirt, Fatima and Pascal from the ETH Zürich for the support during the AMS and paleomagnetic investigations. The constructive reviews of Frantísek Hrouda and M. Hounslow are gratefully acknowledged.

Financial support was provided by the DFG-Graduiertenkolleg 273 (Fluid-Rock Interaction).

And at least, the loveliest thank belongs to my husband Thomas Debray, because *"love is pure - the only treasure"* (Frankie Goes to Hollywood).

Abstract

Rock magnetic properties and petrological investigations of the magnetite-bearing Variscan Soultz granite from the EPS-1 borehole (Upper Rhine Graben) provided a significant contribution for the understanding of the "old" (Middle Carboniferous to Permo-Triassic) hydrothermal alteration history. This alteration history is generally subdivided into two stages. Stage I alteration is related to processes during magma cooling and solidification of the plutonic body in Middle Carboniferous times. Stage II alteration is associated with post-emplacement tectonics from Late Carboniferous to Permo-Triassic, such as exhumation of the plutonic body to a paleo-erosion surface, near surface processes beneath the paleo-surface and the influence of the overlying Permo-Mesozoic sedimentary cover. This study focuses on two main scopes: (i) chronological succession of the alteration history of the Soultz granite, and (ii) modification of the magnetic properties in relation to the different geological processes mentioned above.

During the stage I alteration the plutonic body solidified, which led to the formation of first permeable fault zones at temperatures ~300 °C, obtained from chlorite-geothermometry. The formation of permeable zones allowed the circulation of O_2-rich fluids, which caused the oxidation of magnetite into martite (hematite) within discrete zones. Granites, which are situated further away from a fault zone remained unaffected, and thus are called "fresh" from the magnetic point of view (magnetic susceptibility, $\kappa > 10 \times 10^{-3}$ SI). The $\kappa(T)$ measurements revealed thermomagnetic behavior typical for multi-domain magnetite in fresh granite and an irreversible thermomagnetic behavior in altered granite reflecting the oxidation degree of magnetite. Such degree is related to an alteration index (Al-index) obtained from the difference between κ of the heating and the cooling run at room temperature. The AMS (anisotropy of magnetic susceptibilty) fabric in fresh granites is related to the subhorizontal primary magmatic fabric indicating emplacement within a decelerating flow regime. Along with the oxidation of magnetite κ was decreased to values $< 1 \times 10^{-3}$ SI. The primary horizontal magnetic fabric changed to a steeply dipping and NW-SE trending magnetic fabric in the altered granite due to a microcrack-controlled oxidation. This oxidation caused elongated and aligned small magnetite relics within the host mineral martite. Paleomagnetic investigations revealed that this first faulting event took place during Middle Carboniferous. During Late Carboniferous, probably until Perm, the plutonic body was affected by unloading and exhumation. The initial fault zones were reactivated and $\kappa(T)$ curves revealed the formation of pyrite and Fe-carbonates. The AMS fabric in wall rocks of the fault zones evolved from a normal to an inverse fabric due to decreased (single-domain) grain sizes of the magnetite relics. At the same time, the AMS fabric in the cataclastic granites was destroyed by brittle deformation. The exhumation of the plutonic body to a paleo-erosion surface resulted in near surface processes within the upper borehole section . These processes caused an oxidation of pyrite, which led to the circulation of strongly acidic fluids. Such acidic fluids led to the decomposition of Fe-carbonates and martite until they were neutralized by mixing with meteoric fluids, which in turn caused the precipitation of abundant fine-grained hematite. This event led to a widespread hematitization of the upper borehole section. The fine-grained hematite shows paleofield vectors typical for Permo-Triassic. In contrast, fault zones at the bottom of the borehole remained unaffected by this near surface processes. Granites from these fault zones display a reduction of martite back to magnetite caused by the infiltration of organic matter from the overlying Permo-Mesozoic sedimentary cover. In such granites, no relevant paleomagnetic information could be obtain.

Zusammenfassung

Die gesteinsmagnetischen und petrologischen Untersuchungen des Magnetit-führenden Soultz-Granits aus der EPS-1 Bohrung (Oberrheingraben) lieferten einen bedeutenden Beitrag zum Verständnis über die „alte“ (Mittel-Karbonische bis Permo-Triassische) hydrothermale Alteration. Diese ist im allgemeinen in zwei Alterationsstufen unterteilt. Stufe I bezieht sich auf Prozesse während der Abkühlung und Erstarrung des Magmas im Mittel-Karbon, hervorgegangen aus paleomagnetischen Untersuchungen. Stufe II ist assoziiert mit Spät-Karbonischen bis Permo-Triassischen tektonischen Prozessen, die nach der Platznahme des Granitplutons stattfanden: Exhumierung zu einer Paläo-Landoberfläche, oberflächennahe Prozesse und der Einfluss der überlagernden Permo-Mesozoischen sedimentären Decke. Diese Studie konzentriert sich auf zwei Hauptschwerpunkte: (i) die chronologische Abfolge der Alterationsgeschichte im Soultz Granit und (ii) die Modifikation der magnetischen Eigenschaften in Bezug auf die oben genannten geologischen Prozesse. Hierzu wurden drei generelle Methoden aus der Gesteinsmagnetik verwendet: AMS (Anisotropie der magnetischen Suszeptibilität), Untersuchungen der remanenten Magnetisierung und die Temperaturabhängigkeit der magnetischen Suszeptibilität ($\kappa(T)$).

Während der ersten Alterationsstufe erstarrte der Granitpluton, was zu der Bildung von ersten permeablen Störungszonen bei Temperaturen ~300 °C führte, ermittelt mit Hilfe von Chlorit-Geothermometrie. Die Bildung dieser permeablen Zonen erlaubte die Zirkulation O_2-reicher Fluide, welche zur Oxidation von Magnetit zu Martit (Hämatit) innerhalb von diskreten Zonen führte. Granite, die sich in weiterer Entfernung zu den Störungszonen befinden, blieben dabei unbeeinflusst. Vom magnetischen Standpunkt betrachtet werden solche Proben als „frisch“ bezeichnet (magnetische Suszeptibilität, $\kappa > 10 \times 10^{-3}$ SI). Diese $\kappa(T)$ Messungen zeigen einen typischen Verlauf für multi-domain Magnetit und ein AMS (Anisotropie der magnetischen Suszeptibilität) -Gefüge, das mit einem primär subhorizontalen magmatischen Gefüge korreliert und die Platznahme des Magmas in einem sich horizontal ausbreitenden Fließregime widerspiegelt. Aufgrund von Mikroriss-kontrollierter Oxidation von Magnetit nahm die Suszeptibilität ab ($\kappa < 1 \times 10^{-3}$ SI). Das primär horizontale magnetische Gefüge wechselte zu einem steil einfallenden, NW-SE orientierten sekundären Gefüge im alterierten Granit, was am AMS-Gefüge und an orientierten Dünnschliffen beobachtet wurde. Paleomagnetische Untersuchungen zeigen, dass die initiale Bildung von solchen Störungszonen noch während des Mittel-Karbons stattfand. Während der Exhumierung im Spät-Karbon wurden die frühen Störungszonen reaktiviert, was zur Bildung von Pyrit und Fe-Karbonaten führte, die mit Hilfe von $\kappa(T)$ Messungen identifiziert werden konnten. Die Heraushebung zu einer Paläo-Landoberfläche führte zu oberflächennahen Prozessen im oberen Bereich des Plutonkörpers, was die Oxidation von Fe-Karbonaten und Pyrit bewirkte. Die Oxidation von Pyrit führte zur Zirkulation von stark sauren Lösungen, die wiederum den Abbau von Fe-Karbonaten und Martit verursachten. Das Verdünnen der saueren Fluide mit meteorischen Wässern an der Oberfäche resultierte in der Fällung von großen Mengen an feinkörnigem Hämatit im oberen Bereich des Bohrprofils.

Die Störungszonen des unteren Bereichs blieben von diesen Oberflächenprozessen unbeeinflusst, zeigen jedoch eine Reduktion von Martit zurück zum Magnetit, verursacht durch den Eintrag von organischer Substanz in Fluiden aus der überlagernden Permo-Mesozoischen Sedimentdecke.

List of symbols and abbreviations

AF: alternating field

Al-index: alteration index

AMS: Anisotropy of the Magnetic Susceptibility

An: ankerite

ARM: anhysteretic remanent magnetization

B: barite

χ: mass magnetic susceptibility [SI/g]

Cc: calcite

ChRM: characteristic remanent magnetization

CRM: chemical remanent magnetization

DC: direct current

DEK: declination

DFG: Deutsche Forschungsgesellschaft

DIRM: drilling induced remanent magnetization

ETH: Eidgenössische Technische Hochschule Zürich

fO_2: oxygen fugacity

FMQ: fayalite-magnetite-quartz

hb: hornblende

H_C: coercive force

H_{Earth}: geomagnetic field

Hem: hematite

HM: hematite/magnetite

HP: Hopkinson peak

ICP-ES: Inductive Coupled Emission Spectrometer

Fer: ferrite

Fig: figure

GGA: Institut für Geowissenschaftliche Gemeinschaftsaufgaben

GPI: Geologisch-Paläontologisches Institut

GRK: Graduiertenkolleg

INK: inclination

Int: intermediate

IRM: isothermal remanent magnetization

IRMs: saturation of the isothermal remanent magnetization

J: magnetization

κ: volume magnetic susceptibility [SI]

$\kappa(T)$: temperature dependency of the magnetic susceptibility

KTB: Kontinentale Tiefbohrung

ld: large diameter

LNM: Laboratory of Natural Magnetism

MAD: average maximum angular deviation

mag: magnetite

mar: martite

max: maximum

MD: multi-domain

MDF: median demagnetization field

MGCR: Mid German Crystalline Rise

MH: magnetite/hematite

min: minimum

MO: Moldanubian Zone

n: number

norm: normed

NRM: natural remanent magnetization

P`: anisotropy factor

QIF: quartz-iron-fayalite

Q-ratio: Koenigsberger factor

Qz: quartz

RH: Rhenoherzcynian Zone

RM: remanent magnetization

R-SRM: Superconducting Rock Magnetometer

σ_H: maximum horizontal stress

sd: small diameter

SD: single-domain

SEM: scanning microscope

Sid: siderite

ST: Saxothuringian Zone

std: standard deviation

T: shape factor

T_C: Curie temperaure

TH: thermal

T_M: temperature at the Morin transition

T_N: Neél temperaure

T_{UB}: unblocking temperature

T_V: temperature at the Verwey transition

VRM: viscous remanent magnetization

Contents

Chapter I:

Introduction

I. Introduction

Geophysics is of essential importance to understand the solid Earth, particularly on a global scale. Modern ideas of the structure and evolution of continents and oceans are based extensively on discoveries using geophysics. Geophysical methods allow to "look into the Earth" using mostly remotely methods, which detect differences in the physical properties of the subsurface rocks or structures. But geophysics describes the subsurface in physical terms – density, electrical resistivity, magnetism, etc., not in terms of composition, mineralogy, grain-size, etc., which are familiar to the geologist. The combination of conventional geological with geophysical methods is leading to a better knowledge of the processes that take place on the Earth. In this study the influence of the hydrothermal alteration on magnetic properties was investigated using a combination of rock magnetic and conventional petrological methods in order to explain geological and geochemical processes underwent by the Soultz granite.

1. Rock magnetism

One of the most frequently measured geophysical properties for geological applications is the magnetic susceptibility, which is a characteristic material constant describing the magnetization of a mineral phase or whole rock sample. This rock-physical parameter is often used in geological surveys because it provides information about the mineralogical composition and allows rapid, quasi-continuous registration of variations in the rock composition, e.g. in a borehole profile. Therefore, this parameter supports the correlation of data from several borehole profiles (e.g., Loizeau et al. 2004, Nourgaliev et al. 2003). The susceptibility data (susceptibility-log) can be directly measured in the borehole using a borehole measurement tool, or performed on drill cores using a core logger or a portable Kappabridge. For decades, these applications have mainly been used in mineral exploration for predictive exploration models. Such models allow exploration to focus on signatures being appropriate for the regional and prospect scale, which cuts down expenses and time. By now, the acquisition and processing of data has reached a point, which far outstrips the capacity to interpret the surveys (Clark 1999). However, a proper interpretation of such surveys, could supply far more geological information. Therefore, it is significant to understand the relationship between magnetic signatures and geology.

In recent years, the magnetic susceptibility has been used to record paleoclimatic variations in the course of time. The relevance of this material constant as a climate-proxy is based on its sensitivity for the modification of mineral assemblages (e.g., Bloemendal and DeMenocal 1989, Kukla et al. 1988, Peck et al. 1994). In these studies, the frequency of a susceptibility-log is analyzed and correlated to orbital-controlled climatic variations, such as the Milankovitch cycle, due to the occurrence of cyclic sedimentary sequences. The method has been applied for different sedimentary facies, such as fluvial deposits (Nador et al. 2003), marine deposits (Kravchinsky et al. 2003) and hemipelagic deposits (Port 2001). Moreover, the magnetic susceptibility yields possibilities for a precise subdivision of sedimentary sequences. For example, it has been applied to Maastrichtian chalk reservoirs from the Danish North Sea (Stage 2001), where the correlation between wells provided a better understanding of the sedimentary cycles at a submeter scale.

Beside the wide potential to apply magnetic susceptibility to sedimentary rocks, another focus of its use lies in the characterization of magmatic rocks. Here, the magnetic susceptibility is established and used for fieldwork and regional mapping of different magma compositions. This is based on the susceptibility

distribution, which reflects the mineralogical modifications. Such susceptibility distributions are used, for example, to discriminate subaerial and submarine lava flows, both in the field (Zolk 2004) or from borehole and drill core measurements (e.g., Bücker et al. 1999, Kontny et al. 2003). For instance, in contrast to the natural gamma radiation, which shows only a constricted significance for the stratigraphic sequence, the magnetic susceptibility is a sensitive tool for the discrimination of weak modifications in the magneto-mineralogical assemblages as well as in the magneto-structural variations. Such discriminations are also successfully performed on plutonic rocks, where the application of the magnetic susceptibility helps to detect the differentiation trends of magmas or the variations within a single intrusion (e.g., de Wall et al. 2000, Gleizes et al. 1993, Dietl submitted). Ishihara (1977) discovered that granitoid rocks can be classified into weakly magnetic ilmenite-series (S-type) and strongly magnetic magnetite-series (I-type). This classification is based on the availability of ferrous and ferric iron ions in the magma source. In the weakly magnetic series, iron is incorporated into paramagnetic silicate minerals, predominantly as Fe^{2+}, whereas in moderately to strongly magnetic series, significant amounts of Fe^{3+} are incorporated into magnetite.

Not only the bulk magnetic susceptibility as a scalar parameter, but also the directional dependence of the magnetic susceptibility (the anisotropy of the magnetic susceptibility, AMS), is an appropriate tool in rock magnetism. The AMS is used for qualitative and quantitative characterization of petrofabrics because it provides information on the preferred orientation of mineral phases. The use of the AMS for characterization of petrofabrics was first reported by Ising (1942). The application of the AMS for quantitative fabric analysis was first mentioned in Graham (1954). Other studies, dealing with the correlation of AMS to different geological questions, subsequently followed (Hrouda 1982). In recent times, this method is applied widely in the detection of flow directions of magma and lava (e.g., de Wall et al. 2004, Herrero-Bervera et al. 2001) and in the characterization of internal structures of plutonic bodies (e.g., Ferré 2002, Archanjo et al. 1995). Internal structures of intrusions are well reflected by the AMS, which can be related to the intrusion emplacement within a regional tectonic setting (e.g., Bouchez and Gleizes 1995). In spite of the weak magmatic fabric, the magnetic fabric visualizes the preferred orientation of the mineral phases, which led to the conclusion that granite is never isotropic (Bouchez 1997)! Thus, AMS provides clues about the flow fabric of magma and thus about its emplacement, which may range from forceful intrusion via diapirism (Cruden 1990), dyking (Clemens and Mawer 1992), to permitted intrusion assisted by deformation (e.g., Hutton et al. 1990). Structures in deformed rocks can also be characterized using the AMS method (e.g., Ramsay and Huber 1983a, Williams et al. 1994). An overview of the application of AMS in tectonic settings is given by Borradaile and Henry (1997), or in the textbook of Tarling and Hrouda (1993). In sedimentary rocks, the magnetic fabric may reflect the paleoflow direction and also detect the change of the transport direction (King et al. 1998). Specifically in sandstones, the AMS method can serve as a 3d characterization of pore geometry (e.g., Pfleiderer and Halls 1990). AMS study of volcanic ashes, tuffs and ignimbrites gives information about the transport direction, as well (e.g., Palmer and MacDonald 1999, Ort et al. 1986), and reveals the mechanism of the transport movement (Fisher et al. 1993).

Beside such studies, which use the magnetic behavior of rock samples in an induced laboratory field, the analyses of the remanent magnetization of rocks acquired in the Earth magnetic field provide the possibility to reconstruct the paleogeographic position of a given area. Paleomagnetic evidence for Wegener`s theory of the continental drift was taken on in the 1950`s and 1960`s when the revolution in the Earth sciences took place. Terms such as continental drift, seafloor spreading and plate tectonics were understood, and scientists recognized that these dynamic processes are stored in the rocks as paleomagnetic signatures.

Today, paleomagnetism deals with the combination of tectonic and geochronologic applications, based on the theory that the plates are in motion and continually change their shape and position (e.g., Edel et al. 2003, Hirt et al. 1992, Lowrie 1980). A successful application of the paleomagnetic method, however, requires a precise knowledge of the acquisition of the remanent magnetization. The evaluation the paleofield vectors and the proper isolation of the natural characteristic remanent magnetization (ChRM), which is the carrier of valuable geological information, can be complicated due to magnetic overprints. These overprints can be caused by natural processes, such as the alteration of the primary mineral assemblage, thermal activity or the stroke of lightning, but also by artificial overprints, such as drilling induced remanent magnetization as observed in rock samples from deep drillings (Worm and Rolf 1994, Kanamatsu and Niitsuma 2004).

Magnetic properties of rocks are mainly carried by the accessory mineral assemblage, such as iron oxides or sulfides. Unfortunately, accessory or opaque mineralogy is often ignored in conventional petrological investigations, although it can provide clues about the alteration mechanism, for example, during seafloor spreading at oceanic ridges (Merascotti et al. 2000, Wooldridge et al. 1990, Ade-Hall 1971), or metamorphism (Kontny and de Wall 2000, Kontny et al. 1997). While mineralogical alterations caused by geological processes are well documented in geoscientific works, studies concerning alteration of iron-bearing minerals are rarely documented. Recognition of the modification of a rock during geological processes using the aid of magnetic signatures will reduce time wasted targeting and refocus research. Moreover, the knowledge of the variability of magnetic signatures on Earth can also be assigned to rocks from other planets, for example Mars, as resources potentially available. Since granitoid rocks are common in the continental crust, the knowledge about their magnetic properties is of fundamental importance. They show a large variability of magnetic signatures, which are sensitive for mineralogical modification during different geological processes. This dissertation contributes to the topic and highlights the influence of hydrothermal alteration on the modification of different magnetic properties in the magnetite-bearing Variscan granite drilled by the EPS-1 borehole.

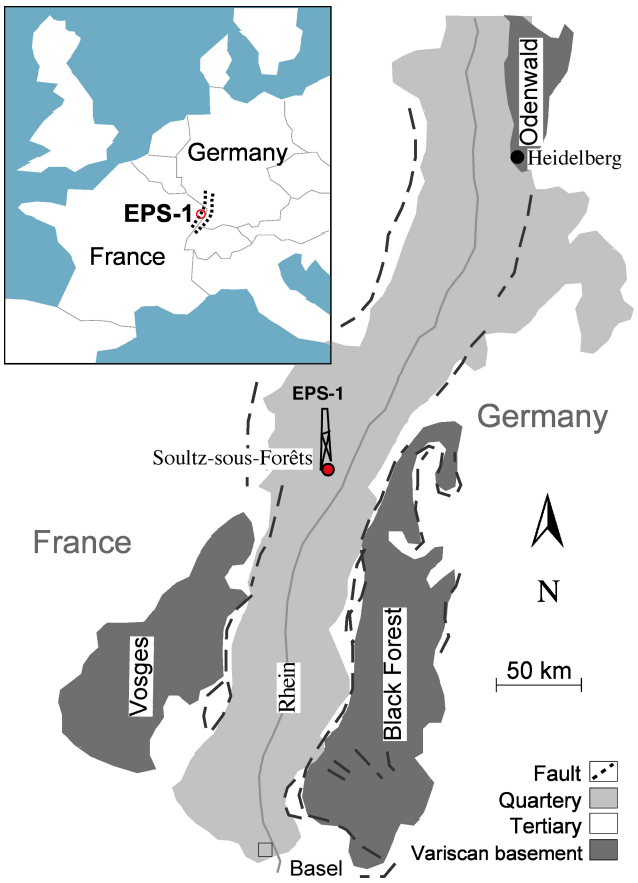

Fig. A: *Location map of the European central Upper Rhine Graben and the EPS-1 drill site at Soultz-sous-Forêts.*

2. The Soultz granite

The Variscan Soultz granite is situated within the Upper Rhine Graben (Fig. A), which is one of the prominent extensional structures in central Europe. It developed since Middle to Late Eocene by reactivations of a complex set of Variscan fault zones (e.g., Schumacher 2002, Ziegler 1996). The Soultz site is the center of the largest anomaly of surface heat flow density (140 mWm^{-2}, Schellschmidt and Clauser 1996) in central Europe and shows a geothermal gradient of 100 °C km^{-1} in the sedimentary cover (Genter 1989). Thus, the

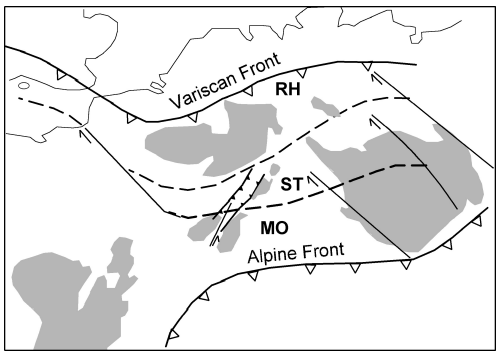

Fig. B: *General geological map of the European Variscan orogen belt (modified after Franke 1995a) and the position of the Upper Rhine Graben. RH: Rhenohercynian Zone, ST: Saxothuringian Zone, MO: Moldanubian Zone.*

Soultz area is in the focus of geothermal energy exploration. The geothermal anomaly at Soultz is not associated with processes at great depth (e.g., rifting) but is the result of deep circulation of meteoric water. The circulation is driven by flow from the topographically higher flanks of the Vosges in the west and Schwarzwald in the east. Along these flanks the fluids are forced to a greater depth and thus carry heat to the horst structure beneath Soultz (Fig. C, Pribnow and Clauser 2000).

Since the magma emplacement during Middle Carboniferous (Alexandrov et al. 2001), the Soultz granite passed a complex hydrothermal alteration history, which started during the Variscan and proceeded until recent times (e.g., Dubois et al. 1996). Together with other adjacent intrusions (Flöttmann and Oncken 1992), the Soultz granite belongs to a generation of subduction related I-type intrusions of the Mid-German Crystalline Rise of the Saxothuringian Zone (Fig. B). Probably, the Saxothuringian Zone was a separate microplate, but with a drift similar to parts of the Bohemian Massif during the Variscan orogeny (Tait et al. 1997). The drift was accompanied by large-scale wrenching and block rotations (Edel et al. 2003) causing numerous fault zones in the Variscan Orogen. A detailed petrographic and microthermometric study of paleofluids, which trapped as fluid inclusions in the veins or microfissures (Smith et al. 1998), indicate a complex alteration history. Dubois et al. (1996) reported that the earliest stage (stage I) was related to late Variscan times with fluids containing rare amounts of CO_2 and H_2O, which was followed by a succession of fluids with moderate salinity (2-7 wt%) trapped under a large range of temperatures between 340 and 180 °C. The second main stage (stage II) was related to post-Oligocene fluid flows and shows fluids, which are rather similar to modern brines; temperature in the range of 130 to 160 °C and a large range of salinity. The large variation of salinities observed in some samples was interpreted to represent a heterogeneous mixing process of different fluids, probably caused by multistage alteration overprints.

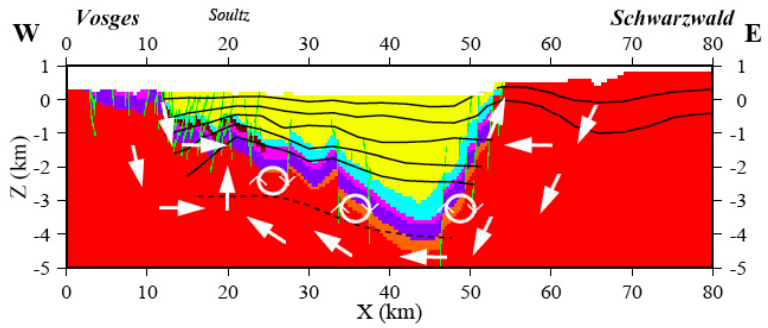

Fig. C: *Schematic diagram of the fluid flow field along the cross section at Soultz-sous-Foêts through the Upper Rhine Graben (from Pribnow and Clauser 2000). Subvertical structures are fault zones. The arrows indicate the direction of flow. Basement: red, Parmian: orange, Buntsandstein: purple, Muschelkalk: pink, Jurassic: blue, Tertiary: yellow.*

The infiltration of large amounts of fluids is related to permeable fault zones with a high fracture density (Genter and Traineau 1991), where the granite was intensively altered (stage II). A characteristic zoning of a fault zone was described by Genter et al. (1995). The central part of a fault zone consists of cataclastic granites showing an intense brittle deformation. In the directly adjacent wall rocks, the fracture density vanishes but the granites still show an intense hydrothermal alteration. With increasing distance from the fracture zone, the hydrothermally altered granites pass into an unaltered rock. Thus, the multistage alteration history of the Soultz granite is additionally complicated due to a spatial relation. Fracture analysis

of the altered Soultz granite (Genter and Traineau 1996, Dezayes et al. 1995, Elsass et al. 1995, Genter et al. 1995) related the observed structures to the tectonic rifting activity of the Rhine Graben during Tertiary. However, although numerous works deal with the alteration of the Soultz granite (e.g., Jacquemont 2002, Genter et al. 1999, Komninou and Yardley 1997, Dubois et al. 1996, Dezaeys et al. 1995, Traineau et al. 1991), the whole alteration history is not completely understood. Particularly, the pre-rift alteration history was neglected in previous studies because of the multistage hydrothermal overprints of the granite, which masks the "old" signatures of the granite.

3. Objectives

This study mainly focuses on two scopes: (1) to reveal the pre-rift alteration history underwent by the Soultz granite and (2) to detect the modification of the magnetic properties during the different hydrothermal alteration episodes, using the combination of rock magnetic and conventional geologic methods. The influence on magnetic properties by the following processes is studied:

- Emplacement mechanism of the plutonic body during Variscan times:
  - Hydrothermal alteration during cooling of the magma (stage I)
  - Transformation from primary to secondary magnetic fabric and its significance for geological questions
- Post-emplacement processes:
  - Hydrothermal alteration related to fault zones (stage II)
  - Hydrothermal alteration during exhumation and uplift
  - Near surface processes of a paleoerosion surface in Permian times
  - Hydrothermal alteration associated with the deposition of the sedimentary cover
  - Paleomagnetic studies in order to assign the chronological evolution to the hydrothermal alteration events

4. Structure of the work

The structure of this work consists of a general introduction and three independent chapters, each focusing on another magnetic method. Finally, the results of these three chapters are discussed in relation to their significance for the hydrothermal alteration underwent by the Soultz granite from the magma emplacement to present times. The three chapters contain abstract, introduction, geological setting, results, discussion and conclusion parts.

Chapter II.1 gives clues about the anisotropy of magnetic susceptibility (AMS) of the Soultz granite and allows an insight into the development of petrofabrics caused by the hydrothermal alteration during the emplacement of the plutonic body and subsequent brittle deformation.
Chapter II.2 unravels the complex remanent magnetization data, which were obtained by alternating field and thermal demagnetization, in order to get paleomagnetic relevant information.
Chapter II.3 shows the thermomagnetic behavior of whole rock and mineral phases using the method of the temperature dependent magnetic susceptibility ($\kappa(T)$), in order to characterize they altered magnetic mineral assemblages.

1.5 Methods, samples and basic principles

The EPS-1 borehole was fully cored to a final depth of 2227 m. Orientations of the drill cores were first measured in a relation to the arbitrary coordinate axes: the long axis of the borehole is assumed to be vertical, and a line drawn along the core give relative north, enabling the reorientation of each drill core. The EPS-1 borehole is deviated to the NE at its base (22° at 2200 m), which was considered during the reorientation of the drill cores. Each drill core is quoted with a core index, which correlates with the sampling depth (compare also Fig. 1.2 in Chapter II.1). Variation in the borehole diameter of the EPS-1 drilling provided drill cores of different sizes. Drilling with a 5.06" drill bit down to a depth of 1997 m recovered core pieces with a large diameter (d = 78 mm). Further below, down to a final depth of 2230 m, a 3.9" equipment was used, providing cores with a small diameter (d = 57 mm). The coring was performed with a diamond core bit cooled by water-based drill mud (Baria et al. 2000). For AMS and magnetization analyses, 1" cylindrical standard specimens were drilled perpendicular to the reference line, using a non-magnetic equipment at the Geological-Paleontological Institute (GPI) in Heidelberg.

The combined methods of rock magnetism and conventional petrology are introduced in more detail in the following three chapters. Thus, herein they are only briefly listed:

- For sampling in the drill core store at Soultz a portable Handkappameter KT-6 (GEOFYZIKA) with a sensitivity of 1 x 10^{-6} SI was used. The measurement on a drill core was carried out in 20 cm intervals. The Handkappameter results were compared with the susceptibility log measured on cores by Rummel and König (1991) resulting in an accordance of the data. The selected drill cores were used for drilling of cylindrical standard specimen with a volume of ~ 10 cm^3.
- Optical examinations of polished thin sections (30 μm) were conducted under the microscope (Leitz, transmitted and reflected light). For the discrimination of magnetic minerals the section was coated with a ferrofluid (G100), which was diluted with distilled water in the ratio 1:10 and covered by a glass slide.
- Backscatter electron images were taken with a Leo 440 scanning electron microscope (SEM) at the Institute for Environmental Geochemistry in Heidelberg.
- XRD analyses on powdered samples were done using a Siemens (Bruker) Diffrac 500 at the GPI of the University of Heidelberg.
- Microanalyses were carried out with a CAMECA SX51 electron microprobe at the Mineralogical Institute of the University of Heidelberg.
- Total determination of major element concentrations in mineral phases was done using an Inductive Coupled Plasma Emission Spectrometer (ICP-ES), commissioned to ACME (Analytical Laboratories) in Vancouver, Canada.
- Temperature dependent behavior of low-field magnetic susceptibility (κ(T)) was performed at the GPI of the University of Heidelberg. The samples were crushed and a sample volume of ~0.25 cm^3 heated. Such a small volume is unproblematic for the fresh granite, which is characterized by a relative homogeneous mineral distribution. In contrast, the heterogeneity of the hydrothermally altered granite causes variation in κ(T) curves, even for the same sample specimen. Therefore, complementary microscopic investigations were performed.
- Natural remanent magnetization (NRM) was measured on whole core pieces using a Cryogenmagnetometer 760 R-SRM (Superconducting Rock Magnetometer), 2G Enterprises (AGICO, Rolf 2000), at the magnetic laboratory of the GGA in Grubenhagen.

- Determination of the directional dependence of the anisotropy of magnetic susceptibility (AMS) was done using the KLY-2 Kappabridge (AGICO) at the GPI in Heidelberg.
- Separation of ferri- and paramagnetic subfabrics was done using a high-field torque magnetometer (Martín-Hernández and Hirt 2001) in the Laboratory for Natural Magnetism (LNM) at the ETH in Zürich.
- Acquisition of remanent magnetization (IRM) was performed using an ASC Scientific Model IM-10-30 Impulse Magnetometer with a maximum field of 2.6 T at the LNM in Zürich.
- Thermal (TH) demagnetization was performed in zero field and the intensities between each steps were measured using a cryogenic magnetometer (2G Enterprises) at the LNM in Zürich.
- Stepwise alternating field (AF) demagnetization using a MI AFD 1.1 demagnetizer (Magnon International) was performed at the GPI of the University of Heidelberg.
- Intensities of the remanent magnetization were measured using a JR-5 / JR-5A spinner magnetometer (AGICO) at the GPI of the University of Heidelberg.

1.6 Fundamentals of magnetism

The ancient Greeks, who lived near the city of Magnesia, and also the early Chinese knew about "strange" stones with the power to attract iron. A steel needle stroked with such a lodestone became magnetic as well, and around 1000 AD, the Chinese realized that such a needle, being freely suspended, pointed north-south. Soon, the magnetic compass spread to Europe. Columbus used it when he crossed the Atlantic Ocean noting that the deviation changed during the voyage. Around 1600 AD, William Gilbert, a physician to Queen Elizabeth I of England, proposed an explanation: the Earth itself is a giant magnet!

Today's geoscientists recognized that all materials possess magnetic properties, which can be correlated to dia-, para- or ferrimagnetic behavior. For a meaningful interpretation of the rock magnetic properties, the knowledge of the magnetic behavior of the included mineral phases is required. Here, a reference should be made to the most important textbooks, for example, Butler (1998), Dunlop and Özdemir (1997), Tarling and Hrouda (1993) and Soffel (1991). An introduction to the most important fundamentals of magnetism referred to in this work, follows.

Magnetization and magnetic susceptibility

Rocks are characterized by two magnetic parameters, which are the *magnetic susceptibility* (κ) and the *magnetization* (*J*). Both depend on the *magnetic field* (*H*), which is expressed by the following equation:

$$H = \kappa \; x \; J.$$

According to this equation, the magnetic susceptibility is a constant of proportionality of magnetization and applied field ($H_{applied}$), for example the geomagnetic field (H_{Earth} = ~40 A/m). Thus the magnetic susceptibility controls the induced part (J_{ind}) of the magnetization. Therefore, it is an important parameter for modeling magnetic anomalies. The remanent part of the magnetization (J_{rem}) remains when removing the magnetic field. Both components of the magnetization ($J = J_{ind} + J_{rem}$) can be separated by calculating the *Koenigsberger ratio* (*Q*):

$$Q = J_{rem} / \kappa \; x \; H_{applied}$$

Normally, material such as steel or iron is considered to be magnetic because a magnet can pick them up. Not only iron-bearing materials show magnetic behavior but also all substances (even water) are affected by magnetism. The magnetic behavior within an induced magnetic field depends on the atomic magnetic moments, which show orbital and spin motions of electrons, and on the relative position of these moments in the mineral lattice resulting in dia-, para- and ferromagnetic behavior. The magnetic susceptibility of rocks with dia- and paramagnetic behavior is independent from the grain size, grain- and phase boundaries, or microcracks. Thus, it is a direct function of the mineralogical composition of a rock. In contrast, the magnetic susceptibility of rocks with ferromagnetic behavior shows a more complex nature, which is dominated by grain size and shape and the intrinsic parameters as well, such as the magnetocrystalline anisotropy and magnetostriction of the ferrimagnetic rock compositions (e.g., Dunlop and Özdemir 1997).

Diamagnetism

Diamagnetic minerals (e.g., quartz, feldspars without incorporated iron) show completely compensated magnetic moments without the influence of a magnetic field. Within a magnetic field, all magnetic moments align antiparallel to the applied field, which cause low induced magnetization and negative values of the magnetic susceptibility. Diamagnetic susceptibility shows no temperature dependent behavior.

Paramagnetism

In contrast to the diamagnetic minerals, the paramagnetic materials (e.g., biotite, amphibole, chlorite, Fe-bearing carbonates) show partially uncompensated spinmoments. None of the magnetic moments show interactions at room temperature and thus their alignment is statistically irregular and the magnetization J = 0 without an applied field. Applying a magnetic field, these randomly oriented magnetic moments align parallel to the field, which cause positive values of the magnetic susceptibility and induced magnetization, which is dependent on the intensity of the applied field. Because the alignment of the resulting magnetic moments can be disturbed by thermal agitation, the paramagnetic susceptibility shows temperature dependent behavior according to the Curie law:

$$\kappa_{para} = C / T,$$

whereby C is the Curie constant and T is the temperature. Paramagnetic minerals show a distinct variation of κ-values, which is caused by the Fe^{2+} and/or Fe^{3+}-content in minerals, but also by the incorporation of other paramagnetic ions such as Mn^{2+}.

Ferromagnetism

Ferromagnetism is caused by strong interaction of paramagnetic moments, which cause a distinct orientation of the uncompensated spinmoments within a crystal lattice and thus in residual magnetic moments. Once aligned parallel to the applied field, these magnetic moments are consistent also outside a magnetic field, which in general is called ferromagnetism. There are several possibilities of the orientation of the magnetic moments within a crystal lattice. Pure ferromagnetism shows a parallel alignment of all uncompensated magnetic moments but this is not realized for natural minerals.

Natural minerals show paired antiparallel alignment of the magnetic moments. When such paired and antiparallel magnetic moments compensate each other, the sum of the magnetic moments is zero and the

minerals show *antiferromagnetic* behavior (e.g., ilmenite). Similar to paramagnetic minerals, a magnetization outside an applied field is not possible and the magnetic information is lost. When applying magnetic field, the induced magnetization is parallel to this field and the magnetic susceptibility shows positive values. At a distinct temperature T_N (Néel temperature), which is characteristic for each mineral, the order of the magnetic moments disappears and the antiparallel coupled magnetic moments of the mineral pass into a statistically randomized, paramagnetic order. The antiferromagnetic κ is therefore temperature dependant according to the Curie-Weiss law:

$$\kappa_{antif} = C / (T + T_N).$$

Numerous natural minerals, such as magnetite ($Fe^{2+}Fe^{3+}O_4$), show unequal magnetic moments in the crystal lattice, which cannot compensate each other. Thus, a resulting magnetic moment exists also outside a magnetic field. Minerals with uncompensated magnetic moments outside a magnetic field are called *ferrimagnetic*. They acquire a remanent magnetization. Similar to the antiferromagnetic order, the ferrimagnetic order passes into a paramagnetic order above a distinct temperature, which is called Curie temperature (T_C). Antiferro- and ferrimagnetic minerals show just below their T_C a jump of κ, which is called *Hopkinson peak* (HP). Above the T_C, the ferrimagnetic minerals show a temperature dependent behavior according to the Curie-Weiss law:

$$\kappa_{ferri} = C / (T - T_C).$$

Anisotropy of the magnetic susceptibility

Ferri-, antiferro- and paramagnetic minerals show a directional dependence of the magnetic susceptibility according to their crystallographic axes. Beside the presence of para- and ferrimagnetic components in a rock sample, this effect can be neglected for the diamagnetic component. The magnetic susceptibility can be described as a second order tensor, which is displayed as a susceptibility ellipsoid with a maximum, intermediate and a minimum axis (Fig. D a). This is used for the quantitative evaluation of petrofabrics in rocks according to the Jelinek-diagram (Fig. D b). The parameter used in this study are the shape factor ($T = (\ln F - \ln L) / (\ln F + \ln L)$) and the degree of AMS defined by the corrected anisotropy factor ($P` = \exp(2(\ln\kappa_{max} - \ln\kappa)^2 + 2(\ln\kappa_{int} - \ln\kappa)^2 + 2(\ln\kappa_{min} - \ln\kappa)^2)$).

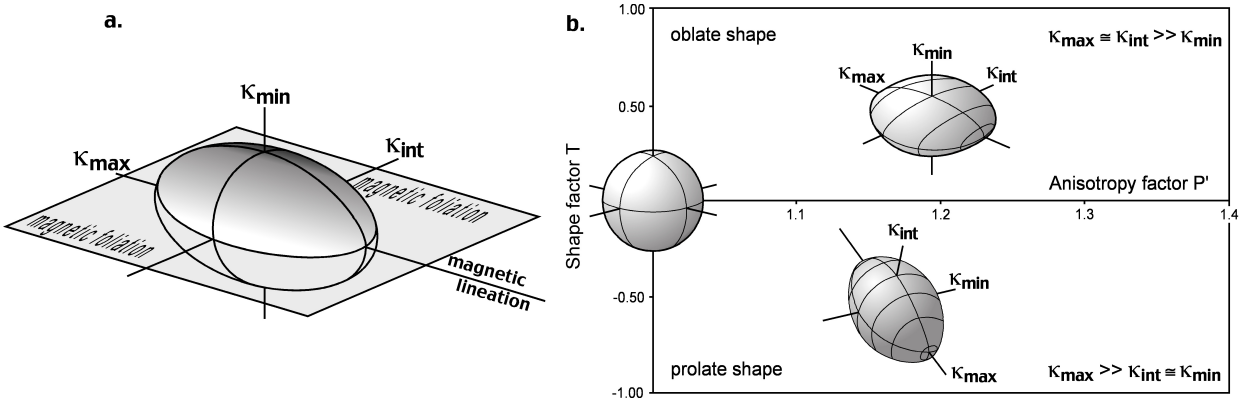

Fig. D: a. *Axes kmax, kint and kmin of the anisotropy tensor of the magnetic susceptibility ellipsoid. The maximum axis (kmax) represents the magnetic lineation. The plane between kmax and kint (intermediate axis) represents the magnetic foliation plane.* ***b.*** *Jelinek diagram (Jelinek 1977) with the shape factor T versus the anisotropy factor P`.*

Remanent magnetization

Natural remanent magnetization (NRM) of a rock is the vector sum of all magnetization vectors acquired during its thermal history and the formation processes of its constituent magnetic minerals. Each of these magnetizations represents a characteristic remanent magnetization (ChRM). A remanent magnetization (RM) acquired during the cooling of the granite pluton is primary and is called thermal remanent magnetization (TRM). Subsequent alteration of a rock can lead to the formation of new magnetic minerals that acquire a RM at temperatures below the Curie temperature representing a secondary magnetization. Formation of a new magnetic mineral in the presence of a magnetic field, either by nucleation and growth to a stable blocking volume or by alteration of an existing magnetic phase, e.g. magnetite to hematite oxidation, results in crystallization or chemical remanent magnetization (CRM). Other remanent magnetizations, which may also contribute to the NRM, are viscous remanent magnetization (VRM) and drilling induced remanent magnetization (DIRM). Both magnetizations are acquired during exposure to weak fields. VRM is acquired during the exposure to the geomagnetic field and, the DIRM is acquired during the exposure to the magnetic field of magnetized core barrel. Such core barrels can produces fields that outweigh the Earth magnetic field.

Magnetic minerals

Magnetite is the most important magnetic mineral on Earth. Magnetite is a cubic mineral with inverse spinel structure. Oxygen anions form a face-centered cubic lattice, with Fe^{2+} and Fe^{3+} cations in interstitial sites. The cation distribution for the divalent cations is confined to octahedral sites while trivalent cations occupy octa- and tetrahedral sites. The exchange interactions between these two sublattices with different magnetic moments (Fe^{3+}: 5 μ_B; Fe^{2+}: 4 μ_B) give magnetite its ferrimagnetic character and the ability to acquire a remanent magnetization. Above ~ -150 °C, the spontaneous magnetization is parallel to the ⟨111⟩ directions, and therefore well-crystalline magnetite is isotropic. Below ~ -150 °C, the easy direction is parallel to ⟨110⟩. The transition between these two easy directions is called Verwey transition. The Curie temperature for pure magnetite is ~ 580 °C. Magnetite shows only a *shape anisotropy*, which depends on the shape of individual grains and only a very weak *coercive force* for large grains. Coercive force is material specific and describes the force, which is needed to rotate the spontaneous magnetization from the easy direction.

Hematite (α-Fe_2O_3) shows antiferromagnetic ordering of its magnetic moments. All cations are Fe^{3+} and occur in (0001) layers alternating with layers of O^{2-} anions. Atomic magnetic moments of Fe^{3+} cations lie in the basal plane. Atomic moments are parallel coupled within one basal plane but they are not exactly parallel coupled between adjacent layers, yielding a net magnetization called as *canted antiferromagnetic*. In addition, hematite shows a defect ferromagnetism caused by lattice defects or nonmagnetic impurity cations (*defect moment*). While the origins of the two contributions to the magnetization are complex and not fully understood, the effect is a weak ferromagnetism of hematite, which enables remanent magnetization acquisition in hematite. The Curie temperature of hematite is ~ 680 °C. Below ~ -10 °C, the spontaneous magnetization changes the direction from the basal plane into the direction normal to the basal plane (parallel to the c-axis), which is called the Morin transition. In contrast to magnetite, hematite shows a strong magnetic anisotropy, which is mainly caused by *magnetocrystalline anisotropy*, which in turn causes a high coercivity.

Chapter II:

Rock magnetic investgations

1. Development of magnetic fabrics during hydrothermal alteration in the Soultz granite from the EPS-1 borehole, Upper Rhine Graben [1]

Abstract: The Variscan, magnetite-bearing Soultz granite is found between 1420 – 2230 m of the EPS-1 borehole situated in the Upper Rhine Graben (France). This chapter focuses on the changes of magnetic properties, which occur during the progressive hydrothermal alteration and fracturing of the Soultz granite after emplacement. The magnetic susceptibility (κ) of the granite is between 10 and 80 x 10^{-3} SI, and suggests that ferrimagnetic minerals are the primary carrier. During cooling and later tectonic and hydrothermal overprints, including the formation of the Rhine Graben, the granite was deformed under brittle conditions and partially altered by hydrothermal fluids. Along with this fluid activity, oxidation of magnetite to hematite (martitization) occurred and reduced κ (< 1 x 10^{-3} SI). AMS analysis on oriented samples documents the history of progressive transformation from primary magmatic fabric to tectonic fabric during hydrothermal alteration and faulting. The fresh granite with multi-domain magnetite grains shows subhorizontal magnetic foliations and randomly oriented magnetic lineations within the foliation plane. This fabric is similar to the magmatic fabric reflected by biotite. Transformation of the magnetic fabric started with localized magnetite oxidation along NW-SE oriented microcracks, which are probably associated with a late-magmatic alteration (stage I). Elongated and co-aligned magnetite relics within the newly formed martite caused a well-defined NW-SE trending magnetic lineation and steeper magnetic foliation. Later alteration associated with intense brittle deformation (stage II) initially adopted this magnetic fabric, but intense cataclasis destroyed it. The geometry and orientation of magnetic fabric clearly indicate a hydrothermal alteration, which relates to the acting tectonic stresses in the post-emplacement history of the Soultz granite.

Introduction

The EPS-1 borehole near Soultz-sous-Forêts is part of the Hot Dry Rock (HDR) project, which drilled through magnetite-bearing, Variscan basement, the Soultz granite, in the depth interval between 1420 – 2230 m. During the late-magmatic cooling of the pluton and the later formation of the Upper Rhine Graben, the intrusive rocks were partially altered by hydrothermal fluids. This alteration has been monitored along the profile by magnetic susceptibility measurements, which indicated a transition from ferrimagnetic to paramagnetic susceptibilities (Rummel and König 1991).

Magnetic fabric analysis using the anisotropy of magnetic susceptibility (AMS) is often used to define and quantify the magnetic fabric (e.g., Bouchez et al. 1987; Tarling and Hrouda 1993; Ferré and Améglio 2000). This method has been applied to a large number of granitoid rocks from different tectonic settings in order to correlate the shape and orientation of the magnetic ellipsoid with tectonic strain and emplacement processes (examples from the Odenwald crystalline complex are given e.g., by Dietl and Stein 2001; Greiling and Verma 2001). While the AMS method has often been used to evaluate the tectonic strain acquired during ductile microstructure development in granitoid rocks (e.g., Hrouda et al. 2002; Ferré and Améglio 2000), very few investigations focused on the influence of hydrothermal alteration and brittle deformation on magnetic fabrics. Changes in magnetic and fractal properties of fractured granites were reported by Nakamura and Nagahama (2001) from a drill core towards the Nojima fault, Japan. In weakly fractured granites, the magnetic fabric can be related to fracturing, while in strongly fractured rocks the AMS became nearly isotropic. In contrast to the Soultz granite, where alteration reduced

[1] *Just et al. 2004*

magnetic susceptibility (Rummel and König 1991), in the Nojima Fault an increase in susceptibility was observed during alteration indicating a new formation of magnetite. This study focuses on the magneto-mineralogical changes and the related magnetic fabric development in the fresh and hydrothermally altered and fractured Soultz granite. A combination of low-field and high-field magnetic methods together with electron backscatter images on polished sections oriented parallel to the magnetic fabric was used. These results should lead to a better understanding of the processes controlling fabric development that reflect tectonic stresses during the brittle, post-emplacement history of an originally magnetite-bearing granite.

Geological setting

The NNW-SSE trending Rhine Rift is one of the most prominent extensional structures in central Europe, which developed since Middle to Late Eocene times by reactivation of a complex set of crustal discontinuities, formed as late to post-Variscan (Permo-Carboniferous) relaxation structures (e.g., Schumacher 2002; Ziegler 1996; van Wees et al. 2000). The reactivation of the Variscan discontinuities was induced by the Alpine Africa-Eurasia crustal convergence. Hereby, the prevailing tectonic stresses influenced the structural development of the localized alteration and fault zones within the Soultz pluton. Enhanced seismicity, abundant mineral water springs and distinct heat flow anomalies are the present-day features of this tectonic structure.

The EPS-1 borehole is located on the western side of the Upper Rhine Graben within a geothermal anomaly (Fig. 1.1). The borehole was cored from 980 to 2230 m and consists of sedimentary cover rocks down to 1420 m underlain by granitic basement. The Soultz granite, belongs to the late to post-tectonic Variscan granitoids, ubiquitous in the European Variscan basement. Alexandrov et al. (2001) dated the magma emplacement at 331± 9 Ma (U/Pb ion-probe, zircon) and classified the

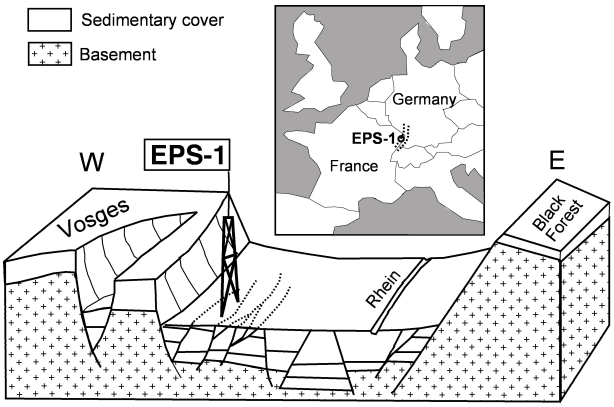

Fig. 1.1: *Location map of the central Upper Rhine Graben (dashed line) and a schematic profile through the rift at the EPS-1 drill site at Soultz-sous-Forêts.*

granite as a monzogranite with high-K calc-alkaline composition. The Variscan age of the Soultz granite is within the range, found for several granitoid intrusions from adjacent basement areas of the Mid-German Crystalline Rise (Flöttman and Oncken 1992). The granitoids were emplaced during the Permo-Carboniferous phase of wrench tectonics (Ziegler 1986). Petrological investigations of the Soultz granite from Stussi et al. (2002) have shown that pluton formation occurred in two different crystallization stages. The first was deep-seated at 11 – 12 km depth and characterized by the crystallization from the liquidus phase (hornblende, rare sphene, allanite, biotite, orthoclase, plagioclase) in a temperature range of 755-790 °C at 3.5 kbar. The second crystallization stage took place at 4.5 – 5.5 km depth, which lead to a consolidation of the granitic body at temperatures of 665-715 °C and pressures of 1.5-2.0 kbar during ascent; this is characterized by the final crystallization of hornblende and magnetite. Genter and Traineau (1996) observed a weak magmatic foliation with subhorizontal inclinations, which was correlated to primary biotite and hornblende.

EPS-1 borehole – magnetic susceptibility and petrography

For sampling in the bore core journal at Soultz a portable Handkappameter KT-6 (Geofyzika, Brno) was used, which has a sensitivity of 1 x 10^{-5} SI and

an operation range between -999 and 9999 x 10^{-3} SI and operating frequency of 10 kHz. The circular surface of the apparatus has a diameter of 6.5 cm and 90 % of the signal come from the upper 2 cm resulting in a measuring volume of ~66.4 cm^3.

Identification of whole rock composition was achieved by means of optical examinations of polished thin sections (30 µm) under microscope (transmitted and reflected light). Backscatter electron images were taken with a LEO 440 scanning electron microscope (SEM) at the Institute for Environmental Geochemistry of the University of Heidelberg. To generate a conductive layer thin sections were coated with carbon in vacuum. Estimations on the major cation composition were carried out using an EDX-apparatus (Link Isis 300, Oxford) with an acceleration voltage of 20 kV.

Based on the magnetic susceptibility log of the drill cores (Rummel and König 1991) (Fig. 1.2) the granite can be subdivided into an upper (1420 – 1550 m) and a lower (1550 – 2230 m) section. The upper section consists of strongly altered granite with low magnetic susceptibility (κ) values (κ < 1 x 10^{-3} SI). The homogenous distribution of the low susceptibilities indicates a persistent alteration. The lower section consists mainly of fresh, unaltered granites with high values in general (κ > 10 x 10^{-3} SI). Three main, discrete fault zones with strongly decreased κ values dissect the lower section; this is also reflected in the susceptibility log (Fig. 1.2). Microscopic examinations showed that oxidation of magnetite into hematite (martitization) during hydrothermal alteration was responsible for the reduction of κ. Traineau et al. (1991) described two main types of hydrothermal alteration within the Soultz granite. The first type (stage I) is propylitic and pervasive. It took place under retrograde conditions during cooling of the magma and affected the whole plutonic body with varying intensities. The second type (stage II) is localized to fault zones and has an argillitic character. It is related to hydrothermally altered cataclastic granites and their hydrothermalized wall rocks.

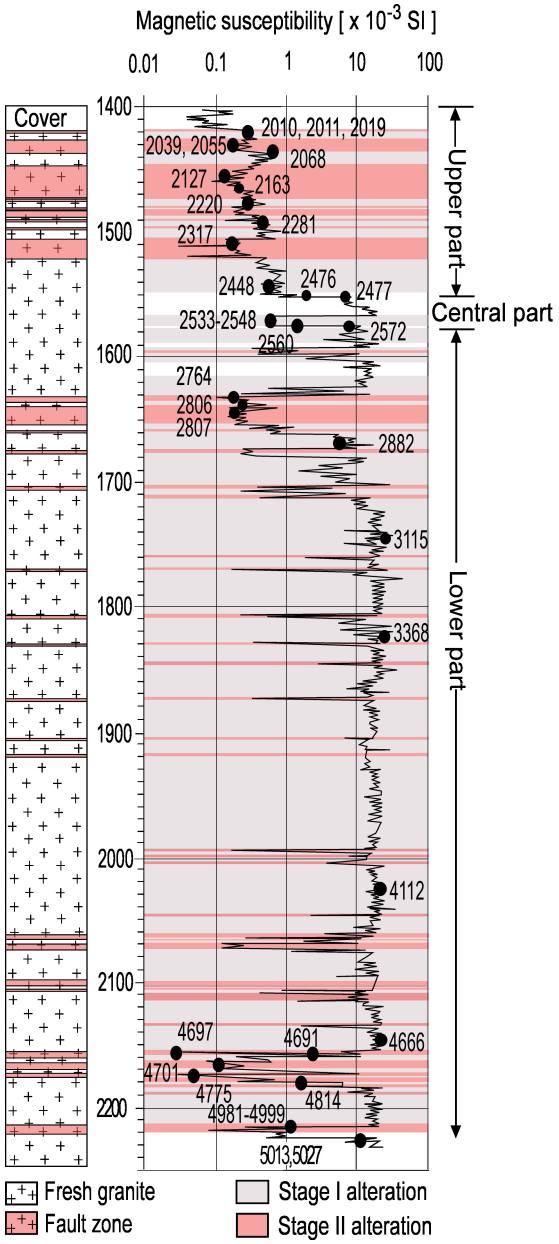

Fig. 1.2: *Lithologic section (modified after Genter and Traineau 1996) and magnetic susceptibility log with data (Rummel and König, 1991) on drill cores at the 1414 to 2230 m depth interval in the EPS-1 borehole. The hydrothermal alteration observed in the cores is related to two stages. Black dots and numbers indicate sample positions, according to the nomenclature of the core index (Genter and Traineau 1991).*

Bulk magnetic susceptibility was measured on cylindrical specimen (~10 cm^3), selected from different localities within the profile (Fig. 1.2). Frequency distribution allows for the definition of susceptibility intervals for the fresh granite, the hydrothermally altered granite of stage I (pervasive alteration) and hydrothermally altered granite of stage II (localized alteration) (Fig. 1.3). The altered

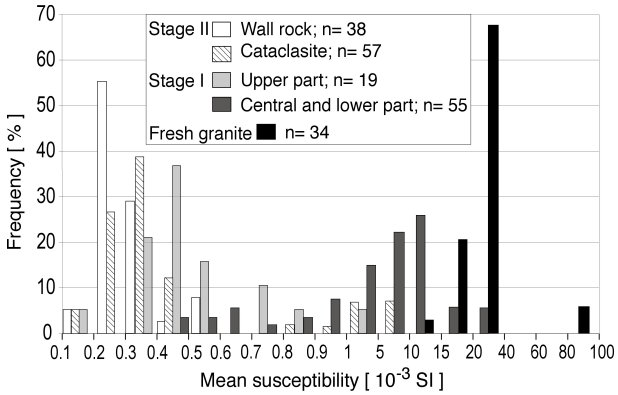

Fig. 1.3: *Frequency histogram of the mean magnetic susceptibility measured on standard specimens (~10 cm³) from cores of the EPS-1 borehole.*

granites of stage II are subdivided into cataclastic granites and their hydrothermally altered wall rocks. Although there is no fresh, unaltered granite sensu stricto within the drill profile, in this study, the term "fresh granite" is used for granites without any evidence of magnetite oxidation. The fresh granite shows a κ interval between 10 and 80 x 10^{-3} SI, whereby almost 70% of the specimens have κ values between 20 and 40 x 10^{-3} SI. The κ values indicate a magnetite concentration of approximately 1 wt% in the fresh granite. The hydrothermally altered granites of stage I show decreased κ values and two maxima in their frequency distribution, one in the upper part (0.4 – 0.5 x 10^{-3} SI) and the second one in the central and lower part (10 – 15 x 10^{-3} SI). This bimodal distribution indicates different alteration and magnetite oxidation intensities during the pervasive alteration. Different alteration intensities are also observed for the later, localized hydrothermal alteration. The cataclastic granites have κ values between 0.8 and 10 x 10^{-3} SI and their hydrothermally altered wall rocks have the lowest susceptibilities between 0.1 and 0.5 x 10^{-3} SI. These hydrothermalized wall rocks have a maximum frequency distribution between 0.2 and 0.3 x 10^{-3} SI, which is characteristic of the most intense hydrothermal alteration in the Soultz granite. In the following, the magnetic minerals and fabrics of the unaltered fresh granite and the subsequent stages of the hydrothermal alteration are described in more detail.

Fresh granite

The high magnetic susceptibilities in the fresh granite, which does not show any evidence of oxidation, are controlled by magnetite with grain sizes between 300 and 500 µm (Fig. 1.4 a, b). The magnetite grains are mostly euhedral or subhedral, and are frequently found in magnetite clusters associated with unaltered biotite and sphene (Fig. 1.4 b). The primary mineral assemblage is comprised of K-feldspar megacrysts (up to 5 cm diameter) in a coarse-grained matrix of diamagnetic quartz, feldspar, paramagnetic biotite and hornblende, as well as accessory diamagnetic apatite and sphene. The primary minerals are partly affected by the early pervasive alteration stage I. This alteration started during the emplacement of the granite and persisted under retrograde conditions during cooling (Jacquemont 2002). During a late magmatic stage (700 °C and 3 – 4 kbar), magmatic epidote was formed due to the decomposition of hornblende. Continued cooling to circa 300 °C caused the formation of paramagnetic hydrogarnet, prehnite and epidote in biotite. An early hematitization of K-feldspar megacrysts (Dubois et al. 1996), observed also in fresh granites, indicates an increase of oxygen fugacity (fO_2) during the cooling history. In addition, small hematite platelets and rods (< 10 µm) grew along the biotite cleavage. The oxidation of magnetite to martite (hematite) occurred during the latest phase of pervasive alteration stage I.

Hydrothermally altered granite

In the Soultz granite, two main hydrothermal alteration stages were previously described by Traineau et al. (1991). This study focus on alteration processes, which affect the magnetic mineralogy. The onset of a gradual decomposition of magnetite into martite was accompanied by a chloritization (Fe-Mg chlorite) of biotite. These alteration processes took place during the latest phase of stage I alteration, where retrograde conditions during the pluton emplacement caused decreased temperatures of ~200 °C (Jacquemont 2002) and increased oxygen

Fresh granite

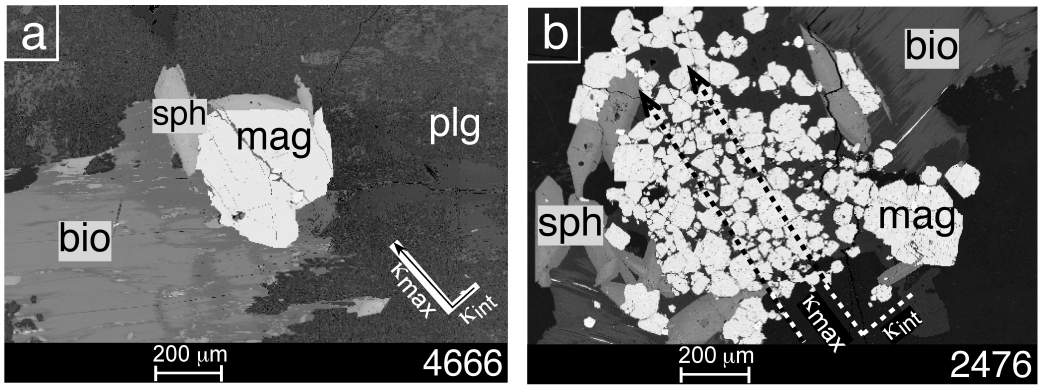

Stage I alteration

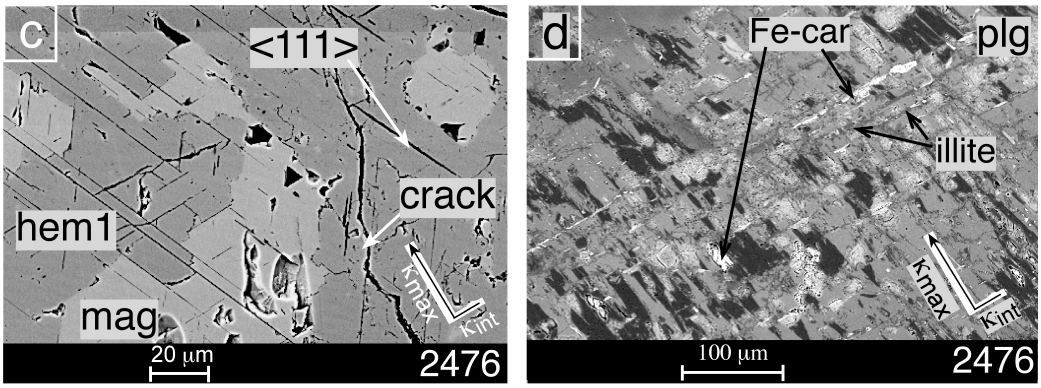

Stage II alteration

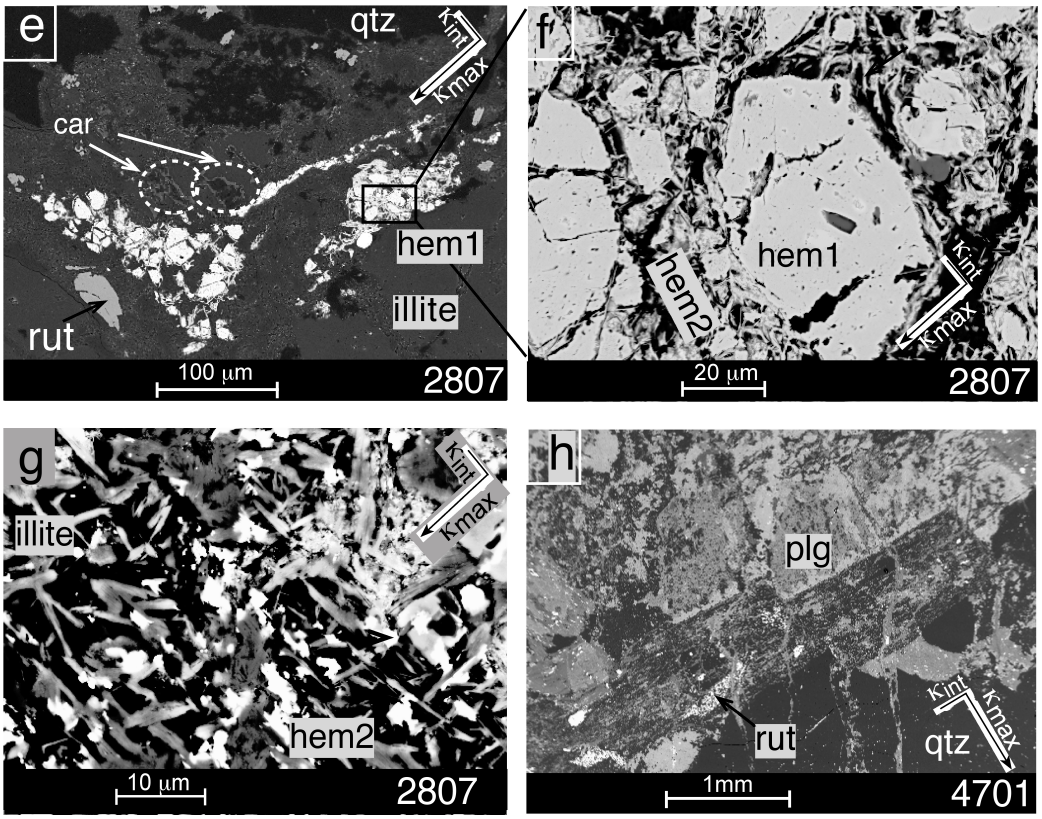

Fig. 1.4: *Micrographs (SEM) from thin sections parallel to the magnetic foliation (kmax/kint) showing typical microfabrics of the fresh and hydrothermally altered Soultz granite (sample locations in Fig. 1.2). Mag: magnetite; hem: hematite; bio: biotite; sph: sphene; rut: rutile; plg: plagioclase; kfs: K-feldspar; qtz: quartz; car: carbonate; cal: calcite.* ***a.*** *Single grain of mag associated with bio and sph surrounded by partly altered plg within fresh granite. Microcrack in mag is parallel to kmax.* ***b.*** *Clusters of mag grains are parallel to the shape preferred orientation of biotite associated with sphene within weakly hydrothermally altered granite.* ***c.*** *Mag oxidized into hem1 (martite) with elongated mag relics with <111> long axis oriented parallel kmax in hydrothermally altered granite.* ***d.*** *Decomposition of plg into Na-rich (dark grey) and Ca-rich (bright grey) plg components. Growth of Ca-Fe-Mg carbonates and illite parallel to crystallographic axis of plg within hydrothermally altered granite.* ***e.*** *Cataclased hem1 (martite) grains.* ***f.*** *Hem1 (martite) is cataclased and dissolved. Precipitation of fine-grained hem (hem2) grains occurred along cracks oriented parallel to the magnetic axis kmax and kint or* ***g.*** *hem (hem2) is associated with illite.* ***h.*** *Progressive illitization in hydrothermalized wall rock accompanied by abundant Ca-Fe-Mg carbonates.*

fugacity, which most likely initiated the magnetite oxidation. The magnetite decomposition is visible in a progressive decrease of ferromagnetic into susceptibility values dominated by paramagnetic phases ($\kappa < 1 \times 10^{-3}$ SI). Martite replacement started in grain boundaries and microcracks, which further evolved in general along the crystallographic axis ⟨111⟩ of magnetite (Fig. 1.4 c). Depending on the alteration intensity magnetite relics of varying grain sizes were retained within the martite grain (Fig. 1.4 c). Shape and orientation of the retaining magnetite relics were controlled by previously existent microcracks within magnetite grains. With advanced hydrothermal alteration of the granite martite was pseudomorphed after magnetite grains. But, in hydrothermally altered granites of stage I, no completely oxidized magnetite grains were observed. Plagioclase and biotite, which were minerals of the primary magmatic assemblage, were altered to illite + calcite + chlorite. Secondary hematite precipitated probably from residual fluids, which circulated during the latest cooling stage of the plutonic body. Similar to hematite, the newly formed minerals pseudomorphed the primary minerals (Fig. 1.4 d). Granites with significantly oxidized magnetite, assigned to the stage I alteration were found only in the depth interval 1550 to 1580 m. This section is referred to as the central part of the borehole profile in this study (Fig. 1.2).

The hydrothermal alteration stage II occurs within faulted and fractured zones showing the strongest alteration intensity of the granite with the strongest oxidation of magnetite. These granites contain inhomogeneously distributed networks of fine veins, mostly filled by secondary minerals such as quartz, illite, hematite and carbonates, which were precipitated from fluids. With increasing distance from a fault zone, cataclasis vanished and wall rock halos of hydrothermally altered minerals developed. Martite (hematite) pseudomorphisms after magnetite were often fractured and a second hematite generation was formed along cracks (Fig. 1.4 e, f). The size of magnetite relics depend on the intensity of the stage II alteration as well as on the intensity of the earlier stage I alteration. Hereby, the magnetite relics can be completely martitized representing the strongest hydrothermal alteration. However, a complete martitization of magnetite is rarely observed in the Soultz granite. In the altered wall rock halos, the primary minerals, particularly feldspars, can be fully dissolved (Fig. 1.4 g, h) and replaced mainly by illite, which pseudomorphosed after the primary minerals. In contrast to stage I alteration, where chlorite replaced the Fe-Mg silicates (biotite, hornblende, chlorite), these phases are also replaced mainly by illite. From the petrographic view, the most obvious difference, compared to stage I, is the higher content of illite.

Results

1. Rock magnetic properties

In order to evaluate the decreasing influence of magnetite during the hydrothermal alteration and the associated increasing content of hematite on magnetic susceptibility and fabric, the rock magnetic

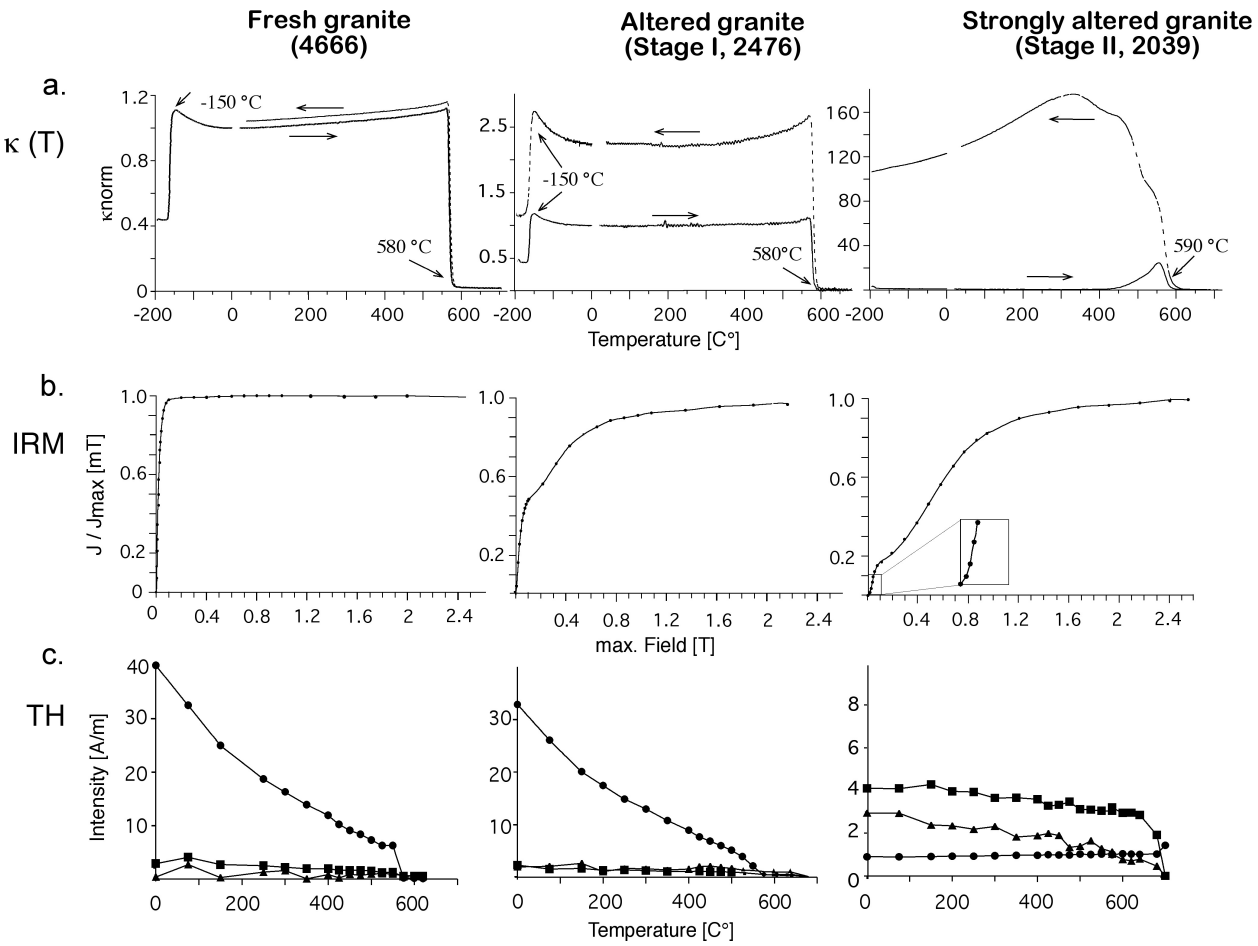

Fig. 1.5: *Rock magnetic properties of fresh and hydrothermally altered granite from stage I and II.* ***a.*** *k(T) curves with susceptibility normalized to room temperature.* ***b.*** *Acquisition of IRM with stepwise magnetization up to 2.6 T.* ***c.*** *Before thermal demagnetization (TH) the samples were magnetized in three directions: x (dots) = 200 mT, y (triangles) = 600 mT and z (squares) = 2.6 T.*

behavior was investigated on representative samples. Fresh and hydrothermally altered granite of different alteration intensities with magnetite relics and without any petrographic evidence of magnetite were analyzed using the temperature-dependence of low-field magnetic susceptibility (κ(T)), isothermal remanent magnetization (IRM), and stepwise thermal demagnetization (TH) experiments of a multi-component IRM (Fig. 1.5).

The κ(T) measurements were done at GPI Heidelberg using a KLY-2 Kappabridge, combined with the CS-2/CS-L furnace apparatus of AGICO (Hrouda 1994). IRM acquisition curves were obtained with a maximum field of 1 T using an ASC Scientific Model IM-10-30 Impulse Magnetometer at the ETH Zürich. Determination of unblocking temperatures was done by thermal demagnetization (TH) with progressive heating in zero-field. Before thermal demagnetization, the samples were magnetized in three orthogonal directions with different field intensities (x = 200 mT; y = 600 mT; z = 2.6 T) in order to separate the different coercivity components (Lowrie 1990).

Fresh granite

The κ(T) measurements for the fresh granite show a curve typical for multi-domain (MD) magnetite with a reversible heating and cooling run (e.g., Kontny and de Wall 2000; Muxworthy and McClelland 2000). Characteristic features of the MD magnetite are the Verwey transition at –150 °C, no distinct Hopkinson peak and a Curie temperature (T_C) of 585 °C, which indicate the predominance of MD grains of magnetite (e.g., Dunlop and Özdemir 1997). This interpretation is also supported by the remanence experiments. IRM acquisition curves

are typical for a soft magnetic component, which can be saturated at fields well below 100 mT. The thermal demagnetization curves are typical for low coercivity material (x axis), which is demagnetized at 575 °C. indicating magnetite as the magnetic carrier (Fig. 1.5 c). The unblocking of magnetite is sharp and suggests a limited grain size fraction and compositional range.

Hydrothermally altered granite

In the pervasively altered granite of stage I with magnetite relics, the κ(T) measurements still show the T_C of magnetite at 585 °C but in contrast to the fresh granite an irreversible heating and cooling run. Although observed microscopically, hematite was not identified by its T_C. It is assumed that in the Soultz granite hematite content is too low for identification using the κ(T)-measurements, because the magnetic susceptibility of hematite is three orders smaller than that of magnetite. Additionally, hematite was probably modified into magnetite during heating before reaching its T_C and thus only the T_C of magnetite was observed. However, the strong increase of κ, a single T_C of magnetite as well as the Verwey transition at –150 °C during a second cooling run indicate the formation of new magnetite phase during the heating run (Fig. 1.5).

The IRM acquisition curve documents the magnetization of soft and hard magnetic components. Nearly 50% of the bulk magnetization is acquired at fields below 100 mT, characteristic of magnetite, but saturation of the second component requires magnetic fields higher than the peak field of 2.6 T. This behavior is typical for hematite. Thermal demagnetization also indicates the dominance of the low coercivity component demagnetized at 575 °C. However, in contrast to the fresh granite, this hydrothermally altered sample shows a wider temperature range of unblocking. This indicates the presence of a wide grain-size spectrum of magnetite. Magnetic behavior of this altered sample is therefore still dominated by the magnetite component while the influence of hematite is subordinate. A grain size reduction of magnetite due to a partial reaction to hematite (martite) during hydrothermal alteration as observed by optical microscopy (Fig. 1.4 c) is clearly evident in the magnetic signature.

κ(T) measurements of granite with the most intensive hydrothermal alteration do not show the Verwey transition in the low-temperature run. During the heating run, an increase in magnetic susceptibility is observed at temperatures above 450 °C, which is interpreted as a formation of a strong magnetic phase. This newly formed phase shows a T_C of 590 °C, indicating the formation of cation-deficient magnetite. From the κ(T) magnetite can be excluded as an original phase. A strong irreversibility of the heating and cooling run is observed along with a strong increase in magnetic susceptibility during cooling. In contrast to the less altered sample, a second low-temperature run reveals no Verwey transition and magnetic susceptibility decreases with decreasing temperature. Therefore, the formation of an unstable, maghemite phase is favoured and the formation of pure magnetite during the heating experiment can be excluded.

In the IRM acquisition curve the hard magnetic component predominates the magnetization behavior. However, the IRM curve still indicates the presence of a softer magnetic component. Initial concave IRM curve (see inlay in Fig. 1.5 b) suggests MD hematite (martite) as the magnetic carrier and not magnetite. This agrees with microscopic observations showing no magnetite but large grains of martite (100 - 300 μm) in addition to fine hematite grains < 10 μm. This interpretation is in agreement with studies of Kletetschka and Wasilewski (2001) on the transition between truly multi-domain (>100 μm) and single-domain (SD; < 50 μm) behavior in hematite. The SD hematite grains possess high coercivities and are not saturated at 2.6 T during IRM acquisition. The TH experiments show that the high and intermediate coercivity components are demagnetized at 700 °C indicating hematite as the magnetic carrier. In contrast to the high coercivity component, the intermediate coercivity component shows a wider temperature range of unblocking and probably can be related to the presence of a wide

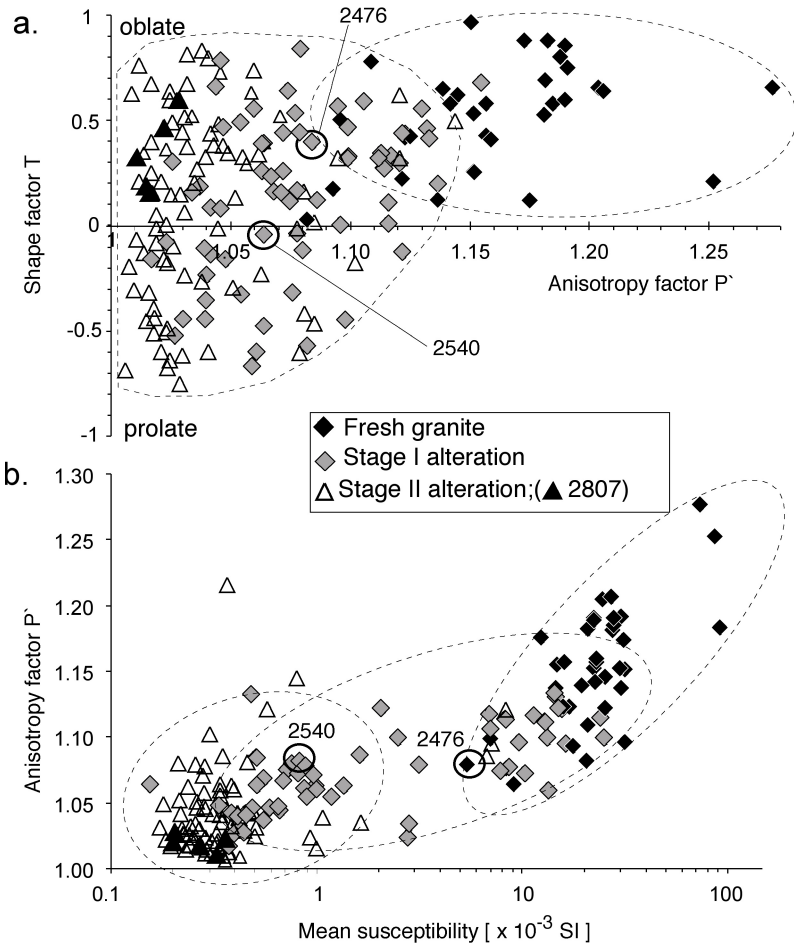

Fig. 1.6: a. *Variation of the shape parameter T with the anisotropy P' (Jelinek 1977) showing oblate shapes for the fresh granite and a strong variation from oblate to prolate shapes in the hydrothermal samples.* ***b.*** *Variation of P' with mean susceptibility. Hydrothermally altered samples of stage I overlap with fresh and as vein altered samples of stage II, for further explanation see text.*

MD hematite grain size spectra.

2. Magnetic fabric

Low field magnetic fabric measurements reflect the bulk, preferred-orientation of all, ferromagnetic, paramagnetic and diamagnetic minerals. The magnetic susceptibility measurements and rock magnetic characteristics presented in the previous sections have revealed a progressive change in the magneto-mineralogy of the Soultz granite from ferrimagnetic behavior in the fresh parts to paramagnetic behavior in strongly altered parts. This change is also documented in the geometry and orientation of magnetic fabrics. Thirty-nine oriented samples were taken from the 1420 to 2230 m granite interval of the EPS-1 borehole. A Kappameter KT-6 (GEOFYZIKA) with a sensitivity of 1 x 10^{-5} SI and an operating frequency of 10 kHz has been used for sample selection, since susceptibility was diagnostic for the fresh and altered granites. Up to 6 cylindrical specimens (1" standard cylinders) per core were prepared with a sample volume of ~ 10.06 cm^3. Determination of the directional dependence of the anisotropy of magnetic susceptibility (AMS) was done using the KLY-2 Kappabridge (AGICO) with a detection limit of 4 x10^{-8} SI and an operation frequency of 920 Hz. Several parameters are used to describe the AMS ellipsoids. The AMS parameter used in this study are the shape factor (T = (lnF – lnL) / (lnF + lnL)) and the degree of AMS defined by the

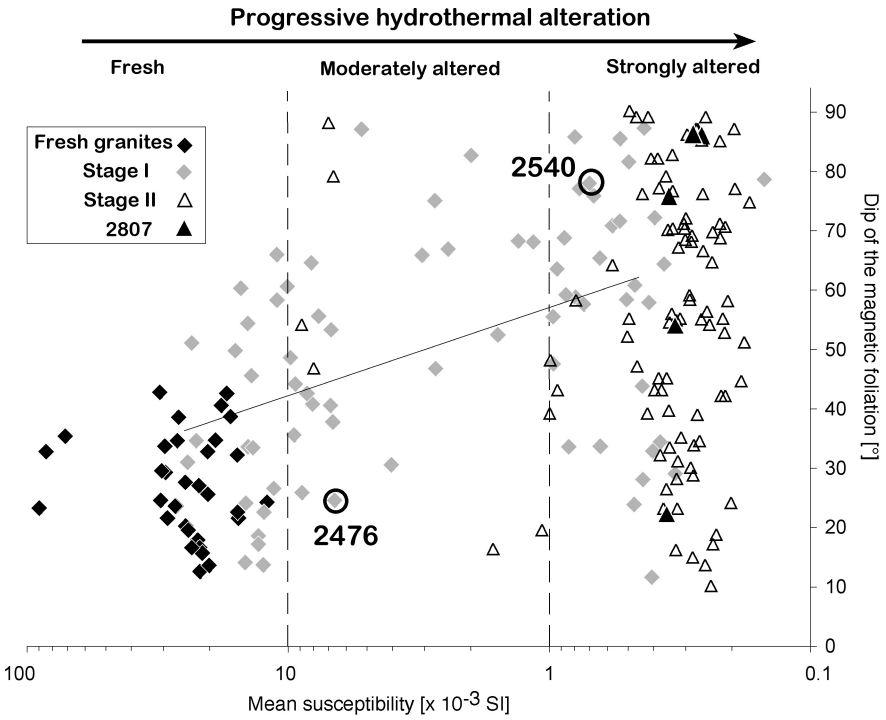

Fig. 1.7: *Mean magnetic susceptibility versus dip of magnetic foliation for fresh (black diamonds) and hydrothermally altered granite of stages I (grey diamonds) and II (open triangles). The solid line represents a changing trend from flat to steep foliation during hydrothermal alteration.*

corrected anisotropy factor ($P` = \exp(2(\ln\kappa_{max} - \ln\kappa)^2 + 2(\ln\kappa_{int} - \ln\kappa)^2 + 2(\ln\kappa_{min} - \ln\kappa)^2)$). Cylinders were reoriented into geographic coordinates to interpret the AMS, using the formation microscanner data given by Genter and Traineau (1991). After AMS measurements, thin sections of oriented specimens parallel to the magnetic foliation plane ($\kappa_{max}\kappa_{int}$-plane) were prepared in order to compare magnetic fabrics with petrofabrics using a scanning electron microscope (SEM).

Anisotropy of AMS ellipsoids

Shape and degree of anisotropy of AMS ellipsoids are displayed in a Jelinek-diagram (Jelinek, 1977) for fresh and altered granites (Fig. 1.6 a). The fresh granites show strongly oblate to neutral ($T > 1$) ellipsoids with high anisotropies ($1.08 < P` > 1.28$). These magnetic fabrics are related to unoxidized magnetite (Fig. 1.4 a, b), which is always associated with biotite in the Soultz granite. The onset of the magnetite oxidation during the hydrothermal alteration caused a decrease in the anisotropy and a breakout of the strictly oblate geometry, so that the ellipsoid shapes became more prolate. With further increase of hydrothermal alteration the anisotropies become nearly isotropic and the ellipsoid shapes cover the whole spectrum from strongly oblate ($T \sim +1$) to strongly prolate ($T \sim -1$) geometries. Figure 1.6 b shows decreasing anisotropy factors with decreasing mean susceptibility for the fresh and hydrothermally altered granites. The fresh granite with significant amounts of magnetite shows a clear linear correlation between the susceptibility and degree of anisotropy. With further decreasing susceptibility, due to hydrothermal alteration, the anisotropy becomes weak and the linear trend changes from steep slope in fresh to flat slope in altered granites of stage I. Samples with hydrothermal alteration of stage II scatter mainly in the field of low anisotropy, and the bulk susceptibility is mainly within the range of typical paramagnetic-dominated values. The low magnetic susceptibility values of localized stage II alteration imply that magnetite oxidation was more intense within the fault zones.

Orientation of AMS ellipsoids

The magnetic foliations of fresh and hydrothermally altered Soultz granite can be

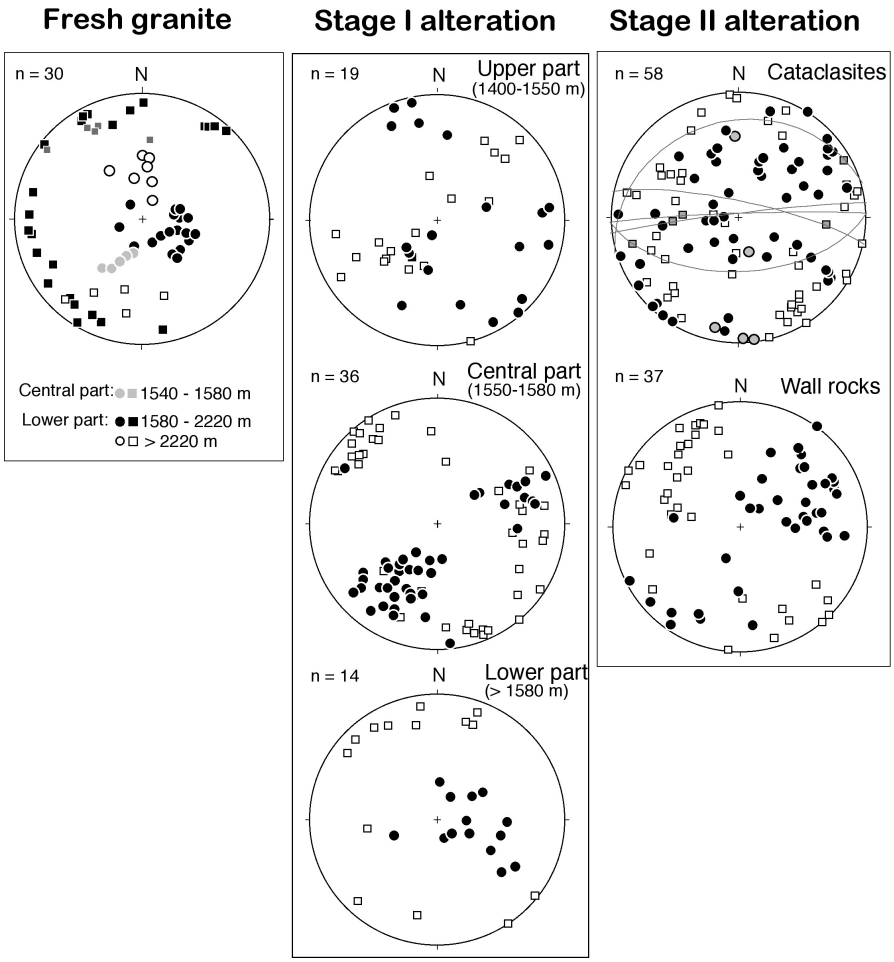

Fig. 1.8: *Lower hemisphere, equal area projection of magnetic lineations (squares) and foliations (circles) in fresh and altered granites with stage I divided into upper part (1420-1550 m), central part (1550-1580 m) and lower part (> 1580 m). Grey symbols and corresponding magnetic foliation planes with E-W trend in cataclastic granites of stage II represent the core sample 2807.*

characterized by a general change from subhorizontal orientation in the fresh granite, to steeper dipping in the altered granite of stage I, and to a random orientation in the strongly altered granites within discrete fault zones (stage II). This trend is accompanied by decreasing bulk susceptibilities (Fig. 1.7).

In the Figure 1.8, the orientation of the low-field magnetic fabric is presented in stereogram subdivided into fresh and hydrothermally altered granites of stage I and II. The stage I alteration is presented for the upper (1400-1550 m), central (1550-1580 m) and lower part (1580-2220 m) of the Soultz granite section, respectively (for definition, see Fig. 1.2).

In the fresh granite the magnetic fabric is carried by magnetite. The magnetic foliation plane (κ_{min}) generally shows subhorizontal orientation with a magnetic lineation (κ_{max}) that is strongly scattered within the foliation plane. However, in the central and in the lower part (below 2220 m) the foliations are slightly steeper and the trend is more distinct with NW-direction and SSW-direction, respectively. The subhorizontal orientation of the magnetic foliation planes in fresh granites is in agreement with observations from Genter and Traineau (1996) who evaluated magmatic foliations from primary biotite and hornblende grain alignment. The agreement of magnetic and magmatic foliation planes and the microscopically observed association of magnetite and biotite imply, that magnetite accommodate the magmatic flow regime in the Soultz granite.

Hydrothermally altered granites of stage I reveal distinct differences in the magnetic fabric orientation

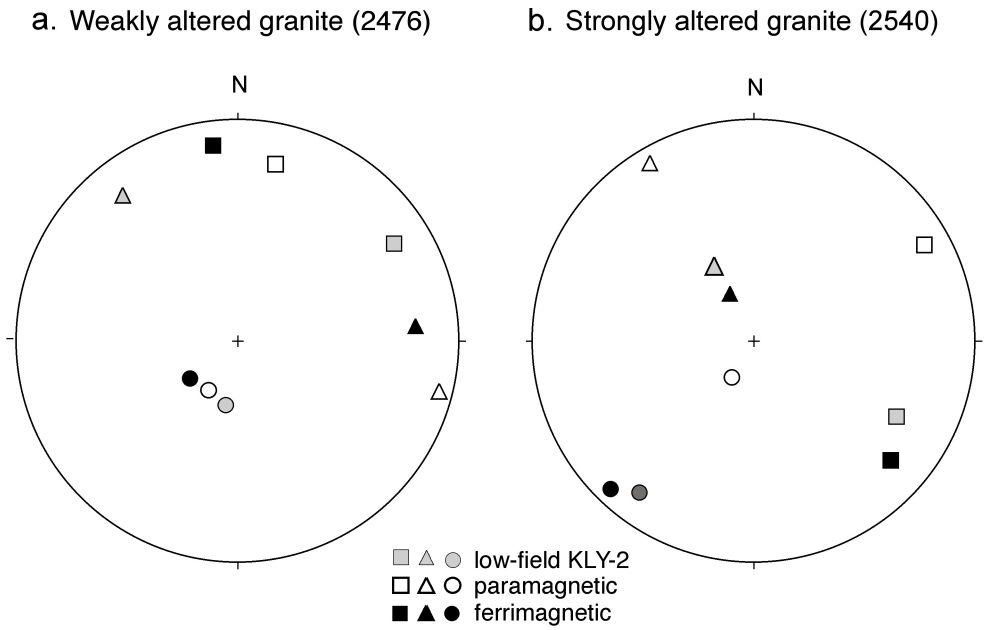

Fig. 1.9: *Separation of ferrimagnetic and paramagnetic fabric by high-field AMS measurements in comparison with low-field KLY-2 AMS data of different hydrothermally altered granite of stage I. Squares represent kmax, triangles kint and circles kmin.* ***a.*** *Weak hydrothermal alteration (sample 2476).* ***b.*** *Strong hydrothermal alteration (core index 2540; sample location see Fig. 1.2).*

within the subdivided sections (upper, central, lower part) of the Soultz granite. The general pattern of preferred orientations in the upper and central part is similar, however, an inversion of the κ_{min} and κ_{max} axes is observed. The magnetic foliations from the central part show a NW-SE trending orientation with varying subhorizontal to steep dip values and subhorizontal lineations. In the upper part the magnetic lineations scatter within a steeply NE-SW oriented plane, while in the central part, this geometry is occupied by the foliation poles. In the lowest part, magnetic fabrics of stage I strongly resemble the pattern evaluated for the fresh granites of the same section. The foliation is generally subhorizontal and the magnetic lineation scattered within the foliation plane. The orientation of AMS ellipsoids in altered granites of stage II within fault zones can be subdivided into cataclastic granites and their hydrothermally altered wall rocks without cataclasis.

The cataclastic granites show no preferred orientations of κ_{max} and κ_{min}, mostly not even in adjacent specimens from the same depth (Fig. 1.8). The random distribution of magnetic foliation poles and magnetic lineations is associated with decreased anisotropy, which can be correlated to the increased fracture density within fault zones. The magnetic fabrics in cataclastic granites show a clear trend of the magnetic foliations only when a limited number of phases dominate the magneto-mineralogy within well-oriented fractures. An example is shown in a localized fault zone at 1640 m depth (sample 2807, Fig. 1.8), where fractures are filled with secondary, fine-grained hematite and acicular illite (Fig. 1.4 g). Magnetite content was almost completely oxidized evident in low susceptibility values (< 0.362×10^{-3} SI) and in $\kappa(T)$ experiments, where no primary magnetite was observed. The quantitatively determined ferromagnetic susceptibility was assigned to hematite with 35% and to paramagnetic components with 65% (separation of para- and ferromagnetic components based on susceptibility versus temperature measurement, Hrouda et al. 1997). Here, an E-W trend of magnetic foliation planes in fractured granite has been observed indicating an E-W trending fault zone. Hematite formed from magnetite (martite) was strongly fractured and partially replaced by a secondary hematite generation precipitated from fluids (Fig. 1.4 e, f). Unlike other cataclastic samples the magnetic foliations in adjacent samples show constant strike directions, because the secondary

hematite associated with paramagnetic illite follow the fracture pattern of the E-W striking fault zone. The magnetic ellipsoids are oblate (Fig. 1.6 a) but show a lineation caused by intersection of secondary fracture planes with small angles to the main fault plane. The small anisotropy factor P` (1.01-1.03) can be explained by hematite and illite within the secondary fracture planes, which are not perfectly aligned.

In contrast to the random distribution of magnetic fabric elements within the cataclastic granites, the hydrothermally altered wall rocks reveal a well-defined magnetic fabric orientation. The foliation planes are preferentially NW-SE oriented and the magnetic lineation has a sub-horizontal NW-SE trend (Fig. 1.8). This geometry is comparable to altered granites of stage I in the central part of the pluton.

High-field separation of ferri- and paramagnetic subfabric

The orientation of low-field AMS fabrics measured with KLY-2 Kappabridge is compared with the subfabrics for ferri- and paramagnetic components, separated using a high-field torque magnetometer (Martín-Hernández and Hirt 2001). This separation (Fig. 1.9) has been carried out for two specimens from hydrothermally altered granites of stage I, which have different magnetite content according to different alteration degrees. Sample 2476 is from a weakly altered section with bulk susceptibility of $\kappa = 9.130 \times 10^{-3}$ SI and still shows the primary magmatic fabric of the granite with a subhorizontal foliation. Sample 2540 is from a strongly altered granite with $\kappa = 0.791 \times 10^{-3}$ SI and represents the altered fabric with a steeply inclined magnetic foliation. These two samples are marked in Figure 1.7, where a steeper inclination for the strongly altered sample is shown.

The high-field separation for the weakly altered sample 2476 (Fig. 1.9 a) shows similar orientations of para- and ferrimagnetic subfabrics with subhorizontal magnetic foliations according to the primary magmatic geometry. The directional properties of high-field measurements indicate that 31% of the anisotropy is carried by the paramagnetic phases and 69% by the ferromagnetic phases. Both are in agreement with the low-field AMS fabric (compare also Fig. 1.8). The torque signal shows also a dependency on applied field (B), which indicates that hematite also contributes to the torque signal. Although this contribution can be separated from the para- and ferrimagnetic contributions, it is not large enough to compute the hematite subfabric, not even in the strongly altered sample 2540. The sample 2540 shows a distinct deviation of para- and ferrimagnetic fabrics (Fig. 1.9 b), whereby 46% of the anisotropy is carried by paramagnetic and 54% by ferrimagnetic signal. The paramagnetic fabric still shows a subhorizontal orientation of the magnetic foliation according to the primary magmatic fabric. In contrast, the ferrimagnetic subfabric shows a subvertical orientation of the magnetic foliation, which is in agreement with the low-field AMS fabric.

The high-field AMS measurements clearly highlight the transformation of magnetic fabric during magnetite decomposition in the course of hydrothermal granite alteration. The low-field AMS fabric of the altered granites of stage I is carried by the ferrimagnetic component, which reflects the preferred alignment of the magnetite relics. The separated paramagnetic fabric is clearly different and is carried by several paramagnetic components mentioned already above. The paramagnetic fabric does not contribute to the low-field anisotropy alongside ferromagnetic magnetite relics.

Discussion

Primary magnetic fabric in the Soultz granite

AMS fabric studies can be used to define the internal structure of granitoid rocks (e.g., Archanjo et al. 1995; Bouchez et al. 1990). In the undeformed state the magmatic fabric reflects the preferred orientation of grains with crystalline and/or shape anisotropy (e.g., Tarling and Hrouda 1993). The fresh Soultz monzogranite has a high-K calc-alkaline

composition and high magnetic susceptibilities typical for granites of the "magnetite series" defined by Ishihara (1977) and characteristic for I-type granites. Together with other clear subduction-related I-type intrusions from the adjacent Northern Vosges, Windstein and Kaiserbach, these rocks indicate a magmatic arc setting in this area (Flöttmann and Oncken 1992).

The ferrimagnetic phase is shown in the Soultz granite to be pure, multi-domain magnetite, which is the main carrier of the AMS. In advanced hydrothermally altered granites the grain sizes of magnetite were reduced. In the studied 700 m granite section of the EPS-1 borehole, the AMS ellipsoids of fresh granites reveal a general anisotropy factor P` in the range from 1.08 to 1.28, which is within typical values for flow fabrics observed also in other granitic magnetite-series (e.g., Ferré et al. 1999; Greiling and Verma 2001). AMS ellipsoids all are oblate but have variable degrees of oblateness (Fig. 1.6 a). The high degree of oblateness is probably due to magnetite forming clusters associated with biotite. The clear positive linear correlation between anisotropy factor and magnetic susceptibility in Figure 1.6 b implicates increased magnetite content. The higher magnetite content allows for better mimicking of biotite crystal and the resulting shape of the magnetite cluster reflects more oblate ellipsoid shapes. Therefore, the strongly oblate shapes ($T < 0.7$) in fresh granites resemble AMS ellipsoids of single biotite crystals (Martín-Hernández and Hirt, 2003). The authors defined a highly oblate shape for biotite ($0.75 < T < 0.99$) and a consistent paramagnetic ellipsoid orientation with the crystallographic structure of the phyllosilicate.

In the Soultz granite, only a weak magmatic foliation is macroscopically observed and reflects the alignment of biotite (Genter and Traineau 1996). The low-field AMS measurements in the fresh granites define a strong foliation since the fabric is well documented by magnetite as the amplification factor. The magnetic foliations show relatively flat dips and a flat random distribution of magnetic lineation (κ_{max}). This flat, oblate geometry is consistent through the whole fresh granite sections (700 m), and therefore is regarded as the significant and primary magmatic fabric of the Soultz granite. However, the orientations of the AMS fabrics in other Variscan late-orogenic granite intrusions differ from those in the Soultz granite. In the Mid-European Variscides, e.g., in the Odenwald magmatic complex (Flöttmann and Oncken 1992; Greiling and Verma 2001; Dietl and Stein 2001) and in the Oberpfalz at the western border of the Bohemian Massif (Leonhard et al. 2001), the observed magmatic fabrics were related to the orientation of NW-SE shortening Variscan tectonic stresses (Ziegler 1986). In the primary magmatic fabric of the fresh Soultz granite, such a relation could not be detected. The distinct flat and planar orientation of magnetic fabrics in the studied granite may indicate a magma emplacement in the center of a batholith with a deceleration flow regime and horizontal spread out of magma. Deceleration flow occurs where channelized magma spreads out into a broader region and thus slows down, resulting in the flattening or oblate strains with high angles to the flow direction (Cruden 1990). This distinct magmatic fabric would imply, that the 331± 9 Ma Soultz granite (Alexandrov et al. 2001) was not effected in the same way as the adjacent intrusions, that were influenced by the transtensional-transpressional stress regime during the late Variscan orogeny (Ziegler 1986).

Magnetic fabric in hydrothermally altered granite

In the Soultz granite, the two hydrothermal alteration stages (pervasive stage I and localized stage II) appear in the strongly altered upper part and in the lower part within fault zones, while the central part is only characterized by stage I alteration. The reduction of magnetic susceptibility due to the reaction of magnetite to martite affects the progressive transformation of magnetic fabrics in both stage I and II alterations. With increasing alteration, the bulk magnetic susceptibility is reduced as well as the anisotropy factor $P` < 1.1$, typical for paramagnetic granitoids (Ferré and Améglio 2000, Bouchez et al. 1987). This study shows that

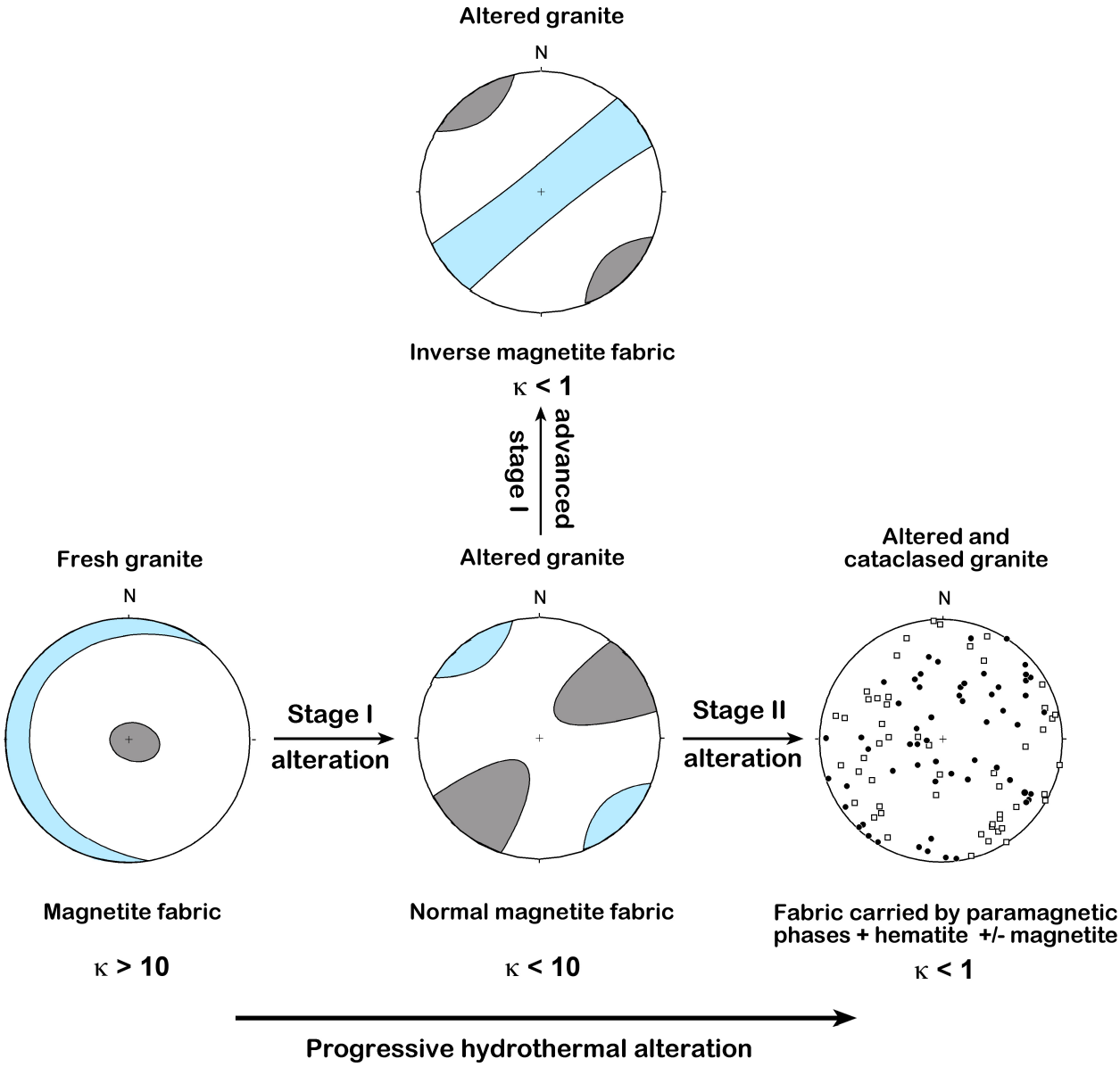

Fig. 1.10: *Development of magnetic fabric during progressive hydrothermal alteration with typical magnetic mineralogy and susceptibility (x 10^{-3} SI). The primary magnetic fabric with subhorizontal magnetic foliation changes to tectonic fabric with steepened NW-SE trends. Intensive cataclasis causes randomly distributed fabrics. Dotted areas (squares) represent magnetic lineations and striped areas (circles) magnetic foliation poles. Magnetic lineation: blue, κ_{min}: grey. Further explanations see text.*

magnetite relics in martite strongly influence the rock magnetic behavior during the progressive hydrothermal alteration. This influence ceases with the strongest degree of hydrothermal alteration when nearly all magnetite is oxidized.

The decreased magnetic susceptibility and anisotropy in the hydrothermally altered granites of stage I and II can be related to the decreased magnetite content as a consequence of oxidation and associated grain size reduction. The formation of martite parallel to ⟨111⟩ long axis of magnetite caused an increased distance of magnetite domains, and therefore the magnetic interactions weakened (Stephenson 1994). With advanced oxidation magnetite disappears and the contribution of paramagnetic minerals to the AMS dominates. The fresh Soultz granite is composed of 40 vol% plagioclase, 19 vol% of paramagnetic, hematitized K-feldspar and 8 vol% of biotite + chlorite (Jacquemont 2002). Along with hydrothermal alteration (stage I and II) paramagnetic illite pseudomorphed after plagioclase and therefore mimic the plagioclase

alignment. In contrast to platy biotite associated with magnetite, feldspars are weakly oriented into the magmatic fabric. Thus, anisotropy is strongly decreased in altered granites without magnetite content. Hydrothermal alteration without cataclasis causes no changes of structural fabric because the paramagnetic alteration minerals mimic the lattice preferred orientation of primary minerals (Fig. 1.4 d). The most frequent alteration mineral is acicular and fine-grained illite (~ 10 μm) that is often accompanied by fine-grained, antiferromagnetic hematite from a second population (Fig. 1.4 f, g,). Variable contributions of ferri-, antiferro- and paramagnetic components on the AMS cause a change from primary, strictly oblate AMS ellipsoids and result into more oblate as well as prolate AMS ellipsoids in the hydrothermally altered granites. Along with this transformation of AMS ellipsoid shape, the orientation of primary magnetic foliation poles in the fresh granites evolves from a horizontal cluster distribution to a general, secondary girdle distribution with NE-SW trending great circle in the altered granites. At the same time, the primary scattered distribution of the magnetic lineation changes to a well defined subhorizontally NW-SE trending distribution pattern (Fig. 1.10). Based on the alteration mineralogy within the alteration zone of the central part of the pluton (1550-1580 m), this characteristic fabric development is assigned to stage I alteration according to Traineau et al. (1991).

In cataclastic-deformed granites, the above mentioned AMS fabric associated with magnetite is destroyed during the stage II alteration. The development of fault zones is characterized by almost randomly oriented microcracks causing randomly oriented magnetite relics. The previous preferred orientation of principal axes of the AMS changes into a random distribution of both foliation poles and magnetic lineations (Fig. 1.10). In contrast, hydrothermalized wall rocks of stage II without cataclasis reveal a pattern of preferred orientation corresponding to the stage I alteration (Fig. 1.8), although the alteration mineralogy can be assigned to the stage II alteration.

A special development during the stage I alteration is observed in the upper part of the granite section (1420 – 1550 m). Here, the altered rocks (stage 1 alteration) show an inverse magnetic fabric with inverted orientation of magnetic foliation as compared with the central part of the pluton (Fig. 1.8). This behavior may indicate an inverse magnetic fabric due to the very small magnetite relics in martite, which behave as single-domain grains and show the lowest magnetic susceptibility for the stage I alteration (Fig. 1.3). Inverse magnetic fabrics related to single-domain magnetite have been described by Potter and Stephenson (1988), Rochette et al. (1999) and Ferré (2002). In single-domain magnetite, the easy magnetic axis fixes the direction of spontaneous magnetization and thus results in zero susceptibility along the long axis.

The evolution from primary to altered magnetic fabric can be discussed in the context of microstructural observations assigned to alteration stages I and II. Two different processes are considered to act as controlling factors during the fabric transformation; these are a microstructural and a stress controlled alteration.

Microstructural and fluid inclusion studies in the Soultz granite were done by Schild et al. (1998), who analyzed three successive, orthogonal microcrack directions in healed quartz and feldspars. One of the microcrack directions is in agreement with the NW-SE trend of κ_{max} in the altered granites and is often accompanied by co-oriented microcracks in magnetite (Fig. 1.4 a). It is assumed that a preferred microcrack formation in magnetite with dominantly NW-SE directions was subparallel to one of the four ⟨111⟩ crystallographic axis of magnetite with the smallest angle to the microcracks. These planes acted as weakened zones that favoured fluid circulation in magnetite. Magnetite oxidation started along these weak zones and caused elongated and NW-SE oriented magnetite relics.

Hydrothermalized wall rocks of the later stage II alteration show magnetic fabric, which corresponds to the geometry of stage I alteration (Fig. 1.8). The alteration minerals of stage II pseudomorphed after

the available mineralogy, as already observed for the stage I. This is also the case, if the granite was already altered during the former stage I alteration. Therefore it is assumed that the ubiquitous NW-SE trending fabrics in the hydrothermally altered granite of stage II are due to the same tectonic setting, which was responsible for the microcrack formation within magnetite during the late magmatic stage.

Conclusions

The magnetic fabrics reflect the primary magmatic flow fabric in the fresh Soultz granite, which had been altered during hydrothermal alteration stages I and II (Fig. 1.10). In the fresh granite, MD and subeuhedral magnetite were identified as the main magnetic carrier of the AMS. Strictly oblate fabrics and enhanced anisotropies are found, which are related to magnetite grains forming clusters. These magnetite clusters mimic the alignment of biotite within the magmatic foliation plane. The subhorizontal magmatic foliation indicates a magma emplacement either due to a decelerating flow regime, which provokes stronger internal than external tectonic stresses or due to internal vertical stresses during the two-stage crystallization of the magma. Therefore, the primary magmatic fabrics of the Soultz granite seems not to be affected by the NW-SE wrench tectonics during the Variscan orogeny, in contrast to adjacent intrusions of similar age at the eastern and western flanks of the Rhine Graben. With further cooling and solidification, the external stress conditions became stronger relative to the internal stress. Now, the solid body could absorb the external stresses (σ_1 = NW-SE), which caused microcrack formation in magnetite with preferred NW-SE orientation. The microcrack formation in magnetite acts as the controlling factor for the development of the alteration fabric during the subsequent hydrothermal alteration stages I and II. During these hydrothermal alteration stages magnetite was oxidized to martite, and illite as well as Fe-carbonates replacing the rock forming minerals became the most important paramagnetic minerals. Therefore, the orientation of steep microcracks is responsible for the steepening of the magnetic foliation. These cracks allowed for circulation of residual fluids during the magma cooling, which caused the pervasive alteration (stage I alteration) of the pluton. The later alteration stage II retained this trend, which is well documented in the hydrothermalized wall rocks within fault zones. This trend is only destroyed by cataclastic deformation, which results in random orientation of the principal axes of the anisotropy ellipsoid. This faulting proceeded during the multiphase formation of the Upper Rhine Graben with changing stress directions and resulted in chaotic microcrack orientations. It could be shown, that magnetite controls the magnetic fabric during the hydrothermal alteration, until it completely oxidizes to martite. In rocks, where the magnetite was completely oxidized the AMS is controlled by paramagnetic minerals, that have a low degree of anisotropy. In such rocks, hematite formation during the hydrothermal alteration stages is not high enough to dominate the AMS fabric.

2. Discrimination of remanence directions in drill cores from progressively altered granite – a long way to achieve paleomagnetic information

Abstract: The magnetite-bearing Variscan Soultz granite from the EPS-1 borehole (Upper Rhine Graben) shows several stages of hydrothermal alteration and brittle deformation along discrete fault zones. Such fault zones consist of central cataclasites and their wall rocks, which pass into the fresh granite. The here presented paleomagnetic studies on reoriented cores show several artificial and natural overprints of remanent magnetization. During the drilling procedure the drill cores were remagnetized by a vertical drilling induced remanent magnetization (DIRM), which in turn has been overprinted by a viscous remanent magnetization (VRM) after recovering the cores to the surface and keeping them in depository. Although the VRM and the DIRM totally remagnetized the soft magnetic fresh and moderately altered granites, in strongly altered and cataclased granites components of hard magnetic natural characteristic remanent magnetization (ChRM) could be separated using alternating field (AF) and thermal (TH) demagnetization. Unstable behavior due to mineral reaction during heating was observed hereby for most of the samples, but it was still possible to separate meaningful paleofield vectors of natural ChRM. Because of the low number of separated vectors statistical analysis could not be performed and therefore the data should be dealt with care. However, comparison of the data with available paleomagnetic data from other Saxothuringian rock suites provides age constraints for the alteration stages of the Soultz granite. Field vectors related to stage I alteration in granites were acquired during cooling and hydrothermal alteration under retrograde conditions and are characterized by coercivities and unblocking temperatures typical for magnetite. Vector orientation correlates with Middle Carboniferous directions. The younger SW- to SSW-oriented B direction with reversed polarity is increasingly dominated by unblocking temperatures typical for hematite and correlates with Late Carboniferous – Early Permian directions. The youngest overprint, the reversed and normal N- to NNE-oriented A directions observed in the Soultz granite are mostly carried by hematite and correlate with Permian – Triassic directions of paleofield vectors. A Late Eocene to present-day impact of the Rhine Graben rift system on the magnetic signature has not been detected. This study clearly indicates older brittle deformation episodes immediately after the magma cooling, which already started during Carboniferous.

Introduction

Paleomagnetic studies play an important role in the reconstruction of continental drift and the associated deformation geometry and processes (e.g., Tauxe et al. 2004, Hirt et al. 1992, Lowrie 1980, Lowrie et al. 1973) and can give some clues about the age relation of related geological processes. A successful application of this method, however, requires a precise knowledge of the magneto-mineralogical history of samples and needs to determine the magnetic remanence acquisition processes involved. This is commonly achieved by paleomagnetic tests, including alternating field (AF) and thermal (TH) demagnetization. Other rock magnetic studies, such as acquisition of isothermal remanent magnetization (IRM) and thermoremanent behavior, give information on the mineralogy and grain size spectra of magnetic mineral phases. Such detailed studies help to unravel the magnetic history of rocks, which may suffer total or partial remagnetization during their geological evolution. Paleomagnetic studies of rock-fluid interactions can provide the determination of the timing in which fluid migration events have occurred (e.g., Elmore et al. 1993) causing polyphase remagnetization of rocks. A polyphase paleomagnetic record was

reported for the Variscan belt (e.g., Zwing and Bachtadse 2000, Edel and Wickert1991, Reisinger et al. 1994), of which the Soultz granite is part. During the magnetic overprints, the whole Variscan belt rotated in a clockwise direction during Middle to Late Carboniferous times, accompanied by large-scale dextral wrenching along NW–SE-trending lithospheric faults. Evaluation of such paleomagnetic information can be complicated when rock samples from deep drillings are investigated (Worm and Rolf 1994, Kanamatsu and Niitsuma 2004). Artificial remagnetization of rocks during or after recovery, for example, drilling induced (DIRM) or viscous remanent magnetization (VRM), can complicate the proper isolation of the natural characteristic remanent magnetization (ChRM), which is the carrier of valuable geological information. An excellent example for such multiple natural and artificial remanence acquisition processes is documented in the presented study for the magnetite-bearing Soultz granite, a Late Variscan I-type intrusion, which passed a complex alteration history related to faulting and fluid circulation since the emplacement until the Rhine Graben rifting.

This study focuses on granite drill cores from the EPS-1 drill hole encountered between 1417 and 2227 m, which allows for a detailed paleomagnetic record from fresh to hydrothermally overprinted granite. Previous work related the cataclastic deformation in the Soultz granite solely to the young alteration history in the context of the Cenozoic formation of the Upper Rhine Graben (e.g., Genter and Traineau 1991, Dezayes et al. 1995). However, recent studies on hydrothermal illites from the Soultz granite (Schleicher et al. 2004) indicate older deformation episodes, which already proceeded during Permian times. Paleomagnetic investigations may however play a significant role in the understanding of the alteration history of the Soultz granite.

Geological setting of the EPS-1 borehole

The Upper Rhine Graben basin, one of the prominent extensional structures in central Europe,

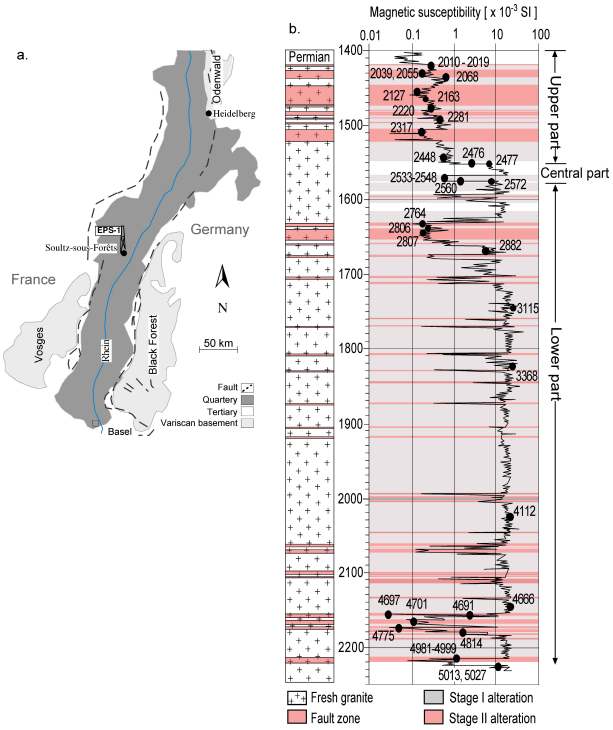

Fig. 2.1 a: *Location map of the European central Upper Rhine Graben and the EPS-1 drill site at Soultz-sous-Forêts.* ***b.*** *Lithologic section (modified after Genter and Traineau 1996) and magnetic susceptibility log with data (Rummel and König, 1991) on drill cores at the 1414 to 2230 m depth interval in the EPS-1 borehole. The hydrothermal alteration observed in the geological section is classified in two stages. Black dots and numbers indicate sample position for this study, according to the nomenclature of the core index (Genter and Traineau 1991).*

developed since Middle to Late Eocene times by reactivation of a complex set of Variscan fault zones (e.g., Ziegler 1996). Because of its high geothermal gradient (100 °Ckm^{-1} in the sedimentary cover, Genter 1989) the Soultz area is in the focus of geothermal energy exploration. Several wells were drilled through the Permo-Mesozoic sedimentary cover into the underlying Variscan basement, one of which is the EPS-1 borehole near Soultz-sous-Forêts (Fig. 2.1 a).

The so-called Soultz granite was recovered below 1417 m down to a final depth of 2227 m, where in-situ temperatures reach up to 160 °C. Alexandrov et al. (2001) dated the high-K calc-alkaline Soultz granite at 331 ± 9 Ma (U/Pb ion-probe, zircon), which, together with other I-type intrusions from the adjacent Northern Vosges, Windstein granite and Kaiserbach granite, respectively, are

assigned to late Variscan magma emplacement in an arc setting (Flöttmann and Oncken 1992). The Soultz granite is a magnetite-bearing intrusion, characterized by high magnetic susceptibilities of 10-80 x 10^{-3} SI, indicating magnetite contents of 0.1-2 vol%. During the subsequent solidification and uplift, a propylitic hydrothermal alteration affected the whole plutonic body (pervasive stage I) followed by argillitic hydrothermal alteration, which was related to discrete fault zones (stage II, Traineau et al. 1991). These fault zones consist of cataclastic granites surrounded by hydrothermally altered wall rocks. Both alteration stages resulted in magnetite oxidation and hematite precipitation, especially in the upper part of the profile, far below the Curie temperature of hematite. The timeframe of hydrothermal alteration and the associated fluid circulation is unclear and led to controversial discussions. However, fluid inclusion studies on quartz from Dubois et al. (1996) indicate a complex and multistage paleofluid trapping from earliest Variscan to Cenozoic. Paleomagnetic investigations of the Soultz granite may help to unravel and assign the periods of hydrothermal alteration related to the complex fluid flow history in the emplacement and Rhinegraben setting.

The primary ferromagnetic mineral of the Soultz granite is magnetite with euhedral or subhedral grain shapes and grain sizes up to 500 µm (see also Fig. 1.4 a, b and Fig. 3.2-II a, b). Such grains frequently form clusters associated with biotite and sphene. Magnetite oxidation caused the formation of hematite during the hydrothermal alteration, which is called martite in this study. Such martite normally shows magnetite relics with varying grain sizes (see also Fig. 1.4 and Fig. 3.2). This initial magnetite oxidation was found in the central part, within a depth interval between 1450 and 1480 m, where altered granites were interpreted to be altered only by a stage I alteration (Traineau et al. 1991). Further alteration is related to discrete fault zones and is called stage II. This stage II caused a brittle deformation (Fig. 1.4 e, f and Fig. 3.2-I c, d, -II g, h) and zonal boundaries of cataclastic granites in the center and hydrothermally altered wall rocks at the rim of a fault zone. From a magnetic point of view the fault zones in the upper part of the pluton (1417 – 1550 m) with high hematite abundance differ from the fault zones in the lower part, where relatively low hematite abundance and the occurrence of pyrite within veins is observed. In contrast to the martite, this hematite precipitated from fluids and has small grain sizes (< 10 µm).

Sampling and methods

As magnetic susceptibility is diagnostic for fresh ($\kappa > 10 \times 10^{-3}$ SI) and altered granites ($\kappa < 1 \times 10^{-3}$ SI; Fig. 2.1 b), samples were selected using a portable Kappameter KT-6 (GEOFYZIKA) with a sensitivity of 0.001 x 10^{-3} SI and an operation range between -999 and 9999 x 10^{-3} SI and an operating frequency of 10 kHz. The circular surface of the apparatus with a diameter of 6.5 cm was put on the surface of the drill core; 90 % of the signal came from the upper 2 cm resulting in a measuring volume of ~66.4 cm^3. In this study the term 'fresh' is used for granites without any evidence of magnetite oxidation, however a weak persistent hydrothermal alteration affected the whole granitic body.

Variation in the borehole diameter of the EPS-1 drilling has provided drill cores of different sizes. Drilling with a 5.06" drill bit down to 1997 m has recovered core pieces with a large diameter (ld-cores) of 78 mm and further below, down to a final depth of 2230 m, a 3.9" equipment has been used, providing cores with a small diameter (sd-cores) of 57 mm. Coring was performed with a diamond core bit cooled by water-based drill mud (Baria et al. 2000). For this study the natural remanent magnetization (NRM) was measured in 1 cm intervals on whole core pieces using a Cryogenmagnetometer 760 R-SRM (Superconducting Rock Magnetometer), 2G Enterprises (Rolf 2000) at the magnetic laboratory of the GGA (Institut für Geowissenschaftliche Gemeinschaftsaufgaben) in Grubenhagen.

For further magnetic investigations 1" plugs were drilled perpendicular to the core length axis

and cut into three cylindrical specimens (volume: ~10 cm^3, diameter: ~2.4 cm) for the ld-cores and two for the sd-cores, respectively (Fig. 2.2). The magnetic susceptibility of a cylindrical specimen with a nominal volume of ~10 cm^3 was measured at the magnetic laboratory of the GPI (Geologisch-Paläontologisches Institut) in Heidelberg using a KLY-2 Kappabridge (AGICO, Hrouda 1994) with a sensitivity of 4 x 10^{-8} SI and an operating frequency of 920 kHz. These susceptibility-values show a good agreement with the susceptibility-values measured with the portable Kappameter KT-6 (AGICO).

For a detailed investigation of the drilling induced remanent magnetization (DIRM), Koenigsberger factor (Q-ratio) analyses of several plugs - cylindrical specimens with a volume of ~1.8 cm^3 and a diameter of 1.4 cm - have been drilled perpendicular to the core axis, providing a profile of six individual specimens for the ld-cores and four specimens for the sd-cores, respectively. All remanence and susceptibility values of the small cylinders were recalculated to the standard volume of 10 cm^3.

Stepwise AF demagnetization was performed at the magnetic laboratory of the GPI in Heidelberg. Twelve steps of different field intensities: 2.5, 5.0, 7.5, 10, 20, 30, 40, 50, 75, 100, 130 and 160 mT were applied using a MI AFD 1.1 demagnetizer (Magnon International). Remanence measurements between each AF step were performed on a JR-5 / JR-5A spinner magnetometer (AGICO). Stepwise TH demagnetization was performed in zero field at the Laboratory for Natural Magnetism (LNM) of the ETH in Zürich by stepwise heating to temperatures of 100, 200, 300, 400, 425, 450, 475, 500, 525, 550, 575, 600, 620, 640, 660 and 680 °C. Remanence measurements between each TH step were performed using a cryogenic magnetometer (2G Enterprises). All separated paleovectors were reoriented due to the reference line of each drill core and corrected for the borehole deviation (Traineau 1991). Because the Soultz area is located on a stable horst structure no further reorientation was necessary. In a final step the results were analyzed using orthogonal vector plots in Zijderveld diagrams and stereographic projections. Where possible, the direction of the natural characteristic remanent magnetization (ChRM) was calculated using principal component analysis (Kirschvink, 1980), whereby a minimum of three AF or TH steps were considered. The different directions revealed only a limited number of vectors and therefore statistical calculations were not accomplished.

In order to detect the carriers of the soft and hard magnetic components, further coercivity spectra analyses were done using the Lowrie method

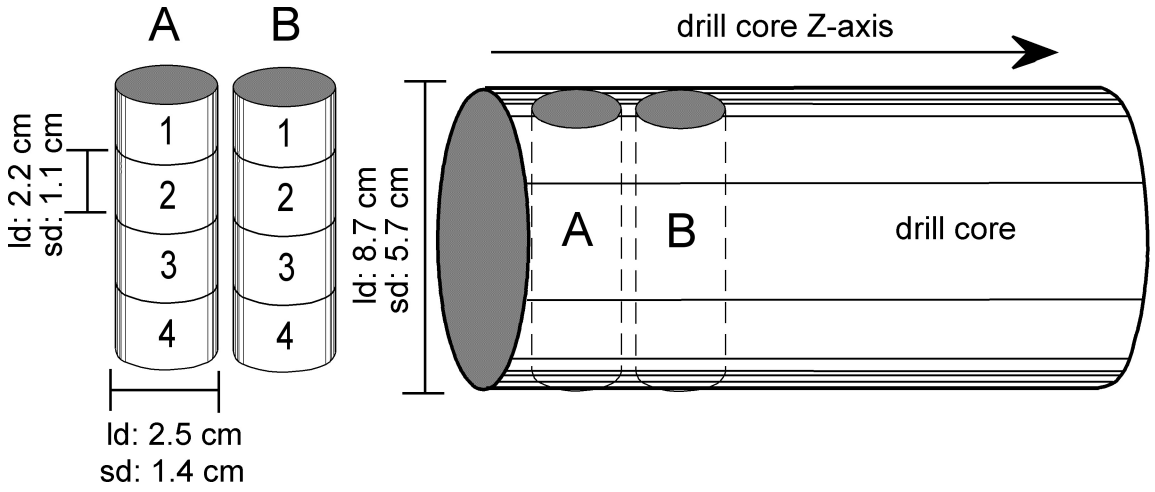

Fig. 2.2: *Graphic diagram of bore core with large diameter (ld-cores) and small diameter (sd-cores) and the manufactured cylindrical specimens (~10 cm3 and ~1.7 cm3) with their plug positions. Ld-cores reveal only three and sd-cores 2 plug positions for standard cylinders with a specimen volume of ~10 cm^3. For Q-ratio analysis standard cylinders with a specimen volume of 1.7 cm3 were prepared resulting in 6 plug positions from the ld-cores and 4 plug positions for the sd-cores due to drilling loss.*

(Lowrie 1990): the sample is rotated parallel to the sample orthogonal axis, exposing the axis to different field intensities during IRM acquisition using an ASC Scientific Model IM-10-30 Impulse Magnetometer with a maximum field of 2.6 T, which was performed at the ETH in Zürich. First, a field of 2.6 T was applied parallel to the Z-axis, which represents the hard magnetic component; subsequently, a field of 600 mT was applied parallel to the Y-axis, which represents the medium magnetic component and finally, 200 mT were applied parallel to the X-axis, which represents the soft magnetic component. The intensity of the magnetization (J) between the individual TH steps was converted to the three orthogonal axes according to the equation: $F = \sqrt{X^2+Y^2+Z^2}$. The applied field value marks the approximate limits of the coercivity spectra of hematite and magnetite, which are the magnetic carriers in the Soultz granite. Subsequent TH demagnetization of the three orthogonal components yields the relative quantities and unblocking temperature spectra of the phases.

Results and interpretations

1. Sample characteristics

The frequency distribution of the intensity of NRM (Fig. 2.3) reflects the gradual decomposition of magnetite, with the highest intensities in the fresh and the lowest in altered granites. Fresh granites reveal wide spectra of NRM intensities between 10 and several 100 mA/m, reflecting an inhomogeneous distribution of magnetite, which is also documented in varying susceptibilities (Fig. 2.4). The hydrothermally altered granites show a strong decrease in bulk susceptibility; stage I altered granites reveal higher intensities (up to 400 mA/m) indicating a transition between fresh and altered rocks. Stage II altered granites, which are cataclastically deformed, show a maximum frequency in the range between 10 and 50 mA/m. The wall rocks of such cataclastic granites show the lowest intensities with a maximum frequency < 10 mA/m, indicating the most intense hydrothermal alteration in the Soultz granite.

Coercivity spectra analysis (Fig. 2.5) was performed in a magnetically shielded target area (< 500 nT) in order to characterize the carriers of the remanent magnetization. Coercive forces (H_C) of magnetic minerals commonly show clear differences with low H_C for magnetite ($H_C \leq 300$ mT) and distinct higher H_C for hematite ($H_C \geq 1$ T). The coercivity spectra of magnetite- and hematite-bearing granites were detected by AF demagnetization running up to 160 mT (maximum possible field at the magnetic laboratory in Heidelberg, Fig. 2.5 a). In the fresh granites a soft

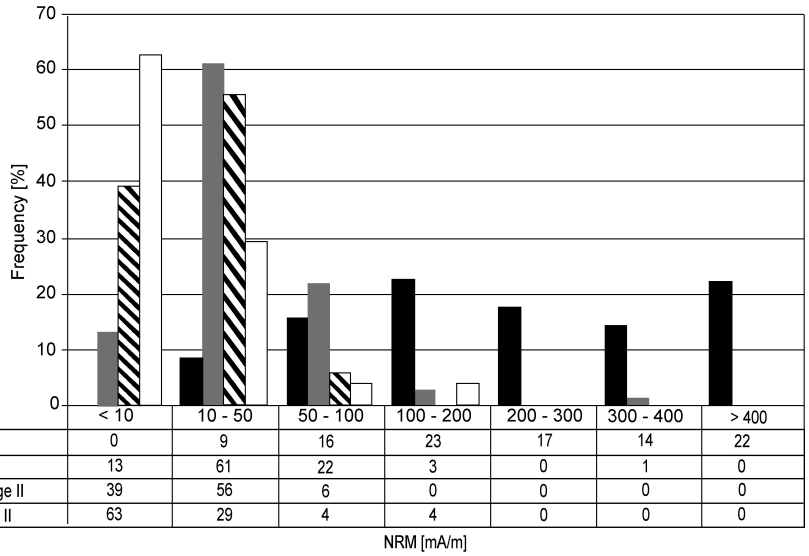

	< 10	10 - 50	50 - 100	100 - 200	200 - 300	300 - 400	> 400
Fresh granite	0	9	16	23	17	14	22
Stage I granite	13	61	22	3	0	1	0
Cataclased granite, stage II	39	56	6	0	0	0	0
Wall rock granite, stage II	63	29	4	4	0	0	0

Fig. 2.3: *Frequency histogram of the natural remanent magnetization (NRM) from different granite facies measured on standard specimens (~10 cm³) from cores of the EPS-1 borehole.*

magnetic behavior typical for magnetite is observed, characterized by the median demagnetization fields (MDF) of < 2 mT and a demagnetized status at 30 mT. According to the soft magnetic behavior for the fresh granite, an IRM in fields up to 2.6 T (Fig. 2.5 b) shows saturation at fields well below 300 mT. The acquired maximum remanence intensity ranges between 30 and 50 A/m. Subsequent analyses of soft and hard magnetic components according to the method of Lowrie (1990) the TH demagnetization reveals unblocking temperatures (T_{UB}) below 575 °C for the soft magnetic component (X-axis, Fig. 2.5 c), indicating magnetite as the magnetic carrier. Only the soft magnetic X-axis shows a significant IRM acquisition, which implicates magnetite as the exclusive carrier of remanent magnetization in the fresh granites.

Hydrothermally altered granites of stage I and II with progressively oxidized magnetite reveal hard magnetic behavior. During AF demagnetization stage I and II altered granites show similar MDF ranging between 3 and 18 mT. However, the cataclastic granites of the upper part are characterized by a high MDF up to 30 mT and by retaining 50% of the initial intensity after AF demagnetization, indicating an increasing contribution of hematite.

The increasing contribution of hematite also affects the magnetic behavior during the IRM acquisition (Fig. 2.5 b). Granites, which still contain magnetite but already show a distinct hematitization,

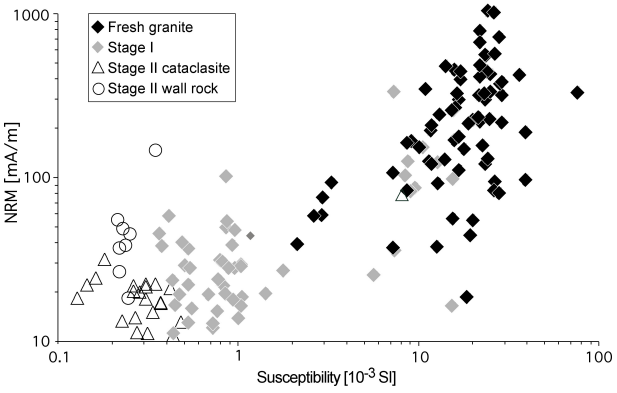

Fig. 2.4: Mean magnetic susceptibility versus natural remanent magnetization (NRM) for fresh, hydrothermally altered granite of stages I, cataclasites of stage II and their wall rocks. Increasing NRM correlates with increasing susceptibility.

are characterized by an initial soft magnetic behavior due to a steep slope below 100 mT and a saturation, which requires fields higher than 1400 mT or even higher than 2600 mT. This initial soft magnetic behavior of such bimodal coercivity spectra is correlated to magnetite relics, which remained within the martite grains and the hard magnetic behavior is correlated to fine-grained hematite precipitated from fluids. TH demagnetization (Fig. 2.5 d) reveals an additional carrier of the soft magnetic component in the altered granites. Two different temperature ranges of demagnetization up to 575 °C and up to 660 °C indicate magnetite and hematite, respectively. Soft magnetic behavior of hematite was reported by Kletetschka et al. (2000) for coarse-grained (> 60 µm) and equidimensional hematite, which shows H_C in the range between 4 and 13 mT. In the Soultz granites, such coarse grain sizes are observed only for magnetite-derived martite. Therefore, the soft magnetic component in the Soultz granite can be carried either by magnetite or coarse-grained hematite (martite) formed during magnetite oxidation. The hard magnetic component is carried only by fine-grained hematite, as indicated by the T_{UB} typical for hematite. Granites with completely oxidized magnetite show a T_{UB} typical for hematite (Fig. 2.5 e) in direction of the hard magnetic Z-axis. On the other hand, Fig. 2.5 d shows a wide unblocking spectra of all axes, X- Y- and Z-axis, indicating a wide grain size spectra of all soft, medium and hard magnetic components. In the direction of the X- and Y-axis T_{UB}s typical for magnetite and hematite are detected, which indicate overlapping coercivities of magnetite and coarse-grained martite. In direction of the hard magnetic Z-axis the wide unblocking spectra point to fine-grained hematite and martite with decreased grain size. Microscopic studies have shown that in such samples the grain sizes of coarse-grained martite (up to 500 µm) is reduced and partially replaced by a hematite (< 10 µm) precipitated from fluids. An abundant occurrence of fine-grained hematite is typical for cataclastic granites above 1580 m in the borehole profile.

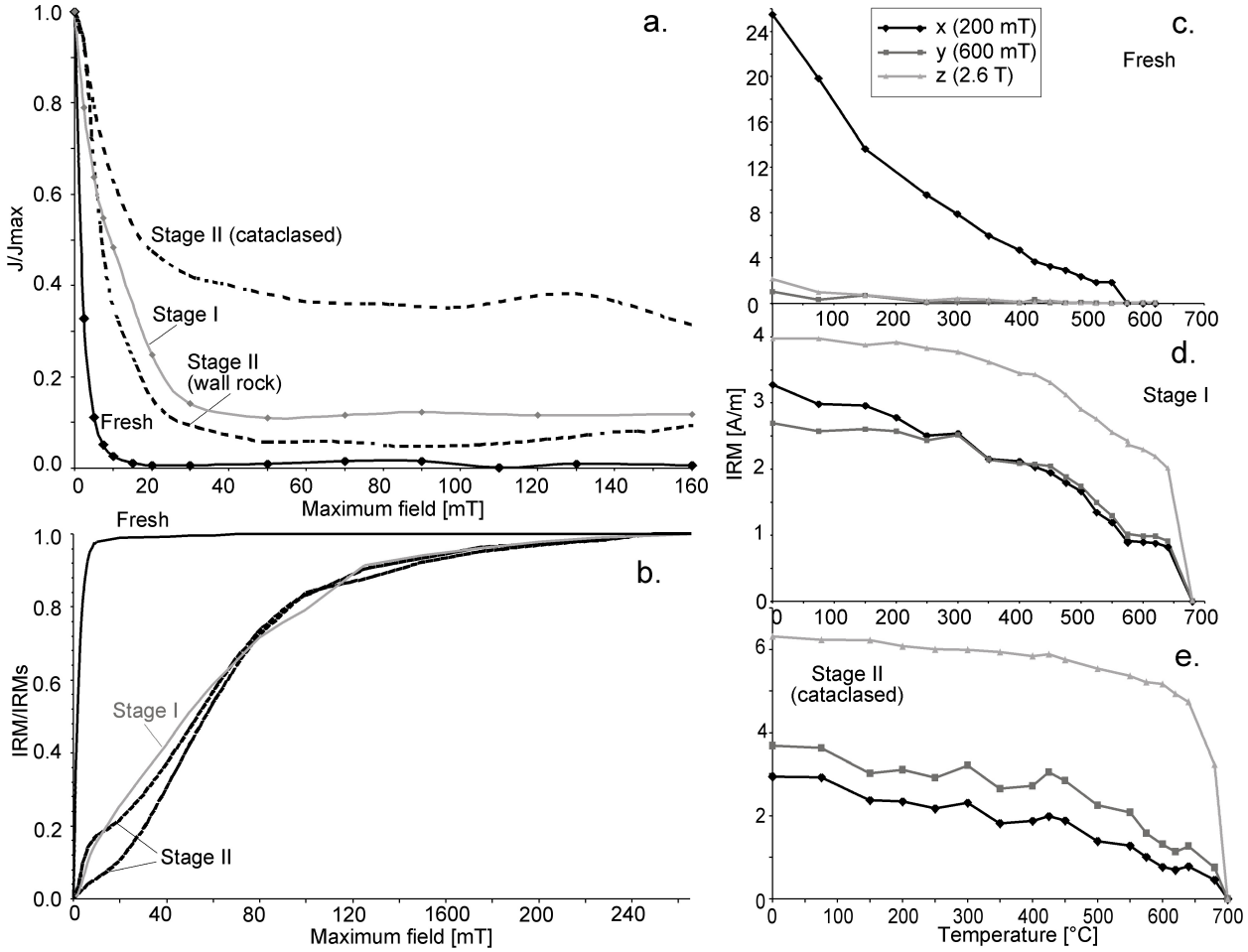

Fig. 2.5: *Coercivity spectra analysis of fresh and hydrothermally altered granites from stage I and II.* ***a.*** *Alternating field (AF) demagnetization up to 160 mT.* ***b.*** *Acquisition of isothermal remanent magnetization (IRM) up to field intensity of 260 mT.* ***c., d. and e.*** *Before thermal demagnetization (TH) the samples were magnetized in three directions: x (diamonds) = 200 mT, y (squares) = 600 mT and z (triangles) = 2.6 T.*

2. Natural remanent magnetization and the effect of drilling induced and viscous remanent magnetization

Measurements of the NRM of whole cores revealed distinct differences in the inclination (Fig. 2.6). Cores with a large diameter (ld-cores, d = 78 mm) generally show steep inclinations (70 - 90°), whereas cores with a small diameter (sd-cores, d = 57 mm) show a wide range of inclinations in relation to the degree of alteration. The sd-cores from fresh granites show flat inclinations (up to 45°) and the altered cores (stage I and II) reveal steeper inclinations (50 - 75°). As the present ambient field at the Soultz area has an inclination of 55° and no steeper inclinations occurred since the formation of the granite, the steep inclinations observed in the Soultz granite are interpreted to be caused by a DIRM. The problem of DIRM has been known for a long time (e.g., Audunsson and Levi 1989, Fuller et al. 1998, de Wall and Worm 2001) and generally steep positive inclinations in the NRM result from a magnetic overprint parallel to the borehole axis, which is probably caused by a combination of coring and recovery. The distinct difference between the inclination pattern in ld- and sd-cores and the variation of remanence inclinations for fresh and altered granites (Fig. 2.6), suggests on a first glance a less effective DIRM overprint in the fresh cores, which needs to be studied in more detail.

As has been shown by de Wall and Worm (2001), calculations of the Koenigsberger factor (Q-ratio) can support the detection of remagnetization related to drilling operations. They found U-shaped Q-

ratio profiles with distinctly higher values near the core surface compared to the internal parts for plug sections through a drill core. Q-ratio is defined as: Q = RM / κ * H_{Earth}, whereby H_{Earth} is the geomagnetic field and κ is the magnetic susceptibility. The product of both (κ * H_{Earth}) is the induced magnetization in the current Earth magnetic field. DIRM, which is an induced magnetization caused by fields higher than the Earth magnetic field, will show enhanced Q-ratios. For detailed analyses and a better resolution of the magnetic overprint of the DIRM, a plug of 1.1 cm in diameter has been drilled to provide a profile perpendicular to the core's long z-axis (Fig. 2.2). Plugs from ld-cores have provided six specimens, sd-cores four specimens, respectively. Q-ratio versus plug positions for ld- and sd-cores are shown in Fig. 2.7. The fresh granites are characterized by low Q-ratios because magnetite is the remanence carrier, and strongly altered granites show high Q-ratio because hematite is the main remanence carrier. Microscopic studies reveal a positive correlation of the Q-ratio to the degree of magnetite alteration. Granite samples, which still contain unmodified magnetite, have ratios in the range typical for NRM acquisition of multi-domain (MD) magnetite (Parry 1967, Stacy 1967). Slightly decreased ratios towards the core center are observed, which cause a distinct U-shaped profile in the ld-cores. The highest Q-ratios (up to 3.5) occur at the outer plug positions and decreased ratios (mostly < 1.0) at the inner positions, which indicate a stronger DIRM overprint of the core rim. The central part of a drill core, which is minor remagnetized, is characterized by Q-ratios < 0.5 in the fresh and Q-ratios < 1 in the altered granites. The Q-ratio analysis indicates that in the ld-cores remagnetization is more efficient at the rim, which is represented by two specimens at the outer positions (~26 mm) and leave a minor remagnetized part (~26 mm) in center of a drill core (Fig. 2.7). Assuming the same drilling conditions throughout the whole profile and the same geometrical as well as operational constraints of the drilling equipment, the remanence of all plugs of sd-core (d = 57 mm) is expected to be affected by a DIRM. This is indicated

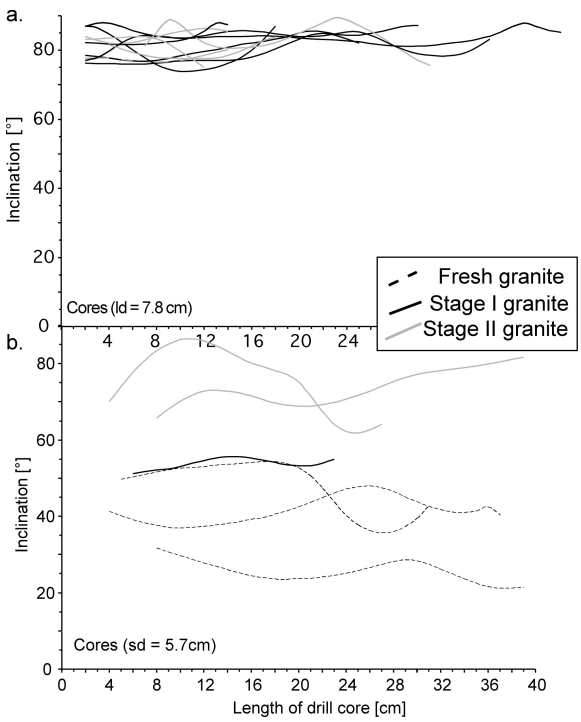

Fig. 2.6: *Reoriented inclination of natural remanent magnetization (NRM) measured on whole drill cores with large diameter (ld) and small diameter (sd) from fresh and hydrothermally altered granites of stage I and II.*

by generally high Q-ratios in the altered sd-cores due to a persistent DIRM overprint.

It can be summarized that altered samples from the Soultz granite must have suffered a considerable overprint by the drilling process, which results in steep inclinations of the remanence vector (> 50°) and higher Koenigsberger ratios. Surprisingly, the DIRM record is not well pronounced in the fresh granites. The fact that these fresh granites with coarse magnetite grains (up to 500 μm) acquire a DIRM less readily than smaller magnetite grains in the hydrothermally altered granites seems to be rather unusual and is not in agreement with the results of other studies that show MD samples to be more susceptible for DIRM acquisition than (single-domain) SD samples (Audunsson and Levi 1989). The reason for the missing DIRM overprint is discussed in the following. Three possibilities are taken into consideration: (i) no acquisition of DIRM in the fresh cores, (ii) deflection of the remanence direction due to magnetic anisotropy of the magnetite fabric in the fresh granites and

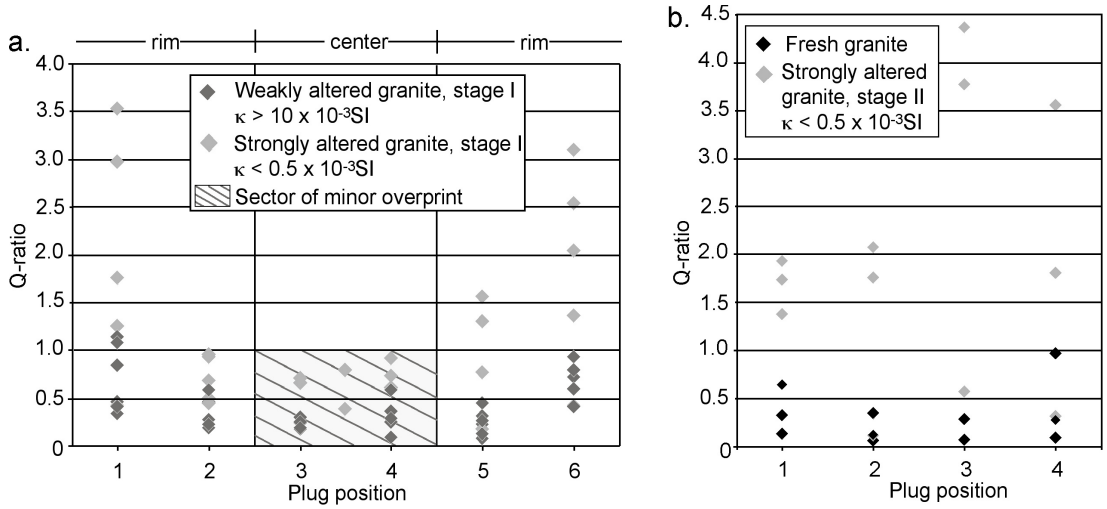

Fig. 2.7: *Koenigsberger ratio (Q-ratio) versus plug positions through core profiles. The weakly altered granites from ld-cores show similar U-shaped profile with relatively low Q-ratios like the fresh granites from the sd-cores. The strongly altered specimens from sd-cores show persistent high Q-ratios, which is in contrast to the U-shaped profile from ld-cores.*

(iii) obliteration by a subsequent remagnetization (VRM). The first case can be excluded because all samples are from the same section and because of the soft magnetic behavior of the fresh granites. The other two possibilities were tested by magnetic experiments as it is shown in the following.

Influence of magnetic fabric anisotropy on the remanence acquisition?

The Soultz granite has distinct magnetic fabrics, which are correlated to different alteration stages, as reported in Chapter II.1. The fresh granite with multi-domain magnetite grains shows a subhorizontal magnetic foliation with randomly oriented magnetic lineations within the foliation plane. The anisotropy factor is highest in the fresh granites ($P` > 1.1$) and decreases during alteration and decomposition of magnetite. The dependence of remanence acquisition on such magnetic fabric anisotropy is evaluated for the sample 3115, that reveals an anisotropy factor $P` = 1.18$. For different spatial orientations between the magnetic foliation plane and the applied field the anhysteretic remanent magnetization (ARM, DC = 0.042 mT; AF = 100 mT) has been registered and the sample was rotated in 22.5° steps around an axis parallel to the magnetic foliation plane (Fig. 2.8). The procedure reveals an anisotropy in ARM acquisition as well as a distinct refraction of the remanence vector for oblique positions in respect to the magnetic fabric axes. Highest ARM intensity (438.9 mA/m) was measured for field directions parallel to the magnetic foliation, where the vector parallels the applied field. However, with rotation of the sample the intensity decreases and reaches its lowest value (209.4 mA/m) for positions normal to the magnetic foliation plane. For this geometry, the remanence vector deviates about 14° from the direction of applied field. The reason for this refraction of the remanence direction probably lies in the critical anisotropy field, or microcoercive force, for MD wall displacement, which is a function of the angle between the domain magnetization and the applied field (Dunlop and Özdemir 1997). This experiment shows a weak dependence of the remanence acquisition on the geometry of the magnetic fabric and does not explain the high deviations from the vertical orientation of the DIRM in fresh granites.

Obliteration of DIRM by VRM

After DIRM remagnetization the cores were recovered to the surface and stored in a horizontal position within the present geomagnetic field. The aim of the following experiment is to clarify if the flat inclinations in the fresh granites are due to a VRM, which was acquired after core recovering. In a first step, a sample (5013) from the fresh granite was demagnetized. Subsequently, the sample was heated up to 160 °C, which is the ambient temperature

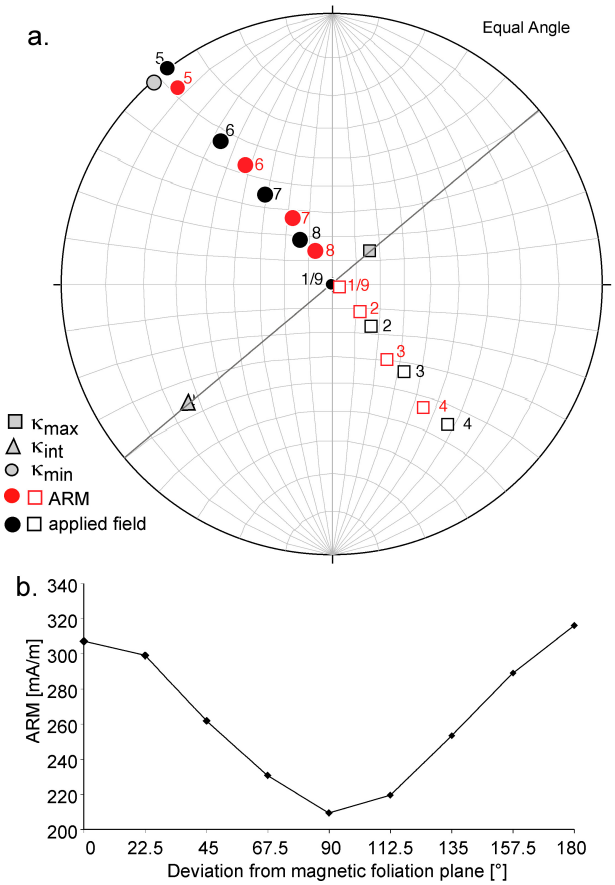

Fig. 2.8: a. *Stereographic projection (lower hemisphere) of the acquisition of anhysteretic remanent magnetization (ARM) in relation to the magnetic fabric of the sample 3368 from the fresh granite. Blank squares represent negative directions.* ***b.*** *Deviation of ARM direction from magnetic foliation plane versus ARM intensity.*

at approximately 2200 m. While holding this temperature for 20 min, a DC field of 0.15 mT was applied within the oven. According to Worm and Rolf (1994) similar values of field intensity were measured during the drilling of KTB (Kontinentale Tiefbohrung). After this procedure, the samples were cooled in a field-free space in order to simulate the conditions during core recovering. The newly acquired remanent magnetization was measured. In a final step the samples were exposed to the present geomagnetic field in a horizontal position and measured after distinct time intervals. The results are shown in Fig. 2.9. Initially, the sample acquires a magnetization parallel to the applied DC field in direction of the drill core axis (Z-axis, Fig. 2.2). The Z-axis correlates with the direction of the acquisition of the DIRM in the Soultz granite. After exposing the sample to the present geomagnetic field for six days the inclination starts to deviate from the original position. After one month also the declination starts to deviate from the original position and turns anticlockwise towards the direction of the present Earth magnetic field. This observation clearly indicates VRM acquisition after recovering and during storage of cores in a horizontal position in the currently existing geomagnetic field. The difference angle between the original direction and the direction acquired after one month is about 30°. In the fresh Soultz granite even higher angles between the DIRM and the NRM were observed, which can be explained by VRM acquisition during contamination with magnetic objects, e.g., components of storage boards.

3. Vector component analyses

At first a stepwise AF demagnetization and subsequently a stepwise TH demagnetization were performed on the same samples for a more detailed analysis of remanent magnetization. This combination allows the discrimination of components with different coercivity and unblocking spectra. For comparison, TH without preexistent AF demagnetization was also performed on three samples. During heating, some magnetic phases, like martite and Fe-bearing carbonates have shown to be unstable during heating. They modify to other magnetic phases, for example maghemite and magnetite, which is described in Chapter II.3 in more detail. The unstable behavior is indicated by increasing remanence intensities and magnetic susceptibilities at temperatures > 500 °C. Samples showing such a behavior were removed from further considerations. Only three samples showed stable behavior during heating up to 690 °C. These samples come exclusively from cataclased granites in the upper part of the borehole profile. In this section martite and the Fe-bearing carbonates are partially decomposed and thus the modification during heating is suppressed (for more details see

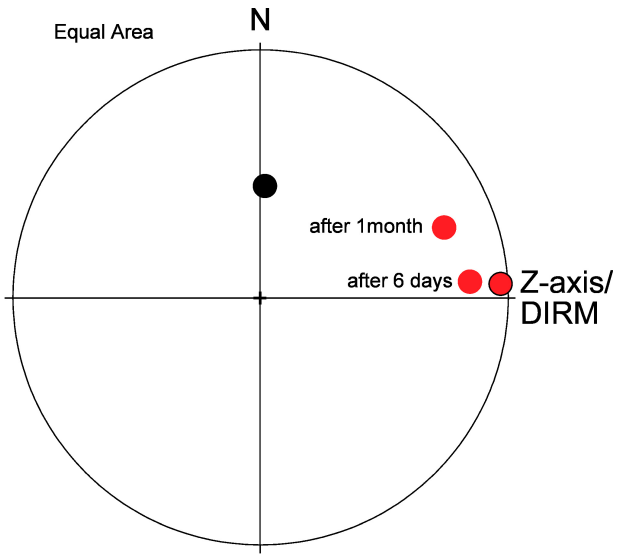

Fig. 2.9: *Stereographic projection (lower hemisphere) of the acquisition of viscous remanent magnetization (VRM) from a fresh granite (core index 5013). The sample acquired a laboratory induced remanent magnetization (red dot with black rim) parallel to the direction of the core long Z-axis, which represents the direction of the drilling induced remanent magnetization (DIRM) in the EPS-1 borehole. After remanence acquisition the sample was stored with respect to the present-day geomagnetic field (black dot) and measured after six days and one month (red dots).*

Chapter II.3). However, the cataclased granites show a strong heterogeneity and therefore TH demagnetization of adjacent specimens can show different demagnetization behavior. Furthermore, all separated vectors revealed erratic declinations and a wide range of inclination angles. However, when treating the vectors in response to their alteration degree, demagnetization procedure and core rim or core center relation, different characteristic components were separated. Hereby, artificial overprints and natural ChRM are identified. The artificial overprints are the VRM and DIRM, which were discussed in the previous chapter. The remaining natural ChRM paleofield directions can be compared to paleofield vectors described for other Variscan rocks.

Remanent overprints – VRM and DIRM

Stepwise AF demagnetization revealed a VRM and a DIRM, which is carried by low coercivity components (Fig. 2.10, compare also Table 2.1 and 2.2). Low coercivity components are present in the fresh granites with $\kappa > 10 \times 10^{-3}$ SI and are mostly demagnetized in fields up to 15 mT because they contain coarse-grained magnetite (up to 500 μm), which is within the threshold of MD magnetite grains. Separated vectors of these granites show relatively flat inclinations and unstable declinations (Fig 2.10 a), which are interpreted to be the VRM (Table 2.1). Weakly altered granites ($\kappa > 1 \times 10^{-3}$ SI) related to stage I alteration also show vectors with flat VRM inclinations but also vectors with steep DIRM inclinations (Fig. 2.10 c). The flat VRM inclinations are associated with declinations showing a tendency to NW or SE orientations, also observed in the fresh granites. These directions are carried by MD magnetite. The steep inclinations of the DIRM (Table 2.2) appear mainly in progressively altered granites with $\kappa < 0.5 \times 10^{-3}$ SI with oxidized magnetite, but which remained as small relics within the martite grains. This oxidation caused a grain size reduction of magnetite and a grain size growth of martite. Samples with a transition from weakly to strongly altered granites carry both the VRM and the DIRM directions. They are separated by AF intervals of 0 – 5/7.5 mT for the VRM component, which is typical for MD magnetite and AF intervals of 7.5/10 – 30 mT for the DIRM component, which is probably carried by both, small magnetite grains and coarse-grained martite because of overlapping coercivities. Hematite is generally assumed to show a hard magnetic behavior, however Kletetschka et al. (2000) reported on a soft magnetic behavior of a MD, coarse-grained (> 60 μm) and equidimensional hematite with H_C in the range between 4 and 13 mT. Such behavior was observed for specimens in the central plug positions of a drill core, which reveal susceptibilities between 0.9 and 3×10^{-3} SI.

Specimens from the rim of a drill core (Fig. 2.10 b) generally show more steep inclinations indicating a stronger DIRM overprint. The more flat inclinations are observed in granites with higher susceptibilities ($\kappa > 1 \times 10^{-3}$ SI) indicating the presence of magnetite relics, whereby the declinations show a distinct NE

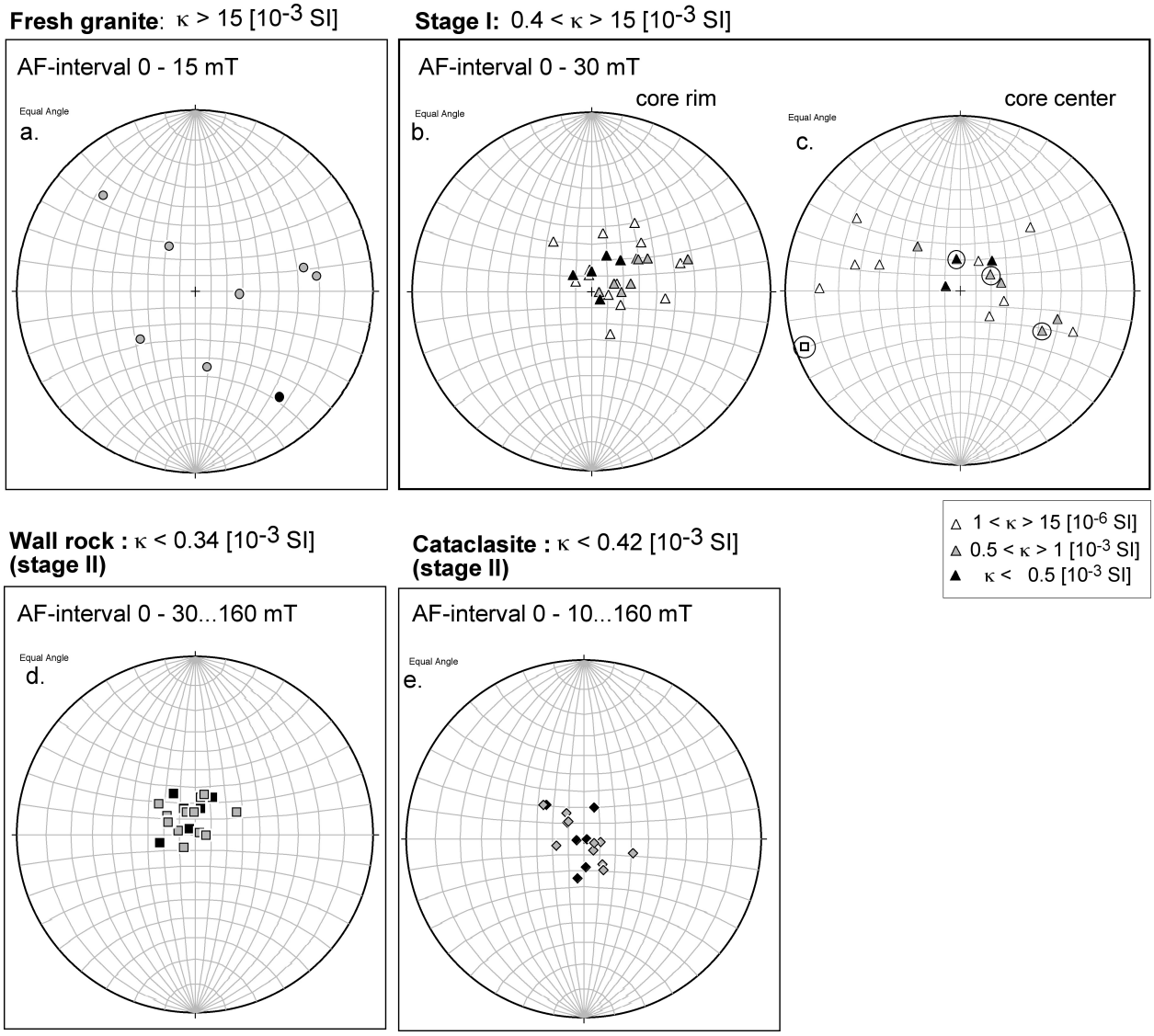

Fig. 2.10: *Stereographic projection in lower hemisphere of low coercivity components separated using AF demagnetization.* ***a.*** *Fresh granites show only VRM. Grey circles = center positions, black circles = rim positions.* ***b.*** *Stage I samples from the rim positions of a drill core.* ***c.*** *Stage I samples from the center positions of a drill core.* ***d.*** *Wall rocks of stage II. Grey squares = center positions, black squares = rim positions.* ***e.*** *Cataclasites of stage II. Grey diamonds = center positions, black diamonds = rim positions.*

orientation. The steepest inclinations are observed in strongly altered granites with $\kappa < 0.5 \times 10^{-3}$ SI. Influence of a post-drilling VRM component is therefore unlikely and the steep inclinations recorded for the whole AF interval (0 – 160 mT) point to a complete DIRM overprint. It can be summarized that the acquisition of the post-drilling VRM depends on the grain sizes of the magnetite relics within the martite grain. DIRM overprint is mostly effective in altered samples with progressive decomposition of magnetite under formation of small sized magnetite relics and coarse-grained martite. Granites, which were overprinted during the stage II alteration show $\kappa < 0.34 \times 10^{-3}$ SI for the wall rocks (Fig. 2.10 d) and $\kappa < 0.42 \times 10^{-3}$ SI for the cataclased granites (Fig. 2.10 e) and indicate a significantly stronger alteration and ubiquitous grain size reduction of magnetite as already suggested in Chapter II.1. In samples with prevailing stage II alteration the inclinations are all steep and no difference between central or rim plug positions can be observed.

The steep DIRM inclinations are removed by AF intensities up to 30 mT. Some samples show steep DIRM vectors during the whole AF range up to

Facies	Specimen		Interval	DEK	INK	MAD
Center plug positions						
wall rock	2010-1B	AF	50 - 400	256	67	3
wall rock	2010-2B	AF	0 - 1650	316	85	3
wall rock	2011-1B	AF	0 - 300	13	73	6
wall rock	2011-3B	AF	0 - 200	336	7	5
wall rock	2019-1b	TH	0 - 300	32	83	5
wall rock	2019-2B	AF	0 - 300	333	61	4
wall rock	2019-3B	AF	0 - 300	25	64	11
cataclasite	2039B-2B	AF	0 - 100	18	69	7
cataclasite	2039B-2B	AF	100 - 1600	311	57	10
cataclasite	2127-2B	AF	50 - 1600	190	65	6
cataclasite	2163-1B	AF	0 - 100	266	85	11
cataclasite	2317-1B	AF	25 - 750	98	88	4
cataclasite	2764-2B	AF	0 - 500	177	72	13
cataclasit	2163-2B	TH	0 - 500	19	82	1
cataclasit	2317-2B	TH	0 - 500	161	79	14
cataclasit	2317-1BAF	TH	0 - 400	118	74	7
stagel	2220-1B	AF	0 - 600	287	80	6
stagel	2281-2B	AF	0 - 300	354	69	3
stagel	2448-1B	AF	25 - 100	47	62	20
fresh/stagel	2476-6B	AF	80 - 150	103	61	9
stagel	2539-3B	AF	0 - 300	79	63	4
stagel	2548-2B	AF	100 - 300	62	68	10
fresh/stagel	2560-2B	AF	0 - 100	31	67	2
fresh/stagel	4691-2B	AF	25 - 300	132	65	9

Facies	Specimen		Interval	DEK	INK	MAD
Rim plug positions						
wall rock	2010-1A	AF	25 - 1650	8	66	4
wall rock	2010-1C	AF	0 - 1600	283	79	2
wall rock	2010-2A	AF	50 - 1600	72	87	1
wall rock	2010-3A	AF	0 - 100	221	79	2
wall rock	2010-3A	AF	200 - 1300	304	69	8
wall rock	2010-3C	AF	0 - 80	96	83	2
wall rock	2010-3C	AF	200 - 1050	339	75	8
wall rock	2011-1A	AF	0 - 200	358	76	2
wall rock	2011-3C	AF	0 - 200	13	64	13
wall rock	2019-1A	AF	50 - 300	310	60	5
wall rock	2019-2A	AF	0 - 300	298	72	6
wall rock	2019-3A	AF	0 - 100	62	60	12
wall rock	2019-3C	AF	50 - 300	294	71	6
cataclasite	2039B-1C	AF	0 - 300	316	75	3
cataclasite	2039B-1C	AF	200 - 800	310	57	8
cataclasite	2039B-2C	AF	0 - 1300	326	70	9
cataclasite	2039B-2a	TH	0 - 450	322	69	2
cataclasite	2127-1C	AF	0 - 100	144	70	8
cataclasite	2127-1C	AF	100 - 1600	257	72	10
cataclasite	2127-2A	AF	0 - 100	99	79	6
cataclasite	2163-2A	AF	0 - 1000	318	75	8
cataclasite	2317-1A	AF	50 - 500	140	81	7
cataclasite	2317-1A	AF	500 - 1600	106	58	10
cataclasite	2317-1C	AF	0 - 500	111	83	6
cataclasite	2764-2C	AF	0 - 500	147	67	8
stagel	2220-1A	AF	0 - 500	359	77	8
stagel	2220-1C	AF	25 - 300	311	74	4
stagel	2281-2A	AF	50 - 300	91	85	3
stagel	2448-1A	AF	25 - 750	22	65	8
fresh/stagel	2476-5A	AF	0 - 150	99	79	4
fresh/stagel	2476-6C	AF	0 - 150	156	61	3
fresh/stagel	2535-1A	AF	0 - 200	356	76	2
fresh/stagel	2535-2C	AF	0 - 75	114	70	4
stagel	2539-2C	AF	0 - 50	131	83	4
stagel	2539-2C	AF	75 - 1600	43	63	10
stagel	2539-3C	AF	25 - 100	90	71	6
stagel	2548-2C	AF	50 - 1200	69	75	8
stagel	2548-3C	AF	25 - 150	78	65	2
fresh/stagel	2560-2A	AF	0 - 200	72	73	3
fresh/stagel	2572-1A	AF	0 - 100	351	79	2
fresh/stagel	4691-3B	AF	100 - 640	303	78	3
fresh	5013-2	AF	0 - 100	93	62	1

Table 2.1: *Paleomagnetic results of VRM directions obtained from the EPS-1 borehole (48.95 ° N, 7.84 ° E) for center and rim plug positions.*

Granite facies	Specimen		Interval	DEK	INK	MAD
Center plug positions						
fresh/stagel	2476-5B	AF	0 -150	305	18	2
fresh/stagel	2476-6B	AF	0 - 50	70	-3	8
fresh/stagel	2534-1B	AF	0 - 75	271	12	5
fresh/stagel	2535-1B	AF	0 - 150	288	38	1
fresh/stagel	2535-2B	AF	0 - 150	110	21	9
stagel	2548-2B	AF	25 - 75	116	35	6
stagel	2548-3B	AF	0 - 100	106	30	10
fresh/stagel	2560-1B	AF	0 - 200	48	33	10
stagel	2560-2B	AF	100 - 400	316	51	15
fresh/stagel	2572-2B	AF	0 - 100	284	26	1
fresh	3368-3B	AF	0 - 100	141	16	1

Facies	Specimen		Interval	DEK	INK	MAD
Rim plug positions						
cataclasite	K111-3	AF	0 - 300	61	30	2
fresh/stagel	2476-6A	AF	25 - 200	53	55	9
fresh/stagel	2534-1A	AF	0 - 150	323	51	4
fresh/stagel	2535-2A	AF	0 - 100	72	35	6
fresh/stagel	2535-2A	AF	100 - 1600	11	53	7
stagel	2539-2A	AF	0 - 700	71	31	4
stagel	2539-3A	AF	25 - 500	59	50	5
stagel	2548-2A	AF	0 - 150	95	45	6
stagel	2548-3A	AF	0 - 550	55	55	2
fresh/stagel	2560-1A	AF	0 - 100	32	41	3
fresh/stagel	2572-2A	AF	0 - 100	45	47	6
fresh	3115-1A	AF	0 - 100	330	58	3
fresh	3368-2C	AF	0 - 200	316	17	7
fresh	3368-3C	AF	0 - 100	171	44	4
fresh/stagel	4691-2A	AF	0 - 50	172	-18	8
fresh	5013-3	AF	0 - 150	78	26	3
fresh	5013-4	AF	0 - 75	229	46	2
fresh	5027-4	AF	0 - 50	83	21	2

Table 2.2: *Paleomagnetic results of DIRM directions obtained from the EPS-1 borehole (48.95 ° N, 7.84 ° E) for center and rim plug positions.*

160 mT indicating a coarse-grained martite as the carrier and/or small MD magnetite with decreased H_C. These small MD magnetite grains and the large martite grains both acquired a DIRM because of their similar and relatively low coercivity, but this coercivity is not low enough for the subsequent VRM acquisition. On the other hand this coercivity is not high enough for conservation of primary remanence directions, because they are totally overprinted by a DIRM. Some samples from the upper part of the granite section show remaining ChRM after the AF demagnetization to 30 mT, which can be explained by smaller grain sizes carrying high coercivities. These samples have been used for a further evaluation of the paleofield vectors.

Natural characteristic remanent magnetization

Vectors, which were separated during AF demagnetization at fields higher than 30 mT, carry a natural ChRM (Fig. 2.11). This ChRM only occurs in the upper part of the borehole profile and reveals different components with different vector orientations (compare also Table 2.3). Vector analysis using the TH demagnetization was only successfully performed in the cataclasites (sample 2039 at 1427 m, 2127 at 1455 m and 2317 at 1508 m; compare also Fig. 2.1 b) because during heating most of the specimens showed unstable behavior and were therefore excluded from further consideration. Consequently, only eight vectors could be separated in total, which prohibited a statistical analysis.

The wall rocks of stage II show in general NW-oriented vectors (component C in Fig. 2.11 a), which are demagnetized up to 160 mT. In the stage I altered granites only two vectors could be separated showing similar orientation. Microscopic studies and coercivity spectra analysis revealed that the carriers of this component C are small magnetite grains, which occur as relics in larger martite grains. In two specimens from cataclasites, again NW-oriented directions are observed (Fig. 2.11 b) during the AF demagnetization as well as during the subsequent TH demagnetization (Fig. 2.11 c). Coercivities higher than 160 mT and unblocking temperatures (T_{UB}) between 400 and 575 °C confirm, that small magnetite relics are the carrier of this component C. At higher temperatures an additional N-oriented direction (component A) occurs, which is carried by hematite indicated by $T_{UB} > 600$ °C. However, component A partially shows also lower T_{UB}s between 500 and 640 °C indicating, that this component is carried by both magnetite and hematite. Similar T_{UB} spectra are also observed for an additional component B, which shows a distinct SW orientation (Fig. 2.11 c). It is assumed that these three components were acquired during different time intervals during the grain size reduction of magnetite. As has been shown in previous chapter, MD magnetite can align its magnetic moments within the Earth magnetic field, unless the grain size is reduced causing increasing H_C and thus frozen magnetic moments. Freezing of the remanent magnetization in the C, B and A direction must have occurred during a successively changing paleoposition of Saxothuringian as already suggested by Edel (2001).

The grain size reduction in general is correlated to a brittle deformation within discrete zones of the granite, which allowed for enhanced fluid circulation resulting in the oxidation of magnetite (further explanation see Chapter II.3, Fig. 3.20). The brittle deformation did not affected significantly the paleofield vectors because the large magnetite grains are cataclastically deformed to grain sizes < 50 μm. Such grains are still within the threshold of MD magnetite, which can readily align within the prevailing Earth magnetic field. Subsequent fluid circulation and accompanying martitization caused a further grain size reduction (< 5 μm) and irregular grain shapes of magnetite resulting in increased H_C and frozen magnetic moments. At the same time the martitization led to an acquisition of a chemical remanent magnetization (CRM) of martite. Butler (1998) reported that if the alteration involves a major change of crystal structure (e.g., magnetite to hematite), acquired CRM records the magnetic direction during alteration. Therefore it is assumed that the host mineral martite carries similar

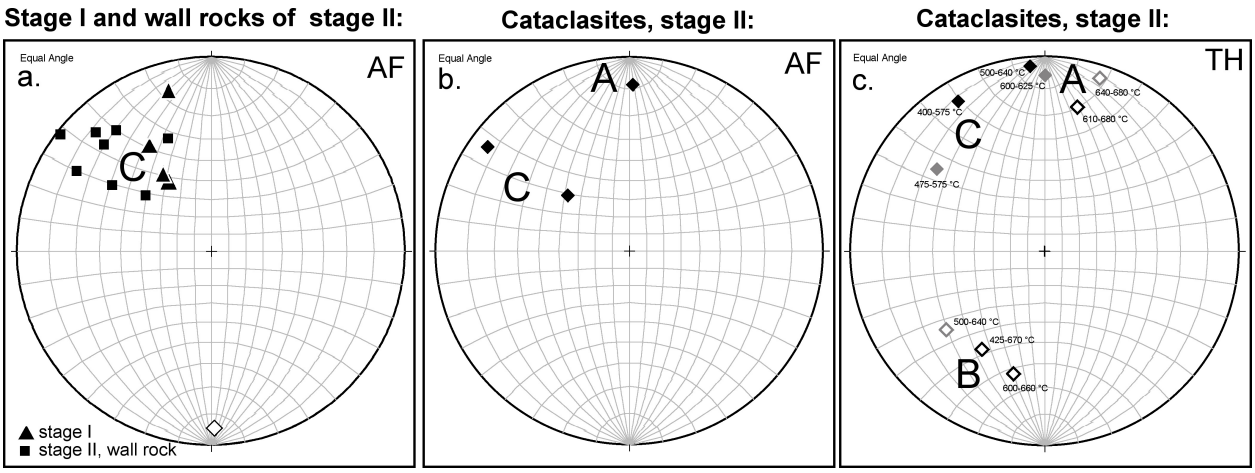

Fig. 2.11: *Stereographic projection in the lower hemisphere of high coercivity components from the upper part of the borehole profile separated using AF and TH demagnetization. Closed symbols represent positive and opened symbols represent negative directions.* ***a.*** *Component C separated in stage I (triangle) and wall rocks of stage II (squares) using AF demagnetization.* ***b.*** *Components C and A separated in cataclasites of stage II (diamonds) using AF demagnetization.* ***c.*** *Components C, B and A separated in cataclasites of stage II (diamonds) using TH demagnetization.*

Granite facies	*Specimen*		*Interval*	*DEK[°]*	*INK[°]*	*MAD*	*Comp.*	*Related time frame*
Center plug positions			[Oe]					
wall rock	2011-1B	AF	300 - 1600	301	12	17	C	Mid Carboniferous
wall rock	2011-3B	AF	500 - 1600	308	1	4	C	Mid Carboniferous
wall rock	2019-2B	AF	300 - 1000	315	14	9	C	Mid Carboniferous
wall rock	2019-3B	AF	450 - 1300	339	26	21	C	Mid Carboniferous
cataclasite	2163-1B	AF	200 - 1600	312	44	15	C	Mid Carboniferous
stageI	2281-2B	AF	300 - 700	328	43	2	C	Mid Carboniferous
cataclasite	2317-1B	AF	750 - 1600	306	6	13	C	Mid Carboniferous
fresh/stageI	2535-1B	AF	900 - 1600	344	9	11	C	Mid Carboniferous
Rim plug positions								
wall rock	2011-1A	AF	200 - 1600	316	9	16	C	Mid Carboniferous
wall rock	2019-2A	AF	300 - 1000	322	13	15	C	Mid Carboniferous
wall rock	2019-3A	AF	200 - 1600	304	27	13	C	Mid Carboniferous
wall rock	2019-3C	AF	400 - 1200	311	42	10	C	Mid Carboniferous
stageI	2220-1C	AF	800 - 1400	358	-5	9	C	Permian
stageI	2281-2A	AF	300 - 1600	328	40	6	C	Mid Carboniferous
cataclasite	K111-3	AF	400 - 1300	7	14	11	A	Triassic
Center plug positions			[°C]					
cataclasite	2127-2BAF	TH	475 - 525	367	4	11	A	Triassic
cataclasite	2163-1BAF	TH	610 - 680	196	-14	7	A	Permian
cataclasite	2317-1BAF	TH	425 - 670	33	-27	7	B	Late Carboniferous
Rim plug positions								
cataclasite	2127-2CAF	TH	400 - 575	330	8	13	C	Mid Carboniferous
cataclasite	2127-2CAF	TH	600 - 660	14	-24	9	B	Late Carboniferous
cataclasite	2317-1AAF	TH	500 - 640	358	2	15	A	Triassic
Directions obtained only from TH demagnetization								
cataclasite	2039b.2a	TH	475 - 575	307	20	6	C	Mid Carboniferous
cataclasite	2039B-2a	TH	600 - 625	0	6	5	A	Triassic
cataclasite	2039B-2a	TH	640 - 680	198	-4	17	A	Permian
cataclasite	2317-2B	TH	500 - 640	51	-24	10	B	Late Carboniferous

Table 2.3: *Paleomagnetic results of natural ChRM directions obtained from the EPS-1 borehole (48.95 ° N, 7.84 ° E) for center and rim plug positions..*

paleofield direction as the magnetite relics, because of the concomitant formation.

Discussion

Granite samples from the EPS-1 drillhole carry complex information of artificial and natural remanence overprints. Artificial overprints like the DIRM was ascertained by calculating Q-ratio in plugs from central and rim positions in relation to the profile of drill core. The relative increase of the Q-ratio from center to rim indicates a more effective DIRM overprint in the altered granites (Q-ratio > 1) than in the fresh granites (Q-ratio > 0.5). In spite of a less effective overprint of the central plug positions, the vector separation of the DIRM overprint in central plugs revealed steep inclinations, too. Together with the VRM experiments these observations indicate that as first the inclination is affected during a magnetic overprint. While the VRM is carried by magnetite only, the steep DIRM is carried by both the relatively coarse-grained magnetite relics and the newly formed martite due to overlapping coercivities. Such magnetic components show a magnetic behavior that is soft enough to be overprinted by the steep DIRM but that is hard enough to be resistant against the subsequent VRM overprint, which was acquired only in fresh granites. For the Soultz granite the following boundary conditions for VRM and DIRM acquisition have been discriminated:

Fresh and stage I altered granite samples with $\kappa > 10 \times 10^{-3}$ SI and a MDF up to 2 mT indicating very low coercivities, revealed only flat VRM directions. On the other hand strongly altered samples of stage I with $\kappa < 0.5 \times 10^{-3}$ SI and a MDF up to 30 mT indicating high coercivities, revealed distinct steep DIRM directions. VRM could not overprint the DIRM in strongly altered samples with high coercivities and the vectors remained steep. Moderately altered stage I granites with moderate degree of magnetite oxidation ($0.5 < \kappa > 10 \times 10^{-3}$ SI) and MDF ranging between 3 and 18 mT indicating moderate coercivities, do show more flat vectors in the center and weakly steeper vectors in the rim positions. However, these vectors are not as steep as the other DIRM vectors. A reason for this observation is the less effective VRM overprint in the rim positions which correlates with the higher DIRM efficiency. The higher DIRM efficiency in the rim positions resulted in only gently deviated vectors from the vertical DIRM directions. In these samples with combined VRM and DIRM remagnetization, the VRM is carried by soft magnetic magnetite only, whereby both, magnetite relics and large martite grains carry the DIRM. Because of overlapping coercivities the AF demagnetization is not appropriate to separate these two components, and vector separation only reveals vectors composed of DIRM and VRM.

In samples containing hard magnetic components, like small magnetite, small martite and fine-grained hematite, the artificial overprints can be cleaned by AF and TH demagnetization up to 30 mT or 450 °C, respectively. The remaining vector directions of natural ChRM help to unravel the alteration history, as discussed in the following.

Significance and implications of the paleofield record

Vector separation of the hard magnetic components was successfully performed only in the rocks from the upper part of the borehole profile: three principal directions of the natural ChRM (A, B and C, Fig. 2.11) were observed. These three ChRM were acquired during a N-S drift and after two sets of clockwise rotations of the Variscides in the Middle to Late Carboniferous times (Edel 2001).

Stage I altered granites and wall rocks of stage II showed similar C components implying coexistent activity of the pervasive, stage I alteration and the stage II alteration with its first event of a brittle deformation in the Soultz granite. The cataclastic deformed granites (core index 2039, 1427 m; 2127, 1455 m; 2317, 1508 m) revealed all three components, A, B and C. The NW-oriented C direction is characterized by unblocking temperatures typical only for magnetite. In contrast to this the A and B

components are characterized by unblocking spectra typical for both magnetite and hematite. Comparing the directions obtained in this study with existing paleomagnetic measurements from the Western Variscides (Northern Vosges, Pfalz, Odenwald and Spessart) and the Eastern Variscides (Moldanubian domain and Bohemian Massif) some clues about the alteration history of the Soultz granite can be given. Edel and Wickert (1991) reported on NW directions in microdioritic rocks, similar to the C directions found in this study, and they correlated these directions to remanent magnetization acquired in the time range 340-325 Ma. This time range correlates with the emplacement (331 ± 9 Ma, Alexandrov et al. 2001) and cooling (325 ± 6 Ma, Rummel 1991) ages of the Soultz granite. In the Soultz granite the C direction is carried by small magnetite relics in martite, which were caused by stage I and continued to decrease their grain sizes during stage II alteration. Similar C directions in cataclased granites confirm the early cataclastic deformation event, which took place immediately after the magma cooling during a late phase of the Variscan orogeny. This interpretation is supported by measurements of the AMS (anisotropy of magnetic susceptibility, Chapter II.1), which showed microcrack formation in magnetite. Microcrack formation is related to a Variscan stress regime. The early cataclastic deformation during cooling allowed for enhanced fluid circulation at relatively high temperatures, which is also implicated by chemical analysis of chlorites from the stage I altered granites (for further information see Chapter II.3). Based on the geothermometer after Cathelineau (1988), this chlorite composition indicates temperatures of approximately 300 °C and elevated fO_2, which was also observed by fluid inclusion study in quartz grains done by Dubois et al. (1996). At such conditions magnetite is not stable anymore and oxidizes to martite.

Similar directions subparallel to the inverse B component were also found in the Frankenstein Complex (Zwing and Bachtadse 2000) and in other adjacent rocks of the Saxothuringian that were correlated to Stephanian ages by Edel and Wickert (1991). Konrad and Nairn (1972) also found similar directions in Stephanian to Early Permian rocks from the Schopfenheim basin, Schwarzwald. As a consequence, the B direction in the Soultz granite has been correlated to Late Carboniferous – Early Permian times. The unblocking behavior indicates magnetite and hematite as the carrier. Because only small magnetite grains are able to carry a stable paleofield direction, the B directions carried by small magnetite grains in the catclasites implicate a grain size reduction due to magnetite oxidation during Late Carboniferous - Early Permian, thus long after the pluton was cooled. This magnetite oxidation was possible because of a second cataclastic deformation event in the Soultz granite, which allowed for fluid circulation. Furthermore, unblocking temperatures implicate that the B direction is also carried by hematite. Microscopic studies revealed different hematite generations. The first one represents decomposed martite and the second one hematite precipitated from fluids. A decomposition of martite caused a grain size reduction similar to the process that has been described for magnetite, which in turn increased the coercivity of martite. Martite, which contains Fe^{3+} can only be decomposed by strongly acidic fluids, which are e.g., formed during pyrite oxidation (see also Chapter II.3). Pyrite is a common mineral in cataclastic rocks from the lower part of the borehole profile, while it is extensively oxidized in the upper part. The pyrite oxidation in turn is caused by the circulation of surface fluids, which implicates increasing surface influence in the upper part of the pluton during exhumation of the pluton in Late Carboniferous to Early Permian times. This is in agreement with an erosion surface during this time interval.

The third vector direction (A) with shallow N-oriented directions is very common in the Variscan belt. The A direction was also found in the Windstein granodiorite as secondary magnetization and in the neighboring Permian Nideck ignimbrite in the northern Vosges as primary magnetizations (e.g., Roche et al. 1962). Reverse A directions were found in igneous rocks from the Saar-Nahe Basin

and in rocks from the Odenwald and Northern Vosges, which were correlated to Triassic times (e.g., Nairn 1960). In the Soultz granite such reverse A component mostly shows high (> 600 °C) and relatively sharp unblocking temperatures typical for small hematite grains. Microscopic studies revealed high amounts of such small hematite grains in the cataclased granites. This suggests a favored hematite precipitation, which started during Permian and lasted up to the Triassic, probably because of the circulation of Fe^{3+}-saturated fluids due to Fe^{2+}-oxidation and Fe^{3+}-leaching in the cataclasites from the upper part of the pluton (for more details see Chapter II.3). Fracture analysis from Genter and Traineau (1996) revealed sub-horizontal joints in these rocks and correlated them to sheet-joints caused by unloading to a paleosurface. Similar old brittle deformation episodes were also observed in episodically grown illites within veins studied by Schleicher et al. (2004). They reported about K-Ar ages of various illite grain sizes obtained from veins from the lower part of the pluton that yielded a mixture of ages ranging between 211 and 280 Ma. This implies that the hydrothermal alteration episode during Permian and Triassic times was not only restricted to the upper part but also affected the lower part of the pluton. Probably, this part was affected by another fluid chemistry.

Conclusions

The presented paleomagnetic studies from hydrothermally altered rocks of the upper part of the pluton unravels the old hydrothermal alteration history in the Soultz granite, which can be correlated to different geological events.

(1) After the magma emplacement at 331 ± 9 Ma (Alexandrov et al. 2001) and due to the magma cooling (325 ± 6 Ma, Rummel 1991) the Soultz granite underwent solidification. This solidification caused the formation of microcracks in magnetite (Chapter II.1), which allowed for preferred fluid circulation and magnetite oxidation under retrograde conditions. Resulting small magnetite relicts (Plate 1 c, d) carry primary C directions acquired during Middle Carboniferous (331-325 Ma) times.

(2) Vector separation in cataclastic granites revealed polyphase faulting. Coexistent with the stage I alteration a first faulting event in discrete zones caused the formation of cataclastic granites, which carry the same C directions as the pervasive stage I altered granites related to small magnetite relicts in martite (Fig. 1.4 c, d and Fig. 3.2-II c, d, g). A second faulting event in cataclased rocks occurred during Late Carboniferous – Early Permian associated with the acquisition of secondary reverse B directions. These directions are increasingly carried by decomposed martite and new precipitated hematite (Fig. 3.2-II e, f) due to increasing influence of surface waters during the exhumation of the pluton.

(3) Progressive exhumation and erosion during Permian caused denudation of the Variscan basement and the formation of a fossil surface at the top of the Soultz pluton. Circulation of surface fluids, which are Fe^{3+}-saturated within the upper part of the pluton (1417 – 1550 m) led to a widespread hematitization of the cataclased rocks. These rocks acquired a chemical remanent overprint during Permian, which lasted into Triassic. This interpretation is based on the shallow positive A directions that change into reverse A directions.

In this study no indication were found for younger remanence overprints during Cenozoic formation of the Upper Rhine Graben, although numerous works (e.g., Dubois et al. 1996, Pauwels et al. 1992, Smith et al. 1998) reported about younger hydrothermal alteration overprints in the Soultz granite. Such younger overprints may be obliterated by the strong DIRM remagnetization or be blurred due to an unstable behavior during TH demagnetization experiments or be blurred due to overlapping coercivity spectra. On the other hand, it is also likely that the special nature of the old paleofluids in the Soultz granite is responsible for the acquisition of a ChRM. The old Carboniferous fluids with high temperatures and elevated fO_2 (Chapter II.3) circulated within fault zones and

enabled martitization of magnetite resulting in small magnetite relicts. Subsequent fluids with high acidity favored Fe^{3+} solubility and after mixing with meteoric water, a subsequent precipitation of fine-grained hematite during Late Carboniferous until Triassic. In contrast to these old fluids, the nature of the modern fluids is controlled by characterized by organic matter (Lédesert et al. 1999), which cause reducing conditions. This observation is also supported by microscopic studies, that revealed reduced martite to magnetite in a fault zone from the lower part of the borehole profile (Fig. 3.2-II h).

Another explanation is probably the reactivation of the old fault zones during younger faulting events. In the upper part, the old hydrothermal alteration events led to stable remanent overprints, which probably could not be overprinted during younger hydrothermal alteration events. These stable remanence carriers are also resistant against the artificial overprints like the DIRM and VRM and therefore preserved the natural ChRM. This study implies that the late Eocene to the present-day development of the Rhine Graben rift system had no effect on the magnetic overprint in the upper part of the Soultz granite.

3. Variations of thermomagnetic behavior and its significance for the pre-rift alteration history of the Soultz granite

Abstract: In this chapter, the magnetic mineralogy is related to the two principal hydrothermal alteration stages I and II of the magnetite-bearing Soultz granite from the EPS-1 borehole (Upper Rhine Graben, France). Interpretation of the temperature dependent behavior of low-field magnetic susceptibility (κ(T)) combined with optical microscopy, microprobe, X-ray diffraction and chemical analysis of single mineral phases provides a better understanding of the pre-rift related alteration history of the Soultz granite, which is described here for the first time in detail.

The stage I alteration is subdivided into a pervasive and a localized event based on the magnetic mineral assemblage. During the pervasive stage I alteration primary rock forming minerals like plagioclase and biotite were altered while accessory magnetite remained without any evidence of oxidation. This type of alteration is without any consequence for the magnetic properties and the granite is called "fresh" from the magnetic point of view. In contrast to earlier studies (e.g., Jacquemont 2002, Genter and Traineau 1995, Traineau et al. 1991) granites from the central part of the borehole profile (1550 – 1580 m) were not affected by the pervasive alteration event, but by an alteration event, which was locally restricted. Thus, this event is called localized stage I alteration. This localized stage I alteration is clearly indicated by the magnetic alteration mineralogy and the associated chlorite chemistry. Such observations imply that fault zones were already formed in the solidified body, during the pluton cooling history. In the vicinity of such fault zones magnetite oxidation to martite occurred. The subsequent stage II alteration is related to post-emplacement tectonics. During the exhumation of the plutonic body, near surface processes in the upper part of the borehole profile caused the oxidation of pyrite, which is a common mineral in the stage II granite from the lower part, but is nearly completely decomposed in the upper part. The oxidation of pyrite led to the formation of strongly acidic fluids and thus to the decomposition of earlier formed martite in the cataclastic granites, and martitization of magnetite in the more distant wall rocks. During the exposure of the Soultz granite to a fossil surface, such acidic fluids probably mixed with meteoric water, which promoted the precipitation of fine-grained hematite. At the bottom of the EPS-1 borehole, a younger event caused a reduction of martite back to magnetite, which is correlated to the infiltration of organic matter from overlying sedimentary cover (Lédesert et al. 1999).

Repeated heating/cooling experiments of whole rock samples from this study clearly indicate that the method of repeated heating/cooling κ(T) measurements, which was suggested by Hrouda et al. (2003), cannot be used in a simple way for determining paleotemperatures in the hydrothermally altered Soultz granite.

Introduction

Interpretation of the temperature dependent behavior of the low-field magnetic susceptibility (κ(T)) of magnetic minerals is of fundamental importance for their identification and was the topic of numerous rock magnetic studies including the investigation of magnetic phases (e.g., Kontny et al. 2004, de Boer and Dekkers 2001, de Boer et al. 2001, Özdemir et al. 1993). However, the interpretation of the κ(T) curves of whole rock samples in respect to determining geological processes, e.g., metamorphism or oxidation, has been the focus of only a few magnetic studies (e.g., Kontny and de Wall 2000, Akimoto et al. 1957). κ(T) measurement shows a high sensitivity to mineralogical composition of para- and ferrimagnetic phases, in contrast to

diamagnetic phases, which display a temperature independent behavior. Accessory minerals, such as iron oxides, sulfides and oxyhydroxides often show ferrimagnetic behavior but are mostly ignored in conventional petrological investigations, despite the fact that they yield detailed information about the geological processes they originated from. Such geological knowledge is, however, important in paleomagnetic or AMS (anisotropy of magnetic susceptibility) studies. For example, primary magnetic minerals with a distinct magnetic behavior are often destroyed or altered into secondary mineral phases during hydrothermal alteration and show modified magnetic behavior. Such modifications can be detected in bulk magnetic susceptibility measurements (e.g., Shunshan et al. 2003, Turunen 2000, Wooldridge et al. 1990). In these cases, the κ(T) measurements can significantly contribute to our understanding of the effects of hydrothermal processes on the magnetic mineralogy.

The identification of magnetic phases using κ(T) curves requires detection of the intrinsic properties, namely the Curie and Néel temperature (T_C, T_N) that lie in the range between room temperature and 700 °C, and the low-temperature magnetic transitions, e.g. the Morin transition (T_M) of hematite and Verwey transition (T_V) of magnetite, which can be detected between 0 and –192 °C. The Morin transition represents hematite's magnetic isotropic point and does not constitute a crystallographic change, whereas the Verwey transition of magnetite represents a transformation from a monoclinic to cubic spinel structure. In a polyphase rock sample, different magnetic phases can occur, and an unequivocal interpretation of κ(T) curves is difficult. For example, the identification of hematite in the presence of magnetite is rare because the magnetic susceptibility of hematite is three orders of magnitude smaller than that of magnetite. Thus, alongside the presence of magnetite, the magnetic signal of hematite disappears in the background noise of the κ(T) curve. In addition to its T_C, hematite can also be identified by its characteristic T_M in the low-temperature range. However, with incorporated impurities or in the case of poorly crystalline hematite the T_M is only poorly developed or completely suppressed (e.g., Bando et al. 1965, Morin 1950). The interpretation of κ(T) curves of whole rock samples containing polyphase paramagnetic minerals is also difficult because the Néel temperature of each phase is often masked by the summation of bulk magnetic susceptibility. Furthermore, mineral reactions may occur during heating despite heating in inert (argon) atmosphere. However, the formation of minor quantities of strongly magnetic minerals when heating a sample containing a distinct para- and antiferromagnetic component does give a characteristic κ(T) curve. Such κ(T) curves can be used for an identification of the original mineralogical composition if it is known how single phased minerals behave during heating. Hematite, for example, is known to produce maghemite on heating in air (e.g., de Boer and Dekkers 2001) and magnetite when heating in argon atmosphere (e.g., Günther 2003). Furthermore, heating Mn-siderite causes the formation of Mn-bearing magnetite (Isambert et al. 2003). In this study it has been tested if such neoformations can be used to characterize the different stages of hydrothermal alteration in the Soultz granite.

Hrouda et al. (2003) proposed the use of mineral reactions during repeated heating/cooling cycles of the κ(T) measurements as a paleotemperature indicator. They hypothesized, that if the sample is heated in 50 or 100 °C steps repeatedly to 700 °C, one can determine the temperature at which the heating and cooling curves start to differ substantially. This temperature is assumed to correspond with the maximum temperature, which affected the rock during its history. However, this hypothesis has not yet been tested in natural field studies. In this chapter, the initial alteration temperature of repeated κ(T) curves will be compared with the temperature derived from the alteration mineralogy in the Soultz granite in order to evaluate this hypothesis for the hydrothermally altered Soultz granite.

The EPS-1 borehole of the Soultz granite was drilled within a geothermal anomaly (140 °C in 2 km depth) in the Upper Rhine Graben, ca. 100 km N of Strasbourg, France. Within the drill cores, the granite was encountered at a depth of 1417 m and lies beneath Permo-Mesozoic sedimentary rocks. Alexandrov et al. (2001) dated the granite emplacement at 331 ± 9 Ma (U/Pb zircon dating). Petrological investigations from Stussi et al. (2002) have shown that the emplacement took place in two different stages. The first stage was deep-seated at 11 – 12 km depth, corresponding to a temperature range of 755-790 °C and a pressure of 3.5 kbar. The second crystallization stage took place at 4.5 – 5.5 km depth, which lead to a consolidation of the granitic body at temperatures of 665 - 715 °C and pressures of 1.5 - 2.0 kbar during ascent. This stage is characterized by the final crystallization of hornblende and magnetite. K-Ar dating gives a cooling age for the whole system (closing temperatures of biotite) at 325 ± 6 (Rummel et al. 1991). During the consolidation of the magma, the formation of microcracks allowed for enhanced fluid-rock interaction and an intensive hydrothermal alteration of the granite body. The fresh and hydrothermally altered granites can be discriminated by their magnetic bulk susceptibility (κ) with $\kappa > 10 \times 10^{-3}$ SI for the fresh and $\kappa < 1 \times 10^{-3}$ SI for the altered granite (Fig. 3.1). The strong decrease of κ is caused by an oxidation of magnetite to hematite (Chapter II.1). Traineau et al. (1991) described two main hydrothermal alteration stages (stage I: pervasive and stage II: vein alteration) that were correlated with autometamorphism during magma cooling under retrograde conditions (e.g., Jacquemont 2002) and brittle deformation during several tectonic settings (e.g., Genter and Traineau 1996) in the Soultz granite. Whereas the pervasive alteration affected the whole plutonic body, the vein alteration was restricted to discrete fault zones with different events of fluid activity (e.g., Komninou and Yardley 1997, Dubois et al. 1996). In this study, the magnetic alteration mineralogy of the Soultz granite comprising oxidized magnetite to martite, precipitated hematite, illite, Fe-bearing carbonate and pyrite was related to these stages of hydrothermal alteration using measurements of the temperature dependence of magnetic susceptibility, microprobe, X-ray diffraction and microscopic analyses.

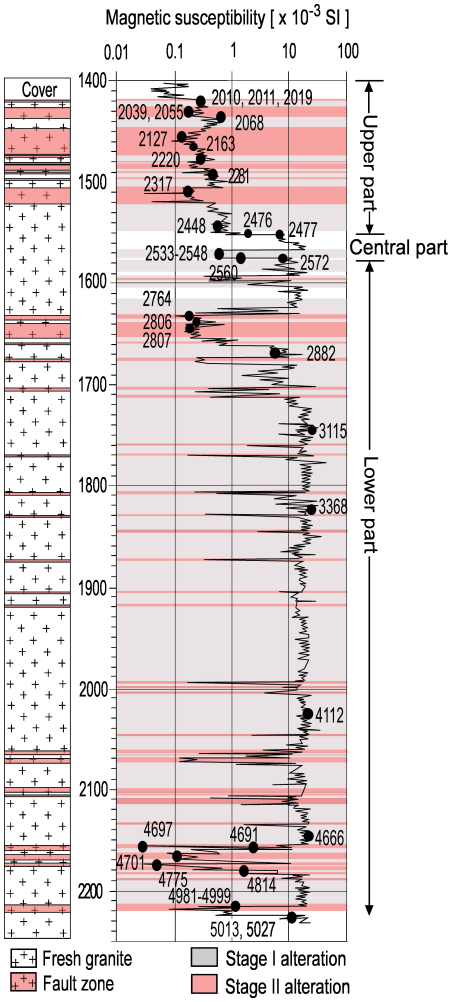

Fig. 3.1: *Lithologic section (modified after Genter and Traineau 1996) and magnetic susceptibility log with data (modified after Rummel and König, 1991) on drill cores from the 1414 to 2230 m depth interval in the EPS-1 borehole. The hydrothermal alteration observed in the cores is related to two stages. Fault zones correlate with increased susceptibilities (< 1 x 10-3 SI). Black dots and numbers indicate sample position for this study, according to the nomenclature of the core index (Genter and Traineau 1991).*

Methods

Temperature dependent magnetic susceptibility (κ(T)) measurements were performed in the temperature range of –192 °C to 700 °C using the KLY-2 Kappabridge combined with the CS-L cryostat and CS-2 furnace of AGICO with a sensitivity of

4 x 10^{-8} SI for a specimen with a nominal volume of 10 cm^3 (Hrouda 1994). Together with five mineral phases (ankerite from quarry Himmelfahrt at Freiberg, Germany; siderite from quarry Pfannenberger Einigkeit at Siegen, Germany; fine-grained hematite from Antiatlas, Morocco; coarse-grained hematite from Banded Iron Formation, Brazil; illite from Silver Hill, Montana, USA) and three vein samples from Soultz granite (hematite, illite and pyrite vein), 22 representative κ(T) curves of whole rock samples of different mineralogy were measured. Hereby, temperatures and susceptibilities were recorded as the sample was warmed up from –192 °C to 0 °C (low-temperature run). A heating and cooling cycle from ambient temperature to 700 °C (high-temperature run) and a repeated heating/cooling cycles from ambient temperature to 700 °C in 50 °C steps were also performed in an argon atmosphere with a flow rate of 100 ml/min and a heating rate of 10 °C/min. The inert gas was used to minimize mineral reactions with atmospheric oxygen during the heating process. The temperature uncertainty is approximately ± 5 °C. The raw data were corrected against an empty furnace run and normalized to the susceptibility magnitude at room temperature before heating (κ_{norm}), or to the sample weight before heating, which is equivalent to the mass susceptibility (χ). An alteration index (Al-index) was calculated representing the difference between the κ_{norm} during cooling and the κ_{norm} in the heating run (Al-index = $\kappa_{Cnorm} - \kappa_{Hnorm}$). The susceptibility bridge operates with an AC field of 300 A/m and a frequency of 920 Hz. The heated sample volume is restricted to ~0.25 cm^3 because higher sample volume cause inconsistency in the sample heating. Such a small volume is unproblematic for the fresh granite characterized by a homogeneous mineral distribution. In contrast, the heterogeneity of the hydrothermally altered granite causes variation in κ(T) curves, even for the same sample specimen. Therefore, complementary microscopic investigations were performed.

Identification of the whole rock mineral assemblages was achieved by means of optical examinations of polished thin sections (30 μm) under an optical microscope using transmitted and reflected light. In order to discriminate and to highlight the small magnetite relics in the host mineral martite, thin sections were covered with a ferrofluid (EMG 807) from Ferrofluidics GmbH, which was diluted with distilled water in the ratio 1:10. The ferrofluid dispersed on the thin section, which was covered by a glass slide, and was attracted by the ferrimagnetic magnetite but not by the antiferromagnetic martite or other weakly magnetic phases. Identification of mineral phases before and after heating was achieved by XRD analyses on powdered samples, using a Siemens (Bruker) Diffrac 500 at the Geological-Paleontological Institute of the University of Heidelberg. Samples were run between 0° and 70° 2θ, with a generator potential of 40 kV, a generator current of 30 mA (using a CuKα radiation), a Ni filter and scan speed of 1°/min. The software used for XRD data analyses was Diffrac AT (version 3.3, © Socabim, 1993).

Mineral chemistry of chlorites and biotites was determined with a CAMECA SX51 electron microprobe at an acceleration voltage of 15kV and a sample current of 20 nA, housed at the Mineralogical Institute of the University of Heidelberg. Calibration was accomplished with the following standards: albite (Na), periclase (Mg) Al2O3 (Al), wollastonite (Si, Ca), orthoclase (K), TiO2 (Ti), Cr2O3 (Cr), rhodonite (Mn) and hematite (Fe). The raw data were corrected with the PAP algorithm of Pouchou and Pichoir (1984).

Determination of major element concentrations in the five mineral phases was done using an Inductive Coupled Plasma Emission Spectrometer (ICP-ES) by ACME (Analytical Laboratories) in Vancouver, Canada. Elements are given as oxides for each element (i.e. Al_2O_3, CaO, Cr_2O_3, Fe_2O_3, K_2O, MgO, MnO, Na_2O, P_2O_5, TiO_2). ACME's Whole Rock package (Group 4A) includes the determination of volatile phases by loss on ignition (LOI), total carbon and sulphur by Leco as well as measurement of Ba, Ni, Sc, Sr, Y and Zr.

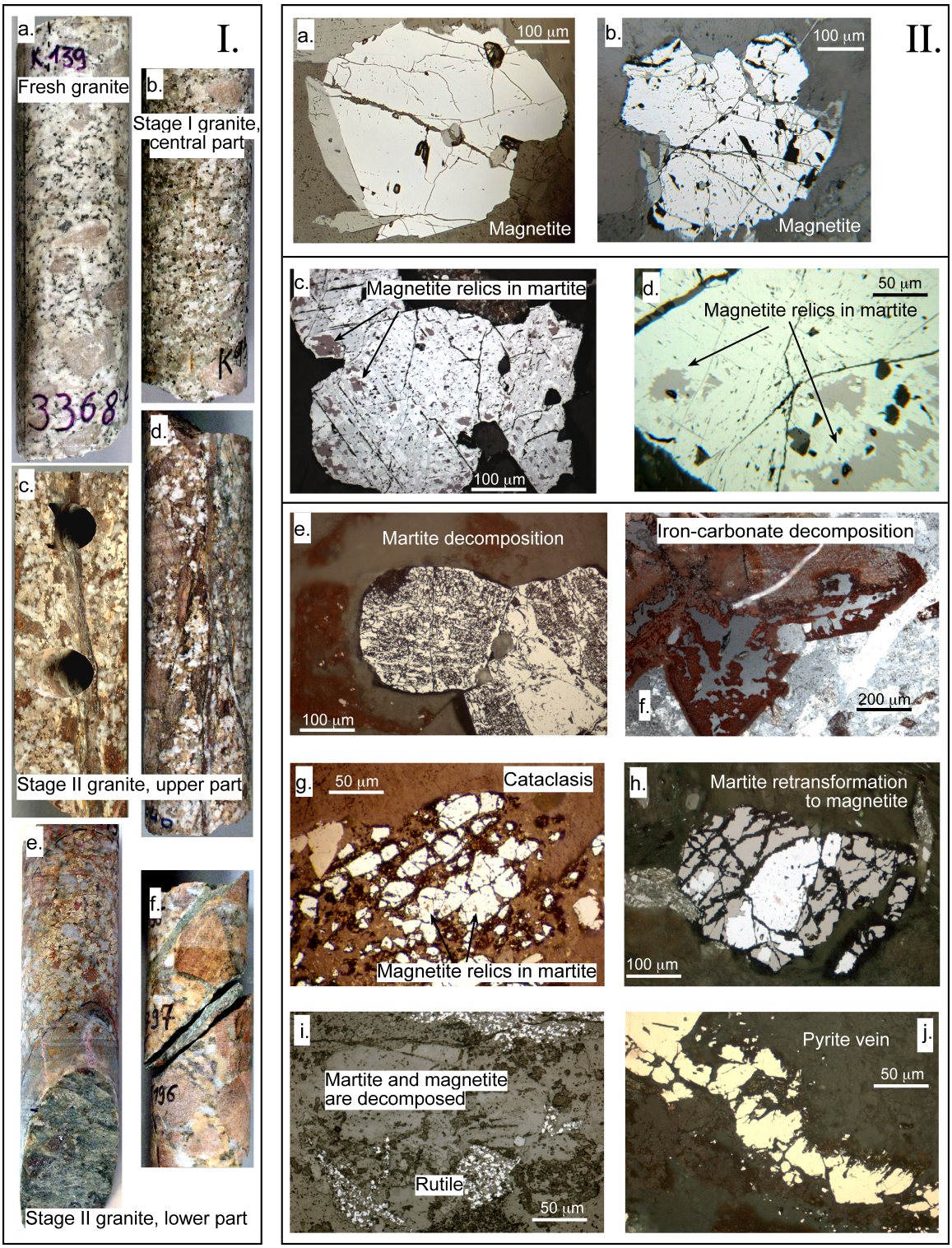

Fig. 3.2: I: *Drill cores from fresh and hydrothermally altered Soultz granite a. Fresh granite (core index 3368).* ***b.*** *Stage I altered granite (core index 2539).* ***c., d.*** *Cataclased granites from the upper borehole section (core index 2055, 2040).* ***e. f.*** *Cataclased granites from the lower borehole section (core index 4989, 4701).* ***II:*** *Reflected light micrographs from fresh and hydrothermally altered Soultz granite (sample locations in Fig. 3.1).* ***a., b.*** *Magnetite from fresh granites (4666, 3368).* ***c., d.*** *Oxidized magnetite and magnetite relics in martite from the central part of the borehole profile (2537 and 2476).* ***e., f.*** *Martite and Fe-carbonate decomposition in the upper borehole section (core index 2039).* ***g.*** *Cataclastically deformed martite with magnetite relics from the upper part (core index 2127).* ***h.*** *Martite modification into magnetite (core index 4986), lower part.* ***i.*** *Martite and magnetite are decomposed, titanite is replaced by rutile (core index 4775), lower part of profile.* ***j.*** *Pyrite vein in the lower part of the borehole (core index 4989).*

Results and interpretation

1. Mineralogical investigations

Fresh granite

The primary mineral assemblage of the fresh Soultz granite (Fig. 3.2-Ia) consists of large pink K-feldspar megacrysts (up to 5 cm in diameter) embedded in a coarse-grained matrix of quartz, plagioclase, K-feldspar, biotite and hornblende, as well as accessory magnetite (up to 500 µm), sphene and apatite. The magnetite shows a pure composition (Table 3.1) and no evidence of oxidation. The grains are mostly euhedral or subhedral (Fig. 3.2-IIa, b) and frequently found in clusters associated with biotite, hornblende and sphene (Fig. 1.4 b). According to Traineau et al. (1991) the pink color K-feldspar megacrysts is caused by a Fe^{3+} substitution in the lattice during crystallization. The pinkish color becomes more intensive and turns into a brick red color close to fault zones. Together with the occurrence of small hematite platelets (< 10 µm) along the biotite cleavage, the formation of hematite suggests increased conditions of oxygen fugacity (fO_2) during the late cooling history of the granite and represents a first episode of hematitization in the Soultz granite. However, magnetite remained unaffected during this pervasive alteration event. The coexistence of magnetite and hematite at 350 °C implies fO_2 conditions around the hematite/magnetite (HM) buffer of approximately $\log[fO_2] = -28$ (Fig. 3.3). This alteration event caused an albitization and sericitization of plagioclase and the chloritization of biotite (Traineau et al. 1991). Plagioclase is widely sericitized and the chemical analysis of biotite shows a composition of $(K_{0.9}\ Na_{0.01})\ (Mg_{1.5}\ Fe_{1.1})\ (Al_{0.05}\ Ti_{0.2})\ [Si_{2.9}\ Al_{1.1}\ O_{10}]\ (OH)_2$ (Table 3.2, sample 4666). Partial chloritization of biotite within the fresh granite led to the formation of Mg-rich chlorites with a chemical composition of $(Fe_{1.8}\ Mg_{3.1}\ Al_{1.1})\ (Si_{3.0}\ Al_{1.0})\ O_{10}\ (OH)_8$ (4666, Table 3.3), which is consistent with the observations of Komninou and Yardley (1997). Based on the geothermometer of Cathelineau (1988) the tetrahedral coordinated Al indicates chloritization temperatures ranged between 231 and 295 °C (Fig. 3.4 a).

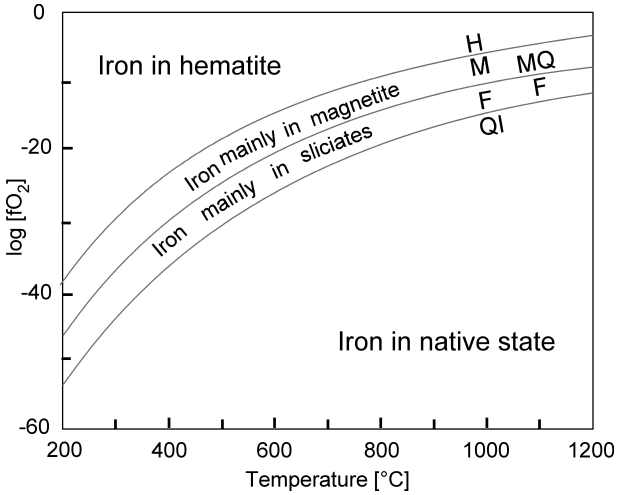

Fig. 3.3: *Plot of oxygen fugacity expressed as log(fO_2), versus temperature showing the relative stabilities of the various oxidation states of iron in the system Fe-Si-O (after Frost, 1991). Below the quartz-iron-fayalite (QIF) buffer iron is present as Fe0; between QIF and the fayalite-magnetite-quartz (FMQ) buffer iron occurs in the ferrous (Fe^{2+}) oxidation state; between FMQ and the hematite-magnetite (HM) buffer iron occurs in both ferrous and ferric (Fe^{3+}) oxidation states; and above HM iron is in the ferric state.*

Stage I altered granite

The stage I altered granite (Fig. 3.2-I b) occurs at a depth interval between 1550 and 1580 m (compare Fig. 3.1). The albitization of plagioclase resulted in the formation of small veinlets of pure calcite (Jacquemont 2002). Chemical analyses of chlorites performed in the study herein (Table 3.3) indicate the formation of a Fe-clinochlore with a chemical composition of $(Fe_{1.8}\ Mg_{2.8}\ Al_{1.3})\ (Si_{2.9}\ Al_{1.1})\ O_{10}\ (OH)_8$ (sample 2540) at temperatures between 239 and 307 °C. This temperature is based on the tetrahedral occupancy of Al (Fig. 3.4 a), which is considered to be a linear dependence of the temperature according to the equation: Temperature [°C] = -61.9229 + 321.9772 (Al^{IV}) (Cathelineau 1988). In contrast to the fresh granite an elevated fO_2 is indicated by the higher Fe/(Fe+Mg) ratio (Fig. 3.4 b), which is considered to be a function of oxygen fugacity (Deer et al. 1992). The quartz fluid inclusion studies of Dubois et al. (1996) described CO_2-rich fluid inclusions in the volatile phase, which supports the conditions of elevated fO_2. As a consequence

	fresh				*stage I*						
sample	4666-1	4666-2	average	std	2540-1-5	2540-1-6	2540-1-8	2540-2-8	2540-2-9	average	std2
Type	**Magnetite**				**Magnetite**						
SiO2	0.02	0.00	0.01	0.02	0.02	0.07	0.00	0.03	0.01	0.03	0.03
TiO2	0.01	0.00	0.00	0.01	0.05	0.08	0.10	0.01	0.26	0.10	0.10
Al2O3	0.06	0.08	0.07	0.01	0.06	0.05	0.16	0.05	0.04	0.07	0.05
Cr2O3	0.10	0.11	0.10	0.01	0.05	0.05	0.11	0.12	0.11	0.09	0.03
Fe2O3	67.97	68.04	68.01	0.05	67.95	68.05	68.12	67.97	68.04	68.03	0.07
FeO	30.52	31.11	30.82	0.42	30.54	30.91	30.91	30.52	31.11	30.80	0.26
MnO	0.02	0.09	0.05	0.05	0.01	0.05	0.06	0.12	0.05	0.06	0.04
MgO	0.02	0.01	0.02	0.00	0.02	0.01	0.00	0.00	0.00	0.01	0.01
CaO	0.00	0.00	0.00	0.00	0.01	0.00	0.00	0.04	0.00	0.01	0.02
Na2O	0.03	0.00	0.02	0.02	0.02	0.00	0.00	0.00	0.00	0.00	0.0
K2O	0.00	0.01	0.00	0.00	0.01	0.00	0.00	0.01	0.02	0.00	0.01
Sum	98.74	99.46	99.10	0.51	98.73	99.27	99.48	98.88	99.63	99.20	0.38
Si	0.00	0.00	0.00	0.00	0.00	0.00	0.00	0.00	0.00	0.00	0.00
Ti	0.00	0.00	0.00	0.00	0.00	0.00	0.00	0.00	0.01	0.00	0.00
Al	0.00	0.00	0.00	0.00	0.00	0.00	0.00	0.00	0.00	0.00	0.00
Cr	0.00	0.00	0.00	0.00	0.00	0.00	0.00	0.00	0.00	0.00	0.00
Fe3+	1.99	1.99	1.99	0.00	1.99	1.99	1.98	1.99	1.98	1.99	0.01
Fe2+	0.99	0.99	0.99	0.00	1.00	1.00	1.00	0.99	1.01	1.00	0.01
Mn	0.00	0.00	0.00	0.00	0.00	0.00	0.00	0.00	0.00	0.00	0.00
Mg	0.00	0.00	0.00	0.00	0.00	0.00	0.00	0.00	0.00	0.00	0.00
Ca	0.00	0.00	0.00	0.00	0.00	0.00	0.00	0.00	0.00	0.00	0.00
Na	0.00	0.00	0.00	0.00	0.00	0.00	0.00	0.00	0.00	0.00	0.00
K	0.00	0.00	0.00	0.00	0.00	0.00	0.00	0.00	0.00	0.00	0.00

	stage I						
sample	540-1-5	2540-1-6	2540-1-8	2540-2-8	2540-2-9	average	std
Type	**Martite**						
SiO2	0.04	0.03	0.04	0.04	0.08	0.05	0.02
TiO2	0.02	0.13	0.04	0.03	0.04	0.05	0.04
Al2O3	0.07	0.14	0.03	0.03	0.07	0.07	0.04
Cr2O3	0.01	0.01	0.10	0.06	0.08	0.05	0.04
Fe2O3	98.24	98.42	98.52	98.38	99.09	98.53	0.33
FeO	0.00	0.00	0.00	0.00	0.00	0.00	0.00
MnO	0.11	0.13	0.07	0.08	0.10	0.10	0.02
MgO	0.01	0.01	0.02	0.01	0.02	0.01	0.01
CaO	0.00	0.00	0.03	0.01	0.00	0.01	0.01
Na2O	0.03	0.00	0.03	0.01	0.02	0.02	0.01
K2O	0.01	0.02	0.01	0.01	0.03	0.02	0.01
Sum	98.65	98.98	98.87	98.69	99.53	98.94	0.35
Si	0.00	0.00	0.00	0.00	0.00	0.00	0.00
Ti	0.00	0.00	0.00	0.00	0.00	0.00	0.00
Al	0.00	0.00	0.00	0.00	0.00	0.00	0.00
Cr	0.00	0.00	0.00	0.00	0.00	0.00	0.00
Fe3+	1.99	1.99	1.99	1.99	1.99	1.99	0.00
Fe2+	0.00	0.00	0.00	0.00	0.00	0.00	0.00
Mn	0.00	0.00	0.00	0.00	0.00	0.00	0.00
Mg	0.00	0.00	0.00	0.00	0.00	0.00	0.00
Ca	0.00	0.00	0.00	0.00	0.00	0.00	0.00
Na	0.00	0.00	0.00	0.00	0.00	0.00	0.00
K	0.00	0.00	0.00	0.00	0.00	0.00	0.00

Table 3.1: *Mineral chemical analyses of magnetite and martite from fresh and stage I altered granites.*

of increased fO_2, magnetite disequilibrated due to the shift from the HM buffer into the hematite field (Fig. 3.3), which caused the oxidation of magnetite to a pure hematite (Table 3.1). Hematite derived from magnetite is called martite and shows small magnetite relics of magnetite (Fig. 3.2-II c, d). The reaction

(1) $2Fe_3O_4 + 1/2O_2 = 3Fe_2O_3$

can occur when Fe^{2+}-bearing and relative fO_2-poor hydrothermal fluids mix with O_2-rich, meteoric fluids. Stage I altered granite, which shows the oxidation of magnetite is restricted to the depth interval between 1550 and 1580 m. Such a spatial restriction is related to a nearby fault zone, which allowed entrance of oxygen-rich fluids. With further distance from a fault zone the intensity of the alteration vanished and magnetite remained unaffected. Thus, the alteration mineral assemblage

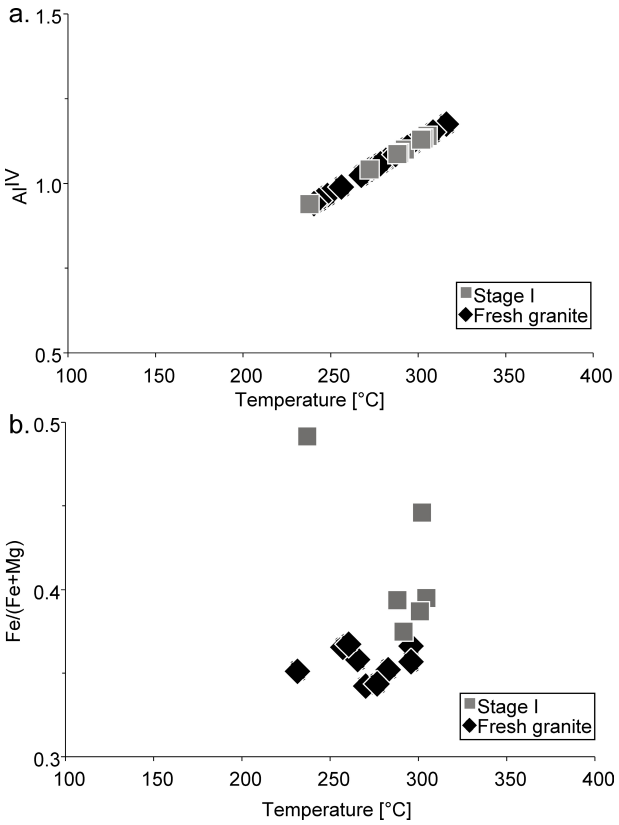

Fig. 3.4: a. *Al on tetrahedral sites (per half formula unit) in chlorites from fresh and stage I altered granites versus temperature, after Cathelineau (1988). The temperature has been calculated using the formula: T °C = -61.9229 + 321.9772(Al^{IV}).* ***b.*** *Plot of the Fe/(Fe+Mg) ratio in chlorites versus temperature from fresh and stage I altered granites. The, Fe/(Fe+Mg) ratio is considered to be a function of oxygen fugacity (Deer et al. 1991).*

of stage I granite indicates indeed a pervasive stage I alteration, whereas the magnetic mineralogy reveals clearly the evidence of a fault-related alteration. This event is called localized stage I alteration.

Stage II altered granite

The stage II altered granite is related to fault zones and subdivided into cataclasites and their wall rocks. The alteration mineral assemblage is characterized by abundant Mg- and Mn-bearing iron-carbonates. Because these granites were affected by a multistage hydrothermal alteration history, they show a strong mineralogical heterogeneity. Moreover, granites from the upper (1417 – 1550 m) and lower (1550 – 2220 m) borehole section are characterized by a different opaque mineralogy. This opaque mineralogy is described in more detail in the following sections. The most significant difference between the upper and lower sections is the presence of hematite and the absence of pyrite in the upper part, whereas in the fault zones of the lower part pyrite is an abundant mineral and hematite is rare.

Upper fault zones

The upper part of the borehole section (1417 – 1550 m) and the fault zone in the depth interval between 1630 and1630 m is characterized by strongly cataclased granites (Fig. 3.2-I c, d and 3.2-II g). In contrast to the fault zones from the lower borehole section, granites from the upper section show a persistent martitization indicated by continuously low κ-values < 1 x 10^{-3} SI (Fig. 3.1). The widespread hematitization gives the granite its reddish color. In the cataclasites martite shows indications of decomposition (Fig. 3.2-Ie). Decomposition of martite requires solution of ferric iron, which is only possible in strongly acidic fluids (maximum pH = 3, e.g. Appelo and Postma 1999) under atmospheric conditions (Fig. 3.19, Mason and Moore 1982). Such low pH-values are reached during volcanic activity, which is associated with dissolving of volcanic gases in acidic thermal waters (e.g., Varekamp 2004). Volcanic activity is well known for the European Variscides during Permian times (e.g., Roche et al. 1962). However, the martite decomposition is restricted to the upper section of the borehole and is not observed in the lower section. In contrast, the lower section is characterized by the occurrence of pyrite within small veinlets (Fig. 3.2-Ij). Regarding the occurrence of accessory mineralogy throughout the whole borehole profile it seems more likely, that the low pH-value was caused by a near surface process in the upper pluton section. Here, O_2-rich meteoric fluids infiltrated into the highly fractured upper section, which is probably related to the exhumation and erosion of the Soultz granite. The infiltration of O_2-rich fluids caused the oxidation of pyrite. This oxidation vanishes with increasing depth and is totally suppressed in the lower section. Thus, pyrite is a common mineral in the fault zones

3.2	fresh	fresh	fresh	fresh	fresh	fresh	fresh	fresh	fresh	fresh	fresh	fresh		
sample	4666-6	4666-7	4666-8	4666-13	4666-14	4666-16	4666-17	4666-18	4666-19	4666-20	4666-21	4666-22	average	sd
Type	Biotite	Biotite	Biotite	Biotite	Biotite	Biotite	Biotite	Biotite	Biotite	Biotite	Biotite	Biotite		
SiO2	37.52	37.45	37.34	36.84	36.26	37.04	37.15	37.29	37.30	37.22	37.31	37.43	37.18	0.34
TiO2	2.68	2.84	2.70	2.73	3.22	3.09	3.18	3.17	3.31	3.35	3.36	3.41	3.09	0.28
Al2O3	13.18	12.99	13.24	13.07	13.11	13.33	13.16	13.22	13.18	13.22	13.25	13.33	13.19	0.10
Cr2O3	0.00	0.00	0.04	0.00	0.00	0.00	0.37	0.00	0.02	0.02	0.00	0.37	0.07	0.14
Fe2O3	0.00	0.00	0.00	0.00	0.00	0.00	0.00	0.00	0.00	0.00	0.00	0.00	0.00	0.00
FeO	17.41	17.28	17.23	17.55	17.70	16.61	16.82	16.77	16.59	16.85	16.89	16.95	17.05	0.37
MnO	0.56	0.70	0.67	0.71	0.73	0.66	0.60	0.67	0.71	0.68	0.67	0.66	0.67	0.05
MgO	14.00	13.59	13.39	13.24	12.61	13.23	13.39	13.30	13.36	13.11	13.22	13.17	13.30	0.32
CaO	0.03	0.03	0.03	0.02	0.05	0.01	0.01	0.01	0.06	0.00	0.00	0.00	0.02	0.02
Na2O	0.10	0.11	0.10	0.10	0.09	0.12	0.11	0.09	0.11	0.07	0.07	0.11	0.10	0.02
K2O	8.86	9.47	9.23	9.27	8.98	9.40	9.35	9.35	9.54	9.47	9.42	9.34	9.31	0.20
Sum	94.35	94.45	93.97	93.53	92.75	93.48	94.13	93.87	94.19	94.00	94.21	94.77	93.97	0.53
Si	2.87	2.87	2.87	2.86	2.84	2.86	2.86	2.86	2.86	2.86	2.86	2.86	2.86	0.01
Ti	0.15	0.16	0.16	0.16	0.19	0.18	0.18	0.18	0.19	0.19	0.19	0.12	0.17	0.02
Al	1.19	1.17	1.20	1.19	1.21	1.21	1.19	1.20	1.19	1.20	1.20	1.20	1.20	0.01
Al(IV)	1.14	1.13	1.13	1.15	1.16	1.14	1.14	1.14	1.14	1.14	1.14	1.14	1.14	0.01
Al(VI)	0.05	0.04	0.07	0.05	0.04	0.07	0.05	0.06	0.05	0.06	0.06	0.06	0.05	0.01
Cr	0.00	0.00	0.00	0.00	0.00	0.00	0.00	0.00	0.00	0.00	0.00	0.00	0.00	0.00
Fe3+	0.00	0.00	0.00	0.00	0.00	0.00	0.00	0.00	0.00	0.00	0.00	0.00	0.00	0.00
Fe2+	1.11	1.11	1.11	1.14	1.16	1.07	1.08	1.08	1.06	1.08	1.08	1.08	1.10	0.03
Mn	0.04	0.05	0.04	0.05	0.05	0.04	0.04	0.04	0.05	0.04	0.04	0.04	0.04	0.00
Mg	1.59	1.55	1.53	1.53	1.47	1.52	1.54	1.52	1.53	1.50	1.51	1.50	1.52	0.03
Ca	0.00	0.00	0.00	0.00	0.00	0.00	0.00	0.00	0.01	0.00	0.00	0.00	0.00	0.00
Na	0.02	0.02	0.01	0.02	0.01	0.02	0.02	0.01	0.02	0.01	0.01	0.02	0.01	0.00
K	0.86	0.93	0.91	0.92	0.90	0.93	0.92	0.92	0.93	0.93	0.92	0.91	0.91	0.02

Table 3.2 (left): *Mineral chemical analyses of biotites from fresh granites. Formula is calculated on the base of 22 oxygen. Analyses are given in wt%.*

Table 3.3 (below): *Mineral chemical analyses of chlorites from fresh (core index 4666) and stage I altered (2540) granites. Analyses are given in wt%.*

3.3	fresh	fresh	fresh	fresh	fresh	fresh	fresh	fresh	fresh			stage I	stage I	stage I	stage I	stage I	stage I		
Sample	4666-7	4666-8	4666-9	4666-10	4666-11	4666-12	4666-13	4666-14	4666-33	average	std	2540-2-1	2540-2-3	2540-2-4	2540-2-5	2540-2-6	2540-3-5	average	std
Type	Chlorite	Chlorite	Chlorite	Chlorite	Chlorite	Chlorite	Chlorite	Chlorite	Chlorite			Chlorite	Chlorite	Chlorite	Chlorite	Chlorite	Chlorite		
SiO2	28.52	28.72	28.82	27.72	27.89	28.07	28.47	29.94	28.79	28.55	0.66	27.36	27.07	29.39	27.70	27.38	27.57	27.74	0.83
TiO2	0.03	0.05	0.06	0.08	0.00	0.04	0.03	0.25	0.06	0.07	0.07	0.01	0.07	0.10	0.04	0.02	0.00	0.04	0.04
Al2O3	16.78	17.48	16.49	18.00	18.05	17.57	17.25	15.42	16.50	17.06	0.85	19.27	20.03	19.61	19.22	18.75	18.22	19.18	0.64
Cr2O3	0.02	0.00	0.01	0.07	0.00	0.03	0.00	0.02	0.03	0.02	0.02	0.02	0.05	0.01	0.04	0.01	0.05	0.03	0.02
Fe2O3	0.00	0.00	0.00	0.00	0.00	0.00	0.00	0.00	0.00	0.00	0.00	0.00	0.00	0.00	0.00	0.00	0.00	0.00	0.00
FeO	19.80	18.86	20.23	19.90	19.69	19.36	19.15	19.70	20.53	19.69	0.52	20.93	22.49	23.47	19.63	20.89	21.03	21.41	1.36
MnO	0.89	0.92	0.83	1.23	1.07	0.93	1.03	0.75	0.85	0.95	0.14	1.34	0.77	0.25	0.99	1.02	1.06	0.90	0.37
MgO	19.93	20.40	19.77	19.44	19.99	20.08	20.61	20.47	19.91	20.07	0.37	17.83	15.55	13.51	18.20	18.41	18.02	16.92	1.97
CaO	0.07	0.06	0.08	0.07	0.04	0.06	0.04	0.13	0.12	0.07	0.03	0.08	0.04	0.11	0.04	0.01	0.01	0.05	0.04
Na2O	0.02	0.01	0.00	0.00	0.00	0.01	0.02	0.03	0.00	0.01	0.01	0.02	0.01	0.06	0.04	0.00	0.03	0.03	0.02
K2O	0.05	0.07	0.03	0.00	0.01	0.00	0.04	0.32	0.01	0.06	0.10	0.05	0.01	0.78	0.03	0.00	0.03	0.15	0.31
Sum	86.09	86.58	86.31	86.50	86.74	86.15	86.65	87.03	86.80	86.54	0.31	86.89	86.10	87.29	85.91	86.49	86.02	86.45	0.55
Si	2.98	2.97	3.01	2.89	2.89	2.93	2.95	3.09	3.00	2.97	0.06	2.85	2.86	3.06	2.90	2.87	2.91	2.91	0.08
Ti	0.00	0.00	0.01	0.01	0.00	0.00	0.00	0.02	0.00	0.01	0.01	0.00	0.01	0.01	0.00	0.00	0.00	0.00	0.00
Al	2.07	2.13	2.03	2.21	2.21	2.16	2.11	1.88	2.02	2.09	0.11	2.37	2.50	2.41	2.37	2.31	2.26	2.37	0.08
Al(IV)	1.02	1.03	0.99	1.11	1.11	1.07	1.05	0.91	1.01	1.03	0.06	1.15	1.14	0.94	1.10	1.13	1.09	1.09	0.08
Al(VI)	1.05	1.10	1.04	1.11	1.10	1.09	1.05	0.97	1.02	1.06	0.05	1.22	1.36	1.47	1.26	1.18	1.17	1.28	0.12
Cr	0.00	0.00	0.00	0.01	0.00	0.00	0.00	0.00	0.00	0.00	0.00	0.00	0.00	0.00	0.00	0.00	0.00	0.00	0.00
Fe3+	0.00	0.00	0.00	0.00	0.00	0.00	0.00	0.00	0.00	0.00	0.00	0.00	0.00	0.00	0.00	0.00	0.00	0.00	0.00
Fe2+	1.73	1.63	1.77	1.74	1.71	1.69	1.66	1.70	1.79	1.71	0.05	1.83	1.99	2.05	1.72	1.83	1.85	1.88	0.12
Mn	0.08	0.08	0.07	0.11	0.09	0.08	0.09	0.07	0.08	0.08	0.01	0.12	0.07	0.02	0.09	0.09	0.09	0.08	0.03
Mg	3.11	3.14	3.08	3.02	3.09	3.12	3.18	3.15	3.09	3.11	0.05	2.77	2.45	2.10	2.84	2.87	2.83	2.64	0.31
Ca	0.01	0.01	0.01	0.01	0.00	0.01	0.01	0.02	0.01	0.01	0.00	0.01	0.00	0.01	0.00	0.00	0.00	0.01	0.00
Na	0.00	0.00	0.00	0.00	0.00	0.00	0.00	0.01	0.00	0.00	0.00	0.00	0.00	0.01	0.01	0.00	0.01	0.01	0.00
K	0.01	0.01	0.00	0.00	0.00	0.00	0.01	0.04	0.00	0.01	0.01	0.01	0.00	0.10	0.00	0.00	0.00	0.02	0.04
Sum	12.05	12.10	12.00	12.21	12.21	12.15	12.11	11.85	12.01	12.08	0.11	9.96	9.88	9.78	9.92	9.98	9.96	9.92	0.07
Fe/(Fe/Mg)	35.79	34.14	36.47	36.48	35.59	35.10	34.28	35.06	36.64	35.51	0.93	39.70	44.80	49.36	37.69	38			

of the lower section but is not observed in the upper section. As reported e.g., by Stumm and Morgan (1996) or Appelo and Postma (1999) meteoric fluids can oxidize pyrite resulting in strongly acidic fluids. The following reactions may occur:

(2) $FeS_2 + 7/2O_2 + H_2O = Fe^{2+} + 2SO_4^{2-} + 2H^+$
(3) $Fe^{2+} + 1/4O_2 + H^+ = Fe^{3+} + 1/2H_2O$
(4) $Fe^{3+} + 3H_2O = Fe(OH)_3 + 3H^+$
(5) $FeS_2 + 14Fe^{3+} + 8H_2O = 15Fe^{2+} + 2SO_4^{2-} + 16H^+$

The oxidation of the sulfide in pyrite to sulfate (reaction 2) releases dissolved Fe^{2+} and acidity into the water. The dissolved Fe^{2+} undergoes oxygenation to Fe^{3+} (reaction 3), which then hydrolyzes to form hydroxide (reaction 4), releasing more acidity to the stream (Stumm and Morgan 1996). The Fe^{3+} can also be reduced by pyrite itself (reaction 5). Sulfide is again oxidized and acidity is released along with additional Fe^{2+}.

The above reactions are restricted to catclasites because pyrite occurs mainly within veins (Fig. 3.2-II j). With further distance from the cataclased granites martite shows no decomposition. This can be explained by fluid-wall rock interactions that neutralize the acidic fluids (e.g., Marescotti et al. 2000). In contrast to the reaction 4, the granites from the upper borehole section show a high content of fine-grained hematite.

Lower fault zones

The studied fault zones of the lower borehole section occur in the depth interval between 2150 - 2180 m, which belongs to a recently active zone of circulating fluids. The second fault zone is in the depth interval of 2210 and 2230 m (Fig. 3.1). Magnetite was oxidized to martite. In contrast to the upper section hematite is not the dominant magnetic mineral. Instead of hematite, illite and pyrite (Fig. 3.2-II j) are now the common minerals in the veins. The magnetic mineral assemblage of these two studied fault zones differs. In the depth of 2157 m (sample 4701), magnetite and martite are not observed. Probably, besides pyrite they were no longer stable during the hydrothermal activity and thus decomposed (Fig. 3.2-II i). In the second fault zone however, magnetite and martite are present. Now, a partial reduction of martite back to magnetite is observed (Fig. 3.2-II h). This accessory mineral assemblage indicates reducing fluids, which are probably associated with younger processes. This can be concluded from the occurrence of organic matter in the lower fault zones reported by Lédesert et al. (1999). These authors described organic matter in fluids from the lower fault zones and related the infiltration of organic matter to overlying sedimentary reservoirs. Such organic matter provides a reasonable explanation for the martite to magnetite reduction, as has been reported, for example, in iron-formations by Morris (1993). This reaction can be expressed as:

(6) $6Fe_2O_3 + CH_2O \rightarrow 4Fe_3O_4 + CO_2$

2. Thermomagnetic analyses of whole rock samples

Temperature dependent magnetic susceptibility ($\kappa(T)$) measurements aid the identification of magnetic minerals. The κ shows a temperature dependent behavior for ferro- and paramagnetic minerals. The changes that occur during heating and cooling of samples can be used to determine the Curie temperature (T_C) for ferrimagnetic minerals and Néel temperature (T_N) for antiferromagnetic minerals. When heated above T_C and T_N the ferrimagnetic minerals lose their magnetic ordering and pass into magnetically disordered or paramagnetic states. During $\kappa(T)$ measurements potential alterations of magnetic phases can cause an irreversible change during heating and cooling runs, reflective of mineral reactions that occur during heating. Such reactions are normally undesired because they blur and complicate the T_C of the original mineralogy and therefore inhibit the identification of ferrimagnetic minerals. On the other hand, such irreversible behavior can be used to calculate an artificial alteration index (Al-index =

$\kappa_{CTroom} - \kappa_{HTroom}$). This Al-index provides a measure of the relative alteration degree of the material after experiment heating and should not be confused with the natural hydrothermal alteration of the Soultz granite. In order to characterize the magnetic mineral assemblage of the hydrothermally altered Soultz granite, κ(T) measurements were performed and correlated to the recognized stages of alteration. Furthermore, the temperature at which thermally induced mineral reactions begin was detected experimentally using repeated cycles of heating and cooling.

Fresh granite

Fresh granites are characterized by ferrimagnetic κ(T) curves typical for magnetite (Fig. 3.5 a, b, d). The low-temperature run shows a Verwey transition (T_V) at –150 °C caused by the change of ordering of Fe^{3+} and Fe^{2+} ions in octahedral sites, which distorts the cubic spinel lattice to a monoclinic structure below T_V. The relatively sharp rise at T_V and subsequent constant κ-values indicate multi-domain (MD) behavior of magnetite. Heating the sample to 700 °C shows an abrupt drop of κ to low values between 580 and 590 °C representing the T_C of pure

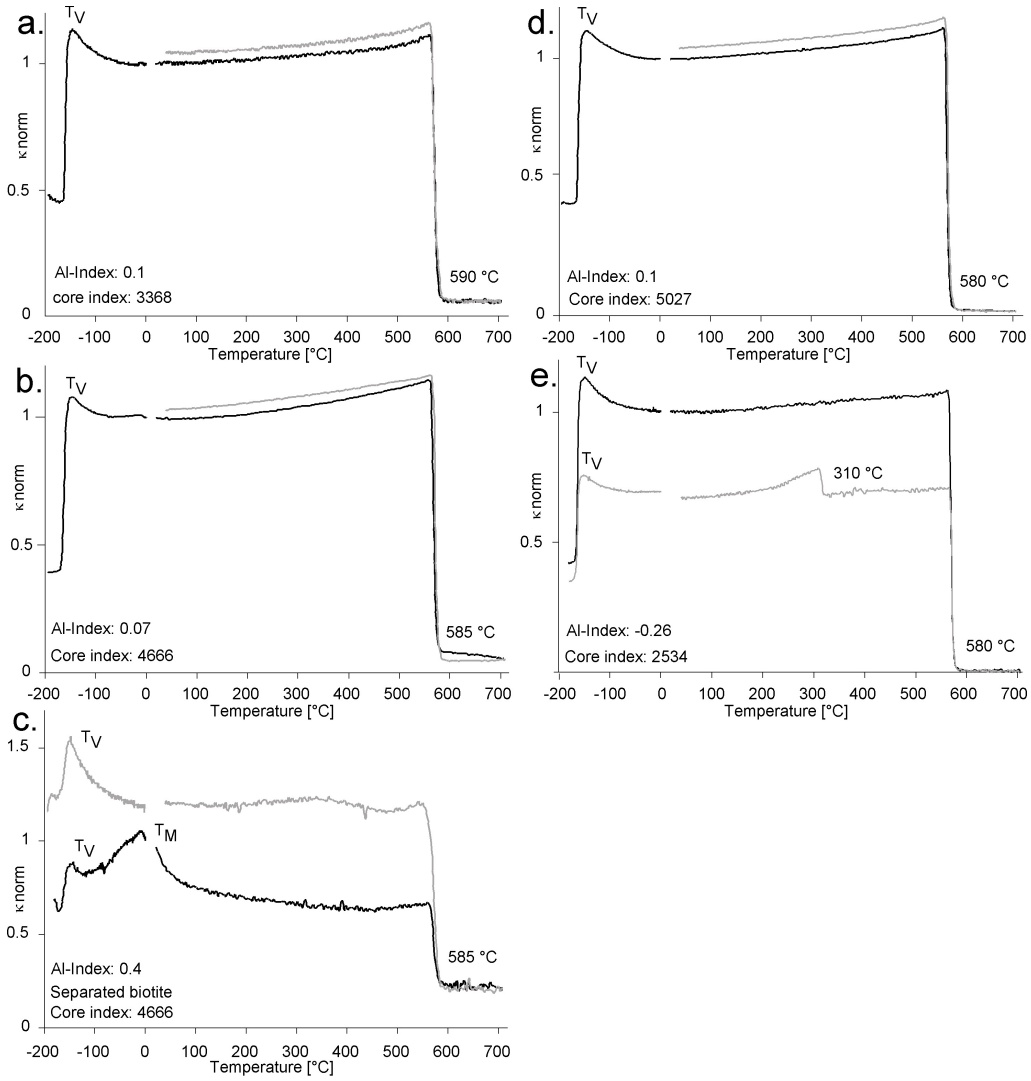

Fig. 3.5: *Normalized magnetic susceptibility (κnorm) as a function of temperature for fresh and stage I altered granites. Black curve represents the heating, grey curve the cooling run. Verwey transitions (T_V) at ~-150 °C and T_Cs (580 – 590 °C) indicate pure, multidomain magnetite. A relative good irreversibility of the κ(T) curves is indicated by small alteration index values (Al-index).* ***a.*** *Core index 3368,* ***b.*** *4666,* ***c.*** *separated biotite from core 4666,* ***d.*** *5027.* ***e.*** *Core index 2534 shows an additional T_C at 310 °C during the cooling run and negative Al-index indicating decomposition of magnetite and neoformation of pyrrhotite from pyrite during heating at temperatures > 580 °C.*

magnetite (compare also Table 3.1). Above T_C the magnetic behavior changes from ferrimagnetic to paramagnetic order. The κ(T) curves of fresh granite show relative good reversibility. However, samples do display some irreversibility with either increasing or decreasing κ-values indicated by a relatively small Al-index (< 0.1). Such changes can be correlated to a particular mineral assemblage. This small positive irreversibility can be correlated to the formation of magnetite during heating of the paramagnetic biotite, which has originally an antiferromagnetic hematite parallel to the cleavage. These features were recognized in biotite separated from the fresh granite using a magnet-separator and a permanent magnet (Fig. 3.5 c). Here, the low-temperature run revealed small amounts of magnetite in addition to hematite, which could be identified by the Verwey transition and Morin transition (T_M), respectively. Below T_M (~ –15 °C) the spontaneous magnetization of hematite changes its direction from lying in basal plane to orienting parallel to the crystallographic c-axis (e.g., Soffel 1991). The Morin transition is related to hematite's magnetic isotropic point and does not represent a crystallographic change, like the Verwey transition of magnetite. The gradual rise to the T_M and the slightly elevated T_M of -10 °C in Fig. 3.5 e can be explained either by the fine grain size of hematite or by impurities in the hematite lattice as reported by de Boer et al. (2001). The irreversible run, with elevated κ in the cooling run, and the distinct peak at T_V confirms the formation of magnetite during the heating experiment.

In sample 2534 (Fig. 3.5 e) the negative irreversibility (Al-index = -0.26) of the κ(T) curves was caused by decreasing κ-values associated with an additional T_C of 310 °C during the cooling run reflecting the formation of pyrrhotite during heating (e.g., Kontny et al. 1997). It is probable that pyrrhotite forms from pyrite during heating, because pyrrhotite was not observed microscopically in the original sample. Decreased κ-values and the negative irreversibility in Fig. 3.5 e indicate, that magnetite became instable during heating to 700 °C in addition to the formation of pyrrhotite. The following reaction may occur during heating:

(7) $Fe_3O_4 + 3FeS_2 \rightarrow 6FeS + 2O_2$

Hereby, magnetite is decomposed on the one hand and on the other hand, oxidized by the released oxygen. In contrast to altered granites, pyrite does not occur in fresh granites, which are distanced to the fault zones. The occurrence of pyrite within this depth interval indicates that pyrite was probably already formed during the localized stage I. Pyrite is a common mineral in stage II granites of the lower borehole section and was later oxidized under near surface conditions. The detection of pyrite in the central part of the profile supports the hypothesis that pyrite was more widespread in the granite before its oxidation by near surface fluids.

Stage I altered granite

The κ(T) curves of stage I altered granite are shown in Fig. 3.6. All curves show magnetite in the heating run with its typical T_V at –150 °C and T_C at 590 °C. Although martite was observed microscopically neither its T_M nor the T_C (~680 °C) were recorded during κ(T)-measurements. The hematite (martite) content is probably too low for identification by κ(T)-measurement because of the relatively low κ of hematite, which is three orders of magnitude smaller than the κ of magnetite. Irreversible behavior of κ(T) curves, with strongly increased κ but similar T_Cs between 585 and 590 °C and T_V at –150 °C during the cooling run, indicate the formation of new magnetite during the heating of all stage I altered samples. In the stage I altered granite the experimentally formed magnetite can be attributed to the alteration of martite. The reaction of hematite to magnetite requires one third of the Fe^{3+} ions in martite to be reduced to Fe^{2+}. The following redox reactions may occur during heating:

(8) $3Fe_2O_3 + H_2 \rightarrow 2Fe_3O_4 + H_2O$

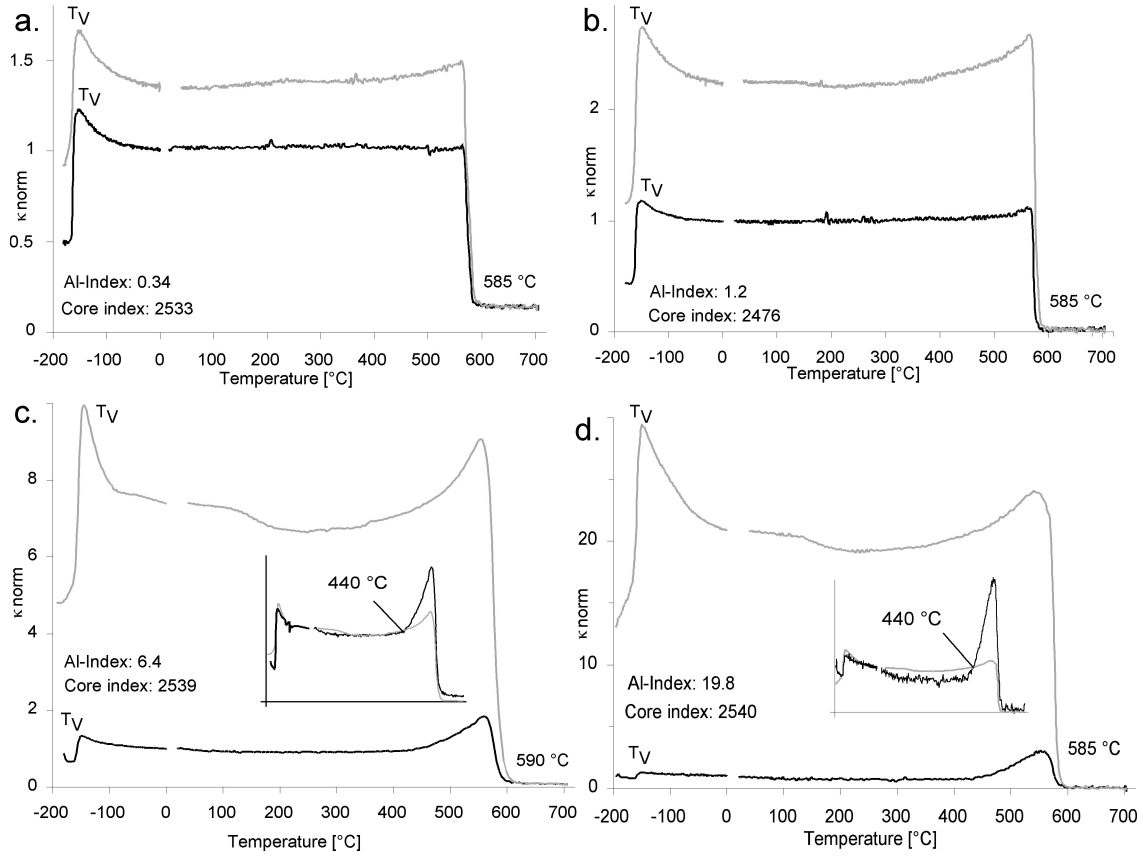

Fig. 3.6: *Normalized magnetic susceptibility (κnorm) as a function of temperature for stage I altered granites from the depth interval between 1550 and 1580 m. Black curve represents the heating run, grey curve the cooling run. Verwey transitions (T_V) at ~-150 °C and T_Cs (585 – 590 °C) indicate pure, multidomain magnetite. Small alteration index (Al-index) indicates a high magnetite content in sample before heating, high Al-index indicates small magnetite content before heating and a formation of magnetite with the same T_C during heating.* ***a.*** *Core index 2533,* ***b.*** *2476,* ***c.*** *2539 and* ***d.*** *2540.* ***Inlays*** *in c. and d. show curves where the heating run is normalized to kTroom of the heating run and the cooling run is normalized to kTroom of the cooling run with intersection points at ~440 °C.*

Hydrogen may originate from tightly held hydroxyl groups in the hematite lattice, which were released by the thermal activation as reported by de Boer and Dekkers (2001). If calcite is present during heating, like in the stage I altered granite, the following reaction may occur:

(9) $CaCO_3 \rightarrow CaO + CO_2$
(10) $CO_2 + H_2 \rightarrow CO + H_2O$
(11) $3Fe_2O_3 + CO \rightarrow 2Fe_3O_4 + CO_2$.

A positive Al-index reflects the amount of newly formed magnetite, which is related to the magnetite content in the original sample. The more martite is present, the more magnetite is formed during heating. Therefore, the Al-index can be related to the degree of magnetite martitization in the stage I altered Soultz granite. Magnetite formation due to the alteration of biotite during heating is here negligible. The low Al-index of 0.34 (Fig. 3.6 a) represents the weakest martitization and a high Al-index of 19.8 (Fig. 3.6 d) the strongest degree of martitization. The Verwey transition is well developed in all samples indicating stoichiometric (Özdemir and Dunlop 1993) and MD (Muxworthy 1999) magnetite relics in the martite grains. The increased peak just before T_C seems to be higher in the cooling run (Fig. 3.6 c, d). Such peaks normally correspond to a Hopkinson peak, which is highest for small grain sizes within the single-domain (SD) threshold. However, when normalizing the cooling run to the κ-value of the cooling run (normally, normalizing only to the heating run), both peaks are seen to behave the opposite way (Fig. 3.6 c, d see inlays). This suggests

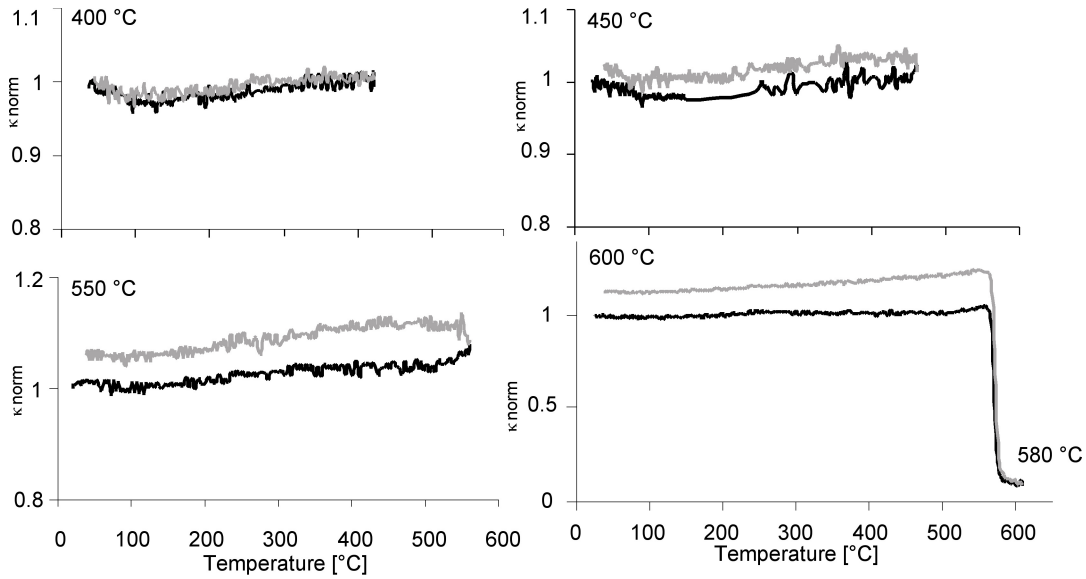

Fig. 3.7: *Normalized magnetic susceptibility (κnorm) as a function of temperature during repeated heating and cooling cycles of stage I altered granite (core index 2540) from the 400 to 600 °C steps. Black curve represents the heating run, grey curve the cooling run. A weak irreversibility starts during the 450 °C step indicating the initial formation of magnetite confirmed by the T_C of 580 °C during the 600 °C step.*

that the strong peak developed during cooling run is an artifact derived from the normalization. The Hopkinson peak of the cooling run is in fact small, which indicates the formation of relatively large grain sizes. The peak observed during the heating run is caused by increasing κ associated with the formation of new magnetite, and does not represent a Hopkinson peak. If this relationships are valid, the intersection points of the heating and cooling curves (inlays Fig. 3.6 c, d) mark the approximately temperature where magnetite begins to form.

In order to determine more precisely, the initial temperature of magnetite formation and the associated irreversibility, repeated heating/cooling experiments were performed (Fig. 3.7). Hereby, the sample is progressively and repeatedly heated and cooled to temperatures of 600 °C done by 50 °C steps. A weak irreversible behavior starts at 450 °C and correlates well with the intersection points in Figure 3.6 c and d (see inlay). By heating the sample repeatedly to 600 °C, the T_C of 580 °C confirms magnetite as the newly formed magnetic mineral.

Stage II altered granite

The κ(T) curves from stage II altered granites (Fig. 3.1) of the upper borehole section are shown in Figure 3.8. The curves of the lower borehole section are shown in Figure 3.9. Samples with martite and small magnetite relics either only show poorly developed T_V, or the T_V is suppressed due to the degree of magnetite oxidation (Özdemir and Dunlop 1993). In contrast to stage I altered granites, where only a single T_C typical for magnetite occurs, the κ(T) curves of stage II altered granites mostly show an additional T_Cs ranging between 200 and 680 °C (Fig. 3.8 and 3.9, compare also Table 3.4). These T_Cs are correlated to the experimental alteration of the stage II mineral assemblage during the heating process. This stage II mineral assemblage shows a strong heterogeneity, with different amounts of the paramagnetic minerals Fe-carbonates, illite, pyrite and antiferromagnetic hematite. These minerals react during the heating process to produce ferrimagnetic minerals with varying T_Cs and Al-indexes, which causes more complex κ(T) curves. The small-scaled heterogeneity of the altered Soultz granite results in different κ(T) curves even from the same sample location. Therefore, a general classification

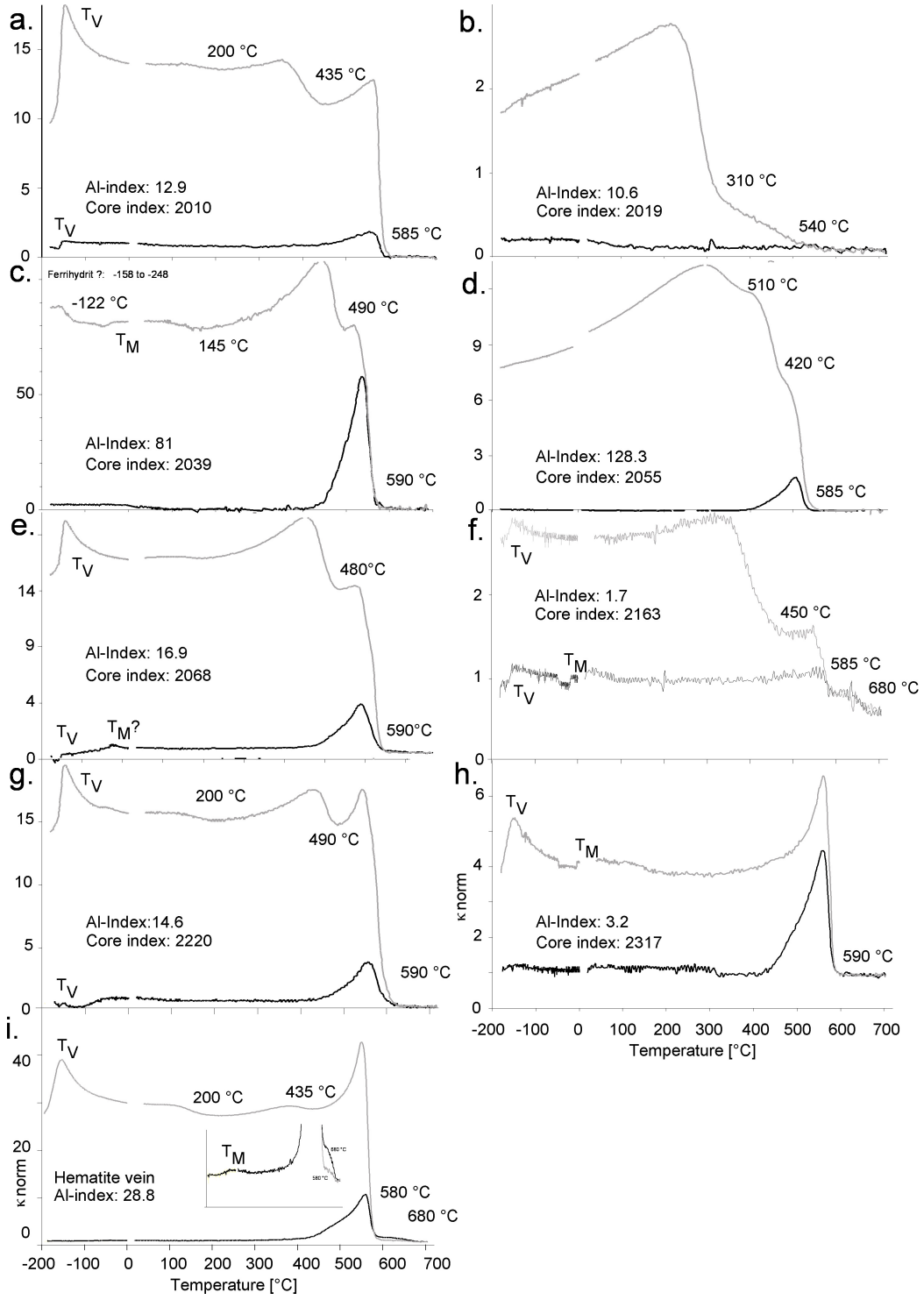

Fig. 3.8: *κ(T) curves showing normalized magnetic susceptibility (κnorm) of stage II altered granites from the* ***upper borehole section****. Black curve represents the heating, grey curve the cooling run.* ***a.*** *Core index 2010: wall rock,* ***b.*** *core index 2019: wall rock,* ***c.*** *core index 2039: cataclasite,* ***d.*** *core index 2055: wall rock,* ***e.*** *core index 2068: cataclasite,* ***f.*** *core index 2163: cataclasite,* ***g.*** *core index 2220: wall rock,* ***h.*** *core index 2317: cataclasite.*

into cataclasites and their wall rocks based on the κ(T) measurements is not possible. The Al-index varies between 0.94 and 128 (Table 3.4) and cannot be correlated to the degree oxidation degree of magnetite, because martite is not the only mineral that reacts during heating to form ferrimagnetic phases. The Al-index of stage II altered granites depends on (i) the type of magnetic mineral assemblage (ferri-, para- or antiferromagnetic minerals), (ii) their readiness to react, and (iii) the availability of

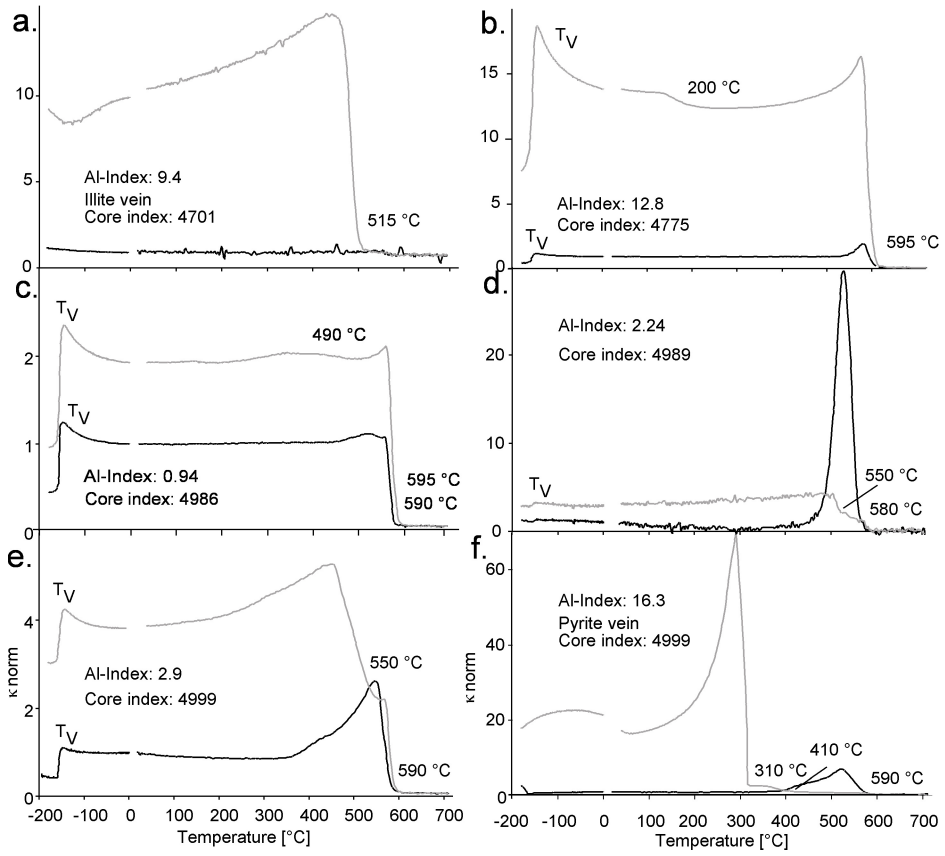

Fig. 3.9: *Normalized magnetic susceptibility (κnorm) as a function of temperature of stage II altered granites from the* ***lower borehole section****. Black curve represents the heating, grey curve the cooling run.* ***a.*** *Core index 4701: cataclasites,* ***b.*** *core index 4775: wall rock,* ***c.*** *core index 4986: wall rock,* ***d.*** *core index 4989: cataclasite,* ***e.*** *core index 4999: cataclasite,* ***f.*** *Pyrite from a vein in core 4999.*

paramagnetic ions.

The κ(T) curves of magnetite- and Fe-carbonate-bearing samples are presented in Figures 3.8 a, e, g and 3.10 c-e. They all show T_V and T_C typical for magnetite in both heating and cooling runs, as well as a positive Al-index. In addition, several T_Cs between 400 and 600 °C occur, which indicates the formation of new ferrimagnetic phases during heating. Similar T_Cs have been already reported by Isambert et al. (2003), who observed a neoformation of Mn-bearing magnetite when heating Mn-bearing siderite. These above mentioned T_Cs are therefore correlated to the modification of Fe-bearing carbonates during heating, which were identified in these samples using optical microscopy. The reaction of Fe- and Mn-bearing carbonates into ferrite and their implications for the magnetic alteration mineral assemblage of the Soultz granite will be discussed later (see Chapter 3 herein: Ferrous carbonates).

Figure 3.8 b shows a κ(T) curve similar to those of stage I altered granites, which indicates magnetite and martite as the dominant magnetic minerals. Samples with progressively oxidized magnetite and abundant Fe-bearing carbonates (Fig. 3.8 b-d) show κ(T) curves with suppressed T_V and a high Al-index. The only two κ(T) curves indicating the presence of hematite, are shown in Fig. 3.8 f and i. Hematite was identified by its T_C at 680 °C and by its poorly developed T_M (hematite vein, Fig. 3.8 i) and relatively well-developed T_M at –10 °C (whole rock sample, Fig. 3.8 f). Poorly developed Morin transition indicates incorporated impurities or poorly crystalline hematite (e.g., Bando et al. 1965, Morin 1950). These samples represent cataclastic granites, which still contain magnetite indicated by its T_V and T_C. The presence of Fe-bearing carbonates are indicated by the formation of a ferrimagnetic phase with a T_C at 450 and 430°C. Although hematite was microscopically identified it could not be recognized in other samples using κ(T) measurements. It is not

Sample	1. Low-temperature	High-temperature (T_C [°C]) Heating	Cooling	2.Low-temperature	Reactant	Product	AI-index
Fresh granite							
2534	VT	580	580, 310	VT	mag, pyrite	pyrrhotite	-0.26
3368	VT	590	590	VT	mag, bio	mag	0.1
4666	VT	585	585	VT	mag, bio	mag	0.05
5027	VT	580	580	VT	mag, bio	mag	0.1
Stage I (1550-1580 m)							
2533	VT	585	585	VT	mag, mar	mag	0.34
2476	VT	585	585	VT	mag, mar	mag	1.2
2539	VT	590	590	VT	mag, mar	mag	6.4
2540	VT	585	585	VT	mag, mar, calcite	mag	19.8
Stage II, upper part (1417 - 1550 m)							
2010	VT	585	585, 435	VT	mar, Fe-car	mag, ferrite	13
2011	VT	590	590, 450	VT	mar, Fe-car	mag, ferrite	2
2019	-	-	540, 310	-	illite, pyrite	ferrite, pyrrhotite	11
2039	-	590	590, 490	MT	mar, Fe-car	hem, mag, ferrite	81
2055	-	585	585, 510, 420	-	mar, Fe-car	ferrite	128
2068	VT, MT	590	590, 480	VT	hem, mar, Fe-car	mag, ferrite	17
2127	-	590	590, 510	VT	mar, Fe-car	mag, ferrite	22
2163	VT, MT	585, 680	680, 585, 450	VT	hem, mar, Fe-car	mag, ferrite	2
2220	VT	590	590, 490	VT	mag, mar, Fe-car	mag, ferrite	15
(hem vein) 2220	-	580, 680	580, 435	VT	mar, Fe-car	mag, ferrite	29
2281	VT	590	590	VT	mag, mar	mag	6
2317	-	590	590	VT, MT	mar	mag, hem	3.2
2764	VT	580	580, 490	VT	mag, mar, Fe-car	mag, ferrite	16
2807	-	580	580	VT	mar	mag	49
Stage II, lower part (2150 - 2227 m)							
(illite vein) 4701	-	-	525	-	illite	ferrite	19
4775	VT	595	595	VT	mag, mar	mag	13
4986	VT	590	595	VT	mag, mar, Fe-car	mag	1
4989	VT	580	580, 550	VT	mag, mar, Fe-car	mag, ferrite	2.2
4999	VT	590	590, 550	VT	mag, mar, Fe-car	mag, ferrite	3
(pyr vein) 4999	VT	590	410, 310	-	Fe-car, pyrite	ferrite, pyrrhotite	16

Table 3.4: *Magnetic minerals identified from κ(T) curves of all measured samples. VT: Verwey transition, MT: Morin transition, bio: biotite, Fe-car: Fe-bearing carbonates, hem: hematite, mag: magnetite, mar: martite, pyr: pyrite.*

clear, if the absence of T_M in such samples is due to the dominance of the magnetite signal or due to a small grain size of hematite or other incorporated impurities (e.g., de Boer et al. 2001, Bando et al. 1965). Another possible explanation could be the complete reaction of hematite to magnetite. The alteration of hematite to magnetite will be discussed later (see Chapter 3 herein: Hematite).

The results of an illite-dominated sample, shown in Figure 3.9 a, differs from the thermomagnetic behavior of other typical stage II altered granites. This illite-dominated sample shows a κ increase during the cooling and not during the initial heating run. Such behavior reflects the formation of a ferrimagnetic phase at temperatures > 515 °C. The modification of illite into a ferrimagnetic behavior will be discussed later (see Chapter 3 herein: Illite).

A sample dominated by pyrite is shown in Figure 3.9 f. Pyrite is a paramagnetic mineral and converts to ferrimagnetic pyrrhotite on heating to ca. 550 – 600 °C in inert atmosphere (Hoare et al. 1988). Pyrite cannot be identified directly, but by the formation of pyrrhotite, which is seen in the cooling run (T_C = 310 °C, Fig. 3.9 f). Although observed microscopically, pyrite could not be identified in other samples from the lower section. It is not clear if the thermo-induced reaction to pyrrhotite is suppressed due to distinct Eh-pH conditions in the test tube, or if the T_C of pyrrhotite is masked by the presence of magnetite, which might be part of the original mineral assemblage or formed during the experiment.

3. Thermomagnetic analyses of mineral phases

Near monomineralic phases of known composition were investigated in order to understand the complex behavior of the κ(T) curves of the altered Soultz granite. The mineral samples such as a fine-grained and coarse-grained hematite, iron carbonates and

Type	*Illite*	*B6*	*9.4-2*	*Siderite*	*Ankerite*
SiO2	49.30	19.95	15.02	6.99	1.77
TiO2	0.55	0.00	0.04	0.00	0.00
Al2O3	24.25	0.15	1.04	0.14	0.09
Cr2O3	-	0.00	0.00	0.00	0.00
Fe2O3	7.32	76.81	80.55	50.28	3.58
FeO	0.55	-	-	-	-
MnO	0.03	0.02	0.07	7.65	1.01
MgO	2.56	0.03	0.16	3.14	5.84
CaO	0.43	0.05	0.35	0.30	12.22
Na2O	0.00	0.00	0.07	0.00	0.00
K2O	7.83	0.00	0.03	0.00	0.00
P2O5	0.08	0.00	0.03	0.00	0.00

Table 3.5: *Whole rock ICP analyses of mineral phases. Analyses are given in wt%. IMT-2 illite: Silver Hill, Montana, USA; HemB6: (coarse-grained hematite) BIF, Brazil; Hem9.4-2 (fine-grained hematite) Antiatlas, Morocco; Siderite: Quarry Pfannenberger Einigkeit, Siegen, Germany; Ankerite: Quarry Himmelfahrt, Freiberg, Germany.*

illite were chosen because they are representative mineral assemblage of the stage II alteration. X-ray diffraction was used for the identification and characterization of the material before and after the magnetic heating experiments.

Hematite

Hematite normally displays a weak ferrimagnetic behavior resulting from the spin-canted antiferromagnetic moment, which disappears above its T_C at ~680 °C. Another characteristic feature of hematite is the susceptibility drop below –15 °C (T_M). In order to study the κ(T) behavior of single hematite-phase, two samples with dominantly fine- and coarse-grained hematite were investigated in detail.

Fine-grained hematite

The fine-grained hematite originated from a fault zone in Precambrian granitoid of the Anti-Atlas, Morocco, and shows some intergrowth with quartz. Chemical analysis revealed that this hematite is relatively pure (Table 3.5) with only 1.04% Al_2O_3 incorporated. In the powdered state, the hematite shows its distinct reddish color. The κ(T) curve (Fig. 3.10 a) shows no T_M in the low-temperature run, which can be caused by impurities, probably the incorporation of Al, or by the small grain size (de Boer et al. 2001). Certainly the absence of T_M in the 9.4-2 hematite more likely reflects the small grain size of this sample. Bando et al. (1965), for example, reported a completely suppressed Morin transition in pure hematite with grains smaller than ~0.02-0.03 µm. During heating the 9.4-2 hematite above room temperature a weak hump and a T_C at 360 °C appears. During further heating, κ subsequently increases to form a distinct peak and a T_C at 685 °C, typical for hematite. The narrow Hopkinson peak (HP) suggests a relatively small distribution of grain sizes within the SD threshold. During cooling, this T_C appears again, indicating that the fine-grained hematite has not been significantly modified during the heating procedure. However during subsequent cooling, a new T_C appears at 570 °C indicating some reactions to magnetite during heating, as is confirmed

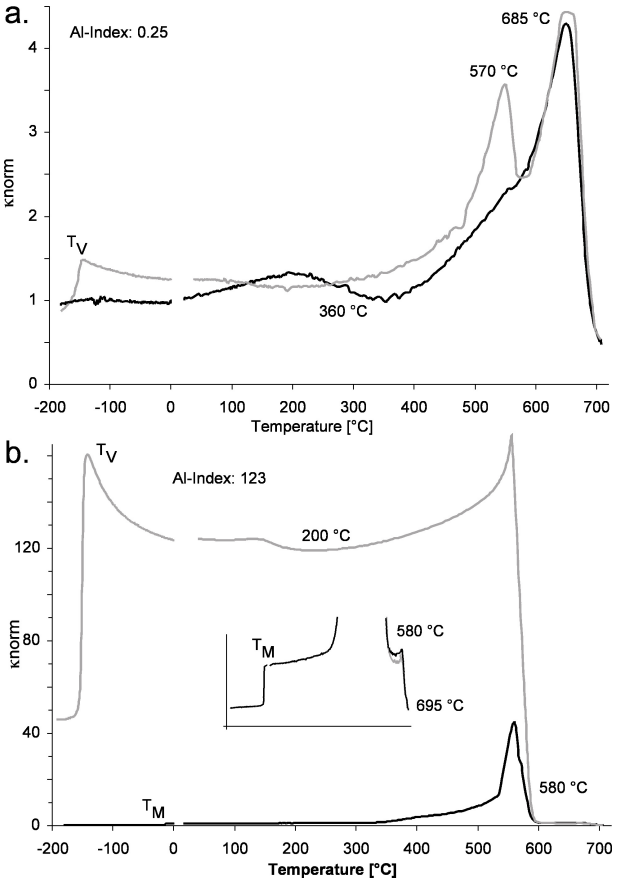

Fig. 3.10: *Normalized magnetic susceptibility (κnorm) of hematite as a function of temperature. Black curve represents the heating, grey curve the cooling run.* ***a.*** *The fine-grained hematite (9.4-2, fault zone in granitoids of the Anti-Atlas, Morocco), shows no Morin transition but a T_C at 685 °C.*
b. *The coarse-grained hematite (B6, Banded Iron Formation of the mine Conceição in Brazil) shows a Morin transition (T_M) at ~ –15 °C and a T_C at 695 °C, which is shown in the figure inlay.*

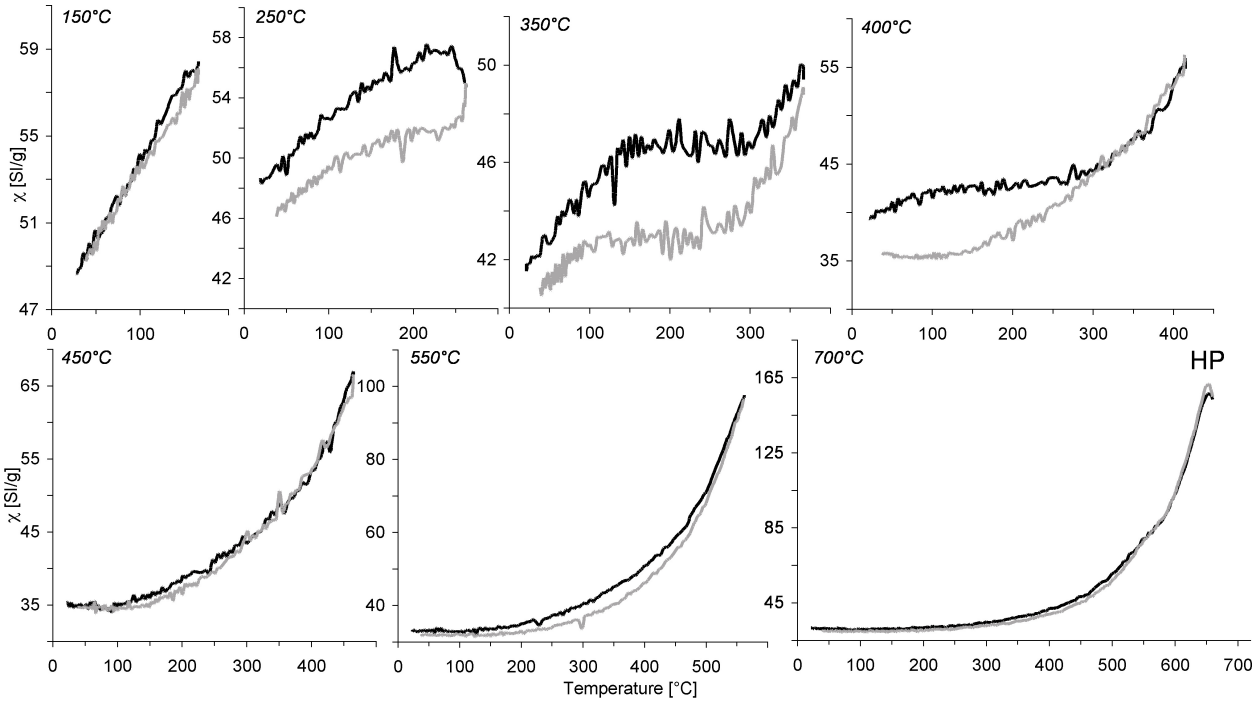

Fig. 3.11: *Magnetic susceptibility normalized to weight (χ) as a function of temperature for fine-grained hematite (9.4-2). Shown are repeated heating/cooling cycles for steps between 150 and 700 °C. Black curve represents the heating, grey curve the cooling run. A weak irreversibility occurs during the 200 °C and disappears during the 450 °C step. Further heating to the 700 °C step indicates no modification of the hematite and a typical T_C of 695 °C. The Hopkinson peak (HP) indicates grain sizes within the singledomain range.*

by the T_V at –150 °C. Normally, magnetite shows a slightly higher T_C between 580 and 590 °C, which in this case is obliterated by the previous hematite peak, hampering the accurate determination of the magnetite T_C. The very low increase in κ at room temperature during the cooling run indicates a very low amount of magnetite is present. The strong and sharp peaks suggest small grain-sizes for both the original hematite and the newly formed magnetite. The absence of the T_M of hematite supports these interpretations. Because no T_C of magnetite was detected in the heating run, the formation of magnetite must have occurred at temperatures > 590 °C. This magnetite probably was formed as an experimental product of the unknown phase with a T_C at 360 °C as this T_C was not observed anymore in the cooling run. De Boer and Dekkers (2001) reported on thermally activated release of incorporated hydroxyl-groups, which triggered the formation of maghemite traces on the surface of well-crystalline hematite planes. The T_C at 360 °C described here may indicate such a maghemite formation. On the other hand, the T_C of maghemite is given to be between 470 and 675 °C (Dunlop and Özdemir 1997). However, the T_C of maghemite is difficult to obtain and depends on the incorporation of impurities and the crystallinity of the precursor (Petrovsky et al. 2004). By further heating, maghemite shows unstable behavior and reacts to magnetite as indicated by the T_C of 570 °C. The κ(T) measurements of the fine-grained hematite in this study shows only a very small Al-index of 0.25 due to the formation of only minor maghemite and magnetite.

Repeated heating/cooling measurements of fine-grained hematite (Fig. 3.11) were performed in order to detect the temperature at which irreversible behavior begins, with the formation of maghemite and magnetite. During all steps a positive slope of κ is observed, with a reversible behavior until the 150 °C step. During the 250 to 400 °C steps the sample starts to behave weakly irreversible, with slightly decreased κ-values in the cooling run. This probably reflects the release of hydroxyl-groups

from the hematite lattice. Steps 450 to 700 °C show relative good reversibility and the last step produces a T_C of 695 °C, typical for hematite. However, no T_M was recognized during the low-temperature run of the heated sample. The missing T_M correlates with the small grain size of hematite sample and is in agreement with the distinctly developed Hopkinson peak at the 700 °C step. In contrast to the first susceptibility cycle up to 700 °C, the formation of maghemite or magnetite is not observed during the repeated κ(T) measurements. It is suggested, that the kinetics of a single heating step to 700 °C measurement differs from the kinetic behavior during repeatedly heating and cooling of the hematite.

Coarse-grained martite

The coarse-grained hematite (~150 µm, B6) sample comes from the Banded Iron Formation (BIF) of the mine Conceição in Brazil (Günther 2003) and shows intergrowth with quartz. For the hematite phase no incorporation into the lattice are indicated by the chemical analyses (Hem B6, Table 3.5). In the powdered state the sample is dark grey colored. The κ(T) curve shows a clear T_M (Fig. 3.10 b, see inlay), which occurs at about -15 °C, typical for pure and well crystalline hematite. The high-temperature run shows a distinct increase of κ above 330 °C and two different T_Cs at 580 and 695 °C typical for magnetite and hematite, respectively. Because no T_V was observed during the low-temperature run, the occurrence of the magnetite T_C during the heating run indicates formation of new magnetite during the thermal treatment. The mechanism, which causes such a reaction of hematite to magnetite in an inert atmosphere, is not fully understood. However, for the reaction of hematite to magnetite a redox reaction is suggested (see reaction 8). The strongly irreversible behavior during the cooling run shows the same T_Cs for hematite at 695 °C and for magnetite at 580 °C and strongly increased κ-values. Regarding the cooling run carefully a decrease of κ at the T_C of hematite can be observed indicating reaction of the coarse-grained hematite to magnetite. Although hematite is still indicated by its T_C after heating, the earlier observed Morin transition does not reoccur during the second low-temperature run. Instead a Verwey transition of newly formed magnetite occurs at -150 °C. The high Al-index of 123 implies the formation of large amounts of magnetite, which probably masks the Morin transition of hematite during the low-temperature run. An additional T_C at 200 °C in the cooling run was observed. A Curie temperature

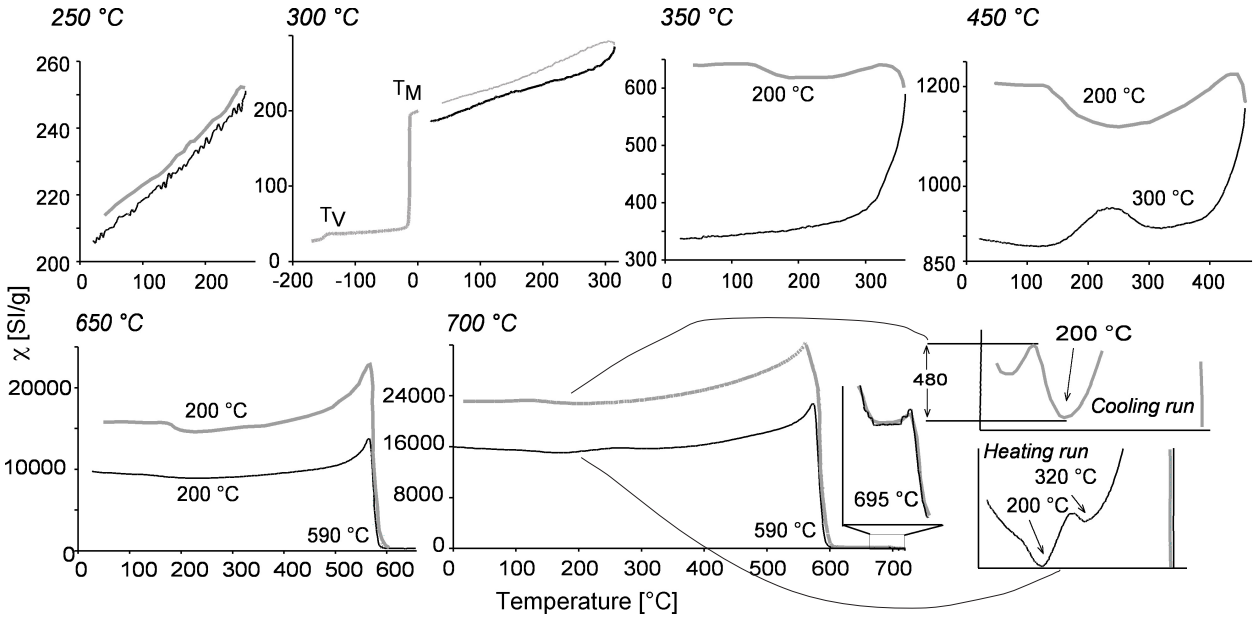

Fig. 3.12: *Magnetic susceptibility normalized to weight (χ) as a function of temperature for coarse-grained hematite (B6). Shown are repeated heating/cooling cycles for steps between 250 and 700 °C from 250 to 700 °C step. Black curve represents the heating, grey curve the cooling run. A weak irreversibility starts during the 250 °C step (more explanation: see text).*

of around 180 °C is known for some ferroxyhite (δ-FeOOH, Murad 1996). The orange coloration and condensation of water at the wall of the glass holder in which the sample was heated is suggestive for the formation of iron oxides or oxyhydroxides.

Repeated heating/cooling experiments of the coarse-grained hematite shows a weakly irreversible trends, which starts with the 250 °C step. Distinct irreversibility was observed after the 300 °C step (Fig. 3.12). A subsequent low-temperature measurement revealed a susceptibility jump at –150 °C indicating the Verwey transition and therefore the formation of magnetite. During the subsequent 350 °C step the formation of a new magnetic phase is also indicated by a T_C at 200 °C in the cooling run, which was already observed during the first heating cycle to 700 °C. This T_C of 200 °C is seen in all cooling runs of the 350 to 700 °C steps but is not typically observed in the heating run of the subsequent steps. Instead, another T_C between 300 and 330 °C occurs during the heating steps of 450, 600 and 700 °C. Such T_Cs occur only during heating, never during cooling, suggesting maghemite reacts to magnetite, as already discussed above and reported by Dekkers (2001). This assumption also implies the coarse-grained hematite contains incorporated hydroxyl-groups. In the final 700 °C step, beside the T_C of magnetite (590 °C), a very faint T_C (695 °C) of hematite is detected indicating not a complete reaction to magnetite. However, no Morin transition is observed. It is assumed, that the missing Morin transition in this case is due to the weak κ of hematite when compared with magnetite and is not due to material properties such as crystallinity or the presence of impurities. The Morin transition probably vanishes in the background noise of the Kappabridge.

Ferrous carbonates

The ferrous carbonates siderite ($FeCO_3$) and ankerite ($Ca(Mg, Fe^{2+}, Mn)(CO_3)_2$) show paramagnetic behavior between the measured

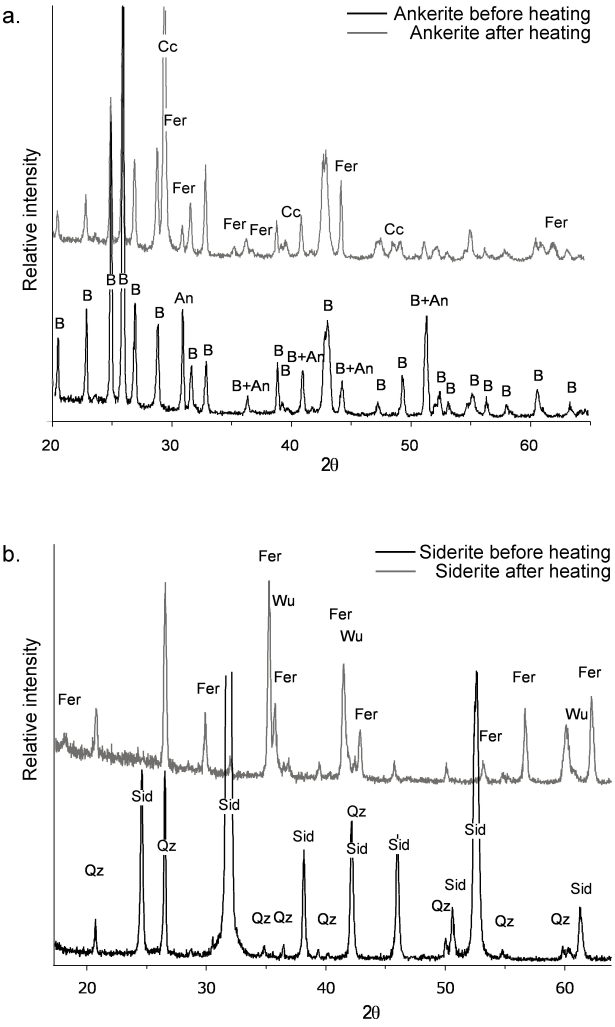

Fig. 3.13: *X-ray diffraction patterns of* ***a.*** *ankerite (quarry Himmelfahrt at Freiberg, Germany) and* ***b.*** *siderite (quarry Pfannenberger Einigkeit at Siegen, Germany), before and after heating to 700 °C. The heated samples clearly show additional peaks belonging to the cubic spinel structure of Mg-Mn ferrites. An: ankerite, B: barite, Cc: calcite, Fer: ferrite, Qz: quartz, Sid: siderite, Wu: wuestite.*

temperature range –192 to 700 °C. Siderite is an isomorph of calcite ($CaCO_3$). Ankerite forms a solid solutions series with dolomite, which in turn is a solid solution between calcite and magnesite ($MgCO_3$). The Fe-Mg layer in carbonates can be filled by Fe^{2+} or by Fe^{2+} and Mn^{2+} (Deer et al. 1966). Frederichs et al. (2003) observed a Néel temperature of siderite to be –236 °C. Magnetic studies of siderite and ankerite show that they oxidize to form ferrimagnetic iron oxides (maghemite and magnetite) by heating to temperatures above 300 °C in air (Isambert et al. 2003, Elwood et al. 1989). For a better understanding of the κ(T) curves of stage II altered Soultz granite,

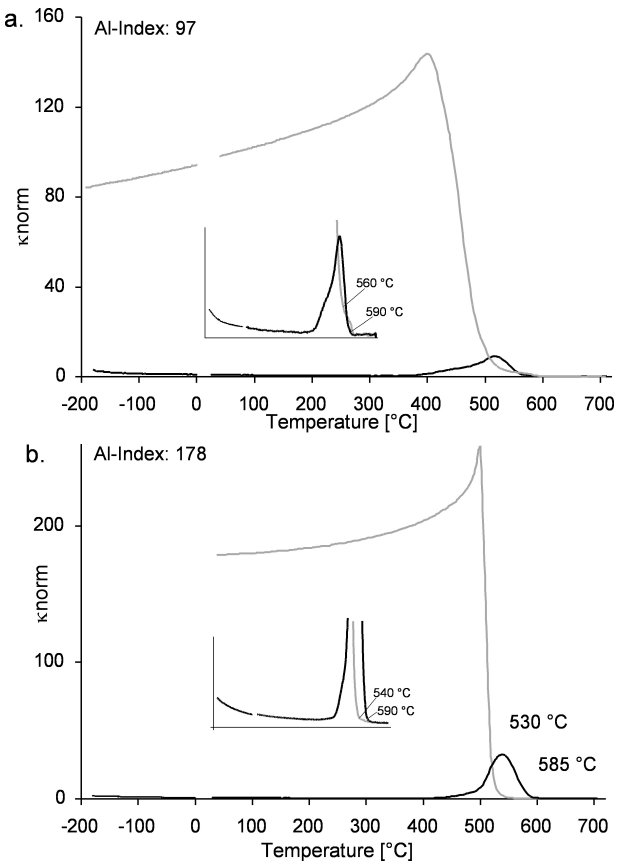

Fig. 3.14: *Normalized magnetic susceptibility (κnorm) as a function of temperature for* ***a.*** *ankerite and* ***b.*** *siderite. Black curve represents the heating, grey curve the cooling run.*

which is characterized by iron-bearing carbonates in addition to minor magnetite and abundant hematite and illite, κ(T) measurements of siderite and ankerite were undertaken. Subsequently the newly formed products were identified using X-ray diffraction.

Ankerite

The ankerite sample from the quarry Himmelfahrt at Freiberg, Germany, shows intergrowth with barite and minor quartz reflected in the X-ray refraction pattern (Fig. 3.13 a). Chemical analysis revealed 5.84 wt% MgO, 3.58 wt % Fe_2O_3 and 1.01 wt% MnO besides 12.22 wt% CaO (Table 3.5). The κ(T) curve of ankerite (Fig. 3.14 a) produces a hyperbola curve during the low-temperature run, which is the typical behavior for paramagnetic minerals. An increase of κ at 380 °C and a T_C of 560 °C during the high-temperature run indicates the formation of a ferrimagnetic phase during heating. This phase behaves unstable during further heating and its T_C at 560 °C disappears in the cooling curve. Instead, T_Cs at 590 and 500 °C appear indicating the formation of stable ferrimagnetic phases at temperatures > 590 °C. The subsequent low-temperature run reveals a positive slope but no Verwey transition. The X-ray diffraction pattern of ankerite after heating (Fig. 3.13 a), indicates new formation of calcite ($CaCO_3$) and Mg-Mn-ferrite ($(Mg, Mn, Fe)_3O_4$), an iron-bearing spinel phase. The following reactions may occurred:

(12) $CaMg(CO_3)_2 \rightarrow CaO + MgO + 2CO_2$
(13) $CaO + CO_2 \rightarrow CaCO_3$.

The siderite component in the solid solution of this ferrous carbonate decomposes preferentially, because siderite already shows unstable behavior

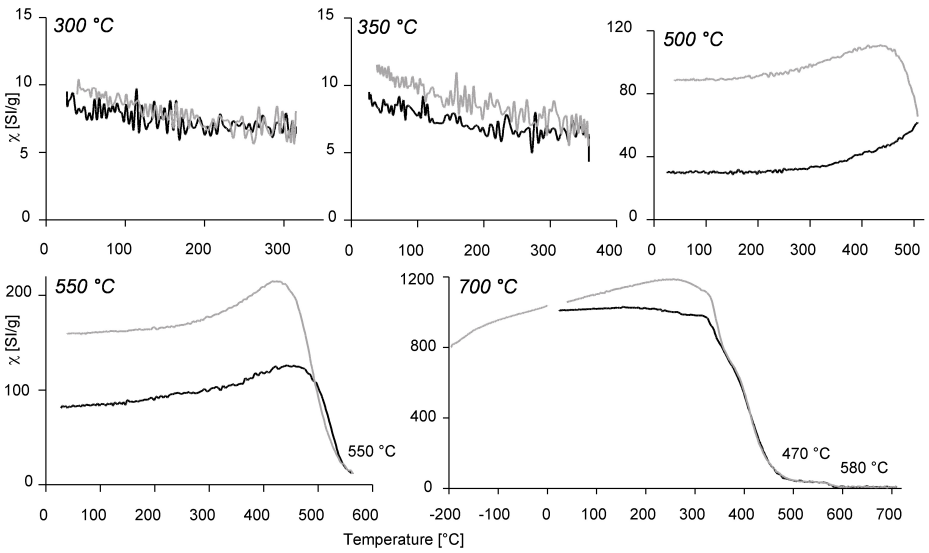

Fig. 3.15:
Magnetic susceptibility normalized to the weight (χ) as a function of temperature for progressively and repeatedly heated and cooled ankerite up to 700 °C. Black curve represents the heating run, grey curve the cooling run. A weak irreversibility starts during the 350 °C step.

at low temperatures (> 300 °C, e.g., Ellwood et al. 1989). This reaction is shown further below (reaction 15). Magnetite-magnesioferrite (Fe_3O_4-$MgFe_2O_4$) solid solutions show T_Cs between 580 and 440 °C and magnetite-jacobsite (Fe_3O_4-$MnFe_2O_4$) between 580 and 350 °C (Dekkers 1997), because the incorporation of non-magnetic ions generally lower the T_C of magnetite. The formation of a ferrimagnetic phase from a paramagnetic phase is also indicated by the relatively high Al-index of ankerite (97).

Repeated heating/cooling cycles of ankerite (Fig. 3.15) show reversible behavior up to the 300 °C step with χ between 5 and 10 x 10^{-6} SI/g, typical for paramagnetic minerals. Heating the sample to 550 °C a newly formed ferrimagnetic phase with T_C at 550 °C is detected, which causes a strong increase in κ up to 100 x 10^{-6} SI/g. During the cooling run this T_C shifts to a lower T_C of 530 °C and upon renewed heating/cooling cycles even to a lower T_C at 470 °C, which is associated with a further increase of κ. Isambert et al. (2003) heated Mn-siderite in an air atmosphere and observed the formation of unstable maghemite, which transformed into hematite after heating to 480 °C and the formation of a Mn-ferrite at 500 °C. This ferrite phase persisted even after heating to 700 °C. According to the observations of Isambert et al. (2003) the phase with a T_C between 530 and 560 °C in the heating curve is assumed to be the unstable maghemite. Further modification to hematite was not observed in the κ(T) curve probably because of heating in the inert argon atmosphere. The shift of the T_C to lower temperatures during the progressive heating and cooling cycles indicates the formation of stable ferrimagnetic spinel phase with a higher incorporation of Mg- and/or Mn-ions.

Siderite

The siderite sample studied comes from the quarry Pfannenberger Einigkeit at Siegen, Germany and has some intergrowth with quartz (Fig. 3.13 b). Chemical analysis revealed that the siderite is Mn- and Mg-rich with 7.65 wt% MnO and 3.14 wt% MgO (Table 3.5). The κ(T) curve of siderite (Fig. 3.14 b) is very similar to that of ankerite (Fig. 3.14 a) and shows a paramagnetic behavior during the low-temperature run. During the high-temperature run κ increases above 370 °C indicating the formation of a ferrimagnetic phase with a T_C of 585 °C. The formation of a ferrimagnetic phase is in agreement with a relatively high Al-index of 178. Although this T_C is typical for magnetite, the irreversibility of

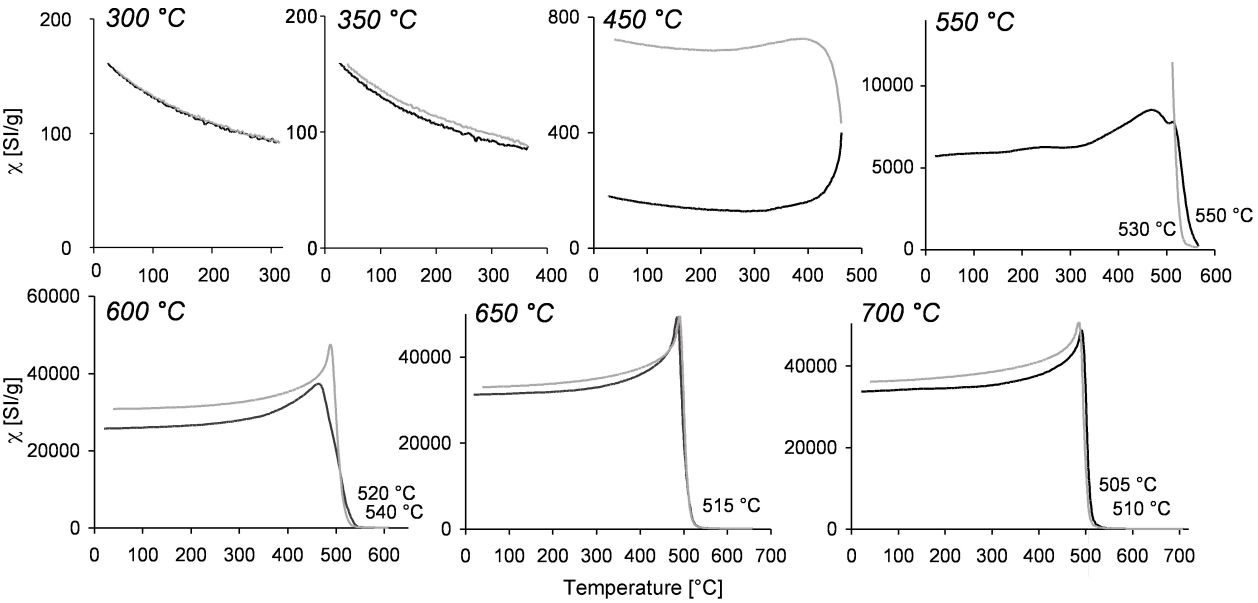

Fig. 3.16: *Magnetic susceptibility normalized to the weight (χ) as a function of temperature for progressively and repeatedly heated and cooled siderite to 700 °C. Black curve represents the heating, grey curve the cooling run. A weak irreversibility starts during the 350 °C step. Note the decreasing T_Cs during the 550 to 700 °C steps.*

T_C strongly suggests that it is unstable maghemite. During further heating maghemite is replaced by a new, stronger magnetic phase with a T_C of 530 °C observed in the cooling run. The X-ray diffraction pattern of siderite after heating (Fig. 3.13 b) indicates the formation of wuestite (FeO) and Mg-Mn-ferrite, a phase also observed after heating of ankerite. Isambert et al. also observed the decomposition of siderite to wuestite and to a ferrite phase. The following reaction may occurred during this heating:

(14) $FeCO_3 \rightarrow FeO + CO_2$
(15) $3FeCO_3 + 1/2\ O_2 \rightarrow Fe_3O_4 + 3CO_2$.

The newly formed magnetite (reaction 15) shows a significant exchange of the Fe^{2+} by Mn^{2+} and Mg^{2+} in the siderite lattice led to an incorporation of these ions into the magnetite lattice reflected by the decreased T_C of magnetite.

Repeated heating/cooling curves of siderite (Fig. 3.16) shows a distinct irreversibility starting during the 400 °C step. This is consistent with the beginning of irreversible behavior observed during the first heating cycle to 700 °C (Fig. 3.13 b). This irreversibility is caused by the formation of a ferrimagnetic phase. This ferrimagnetic phase shows a T_C of 550 °C during the 550 °C step detected in the heating run, which shifts to a T_C of 530 °C during the cooling run. Further heating and cooling steps result in a continued decrease of T_C, which finally produces a T_C of 505 °C in the 700 °C step. The decrease of T_C of magnetite is normally related to Fe substitution by other ions, for example Mn or Mg. Dilution with non-magnetic ions was e.g., reported by Kontny et al. (2004), where Fe substitution by Mg in high-pressure spinel resulted in lower T_C compared to the T_C of pure magnetite. Chemical analysis of the unheated siderite (Table 3.5) shows higher amounts of Mn than in ankerite. In contrast to Mg, which is a non-magnetic ion, Mn is a ferromagnetic ion similar to Fe. Heating Mn-rich (MnO = 7.65 wt%) siderite therefore results in the formation of a spinel phase with a higher χ (~30 x 10^{-3}SI/g, Fig. 3.16) in contrast to heating a Mn-poor (MnO = 1.01 wt%) ankerite. This results in the formation of a new spinel phase with a lower χ (~1 x 10^{-3}SI/g, Fig. 3.15). On the other hand, the X-ray pattern of the original ankerite sample (Fig. 3.13 a) indicates relative high amounts of barite. Because of the lower carbonate content of the ankerite sample, lower amounts of a ferrite phase could be formed during heating. This also explains the low χ of the newly formed ferrite phase during heating of ankerite. However, the T_C of 550 °C observed during the heating run of the 550 °C step is similar for both ankerite and siderite. These similar T_Cs imply the formation of the same, unstable magnetic phase, probably maghemite. During further heating this maghemite modifies to a stable spinel phase of varying T_Cs depending on the availability of Mg and Mn ions, respectively.

Illite

Beside iron carbonates illite is the most common alteration mineral in the hydrothermally altered Soultz granite. The studied illite contains 7.32 wt% Fe_2O_3 and 0.55 wt% FeO (Table 3.5) and has the following structural formula: $(Mg_{0.09}\ Ca_{0.06}\ K_{1.37})[Al_{2.69}\ Fe(III)_{0.76}\ Fe(II)_{0.06}\ Mg_{0.43}\ Ti_{0.06}][Si_{6.77}\ Al_{1.23}]O_{20}(OH)_4$. It is an IMT-2 type clay mineral from Silver Hill, Montana, USA (Olpheny and Fripiat 1979). The κ(T) curve (Fig. 3.17) shows a typical paramagnetic behavior during the heating

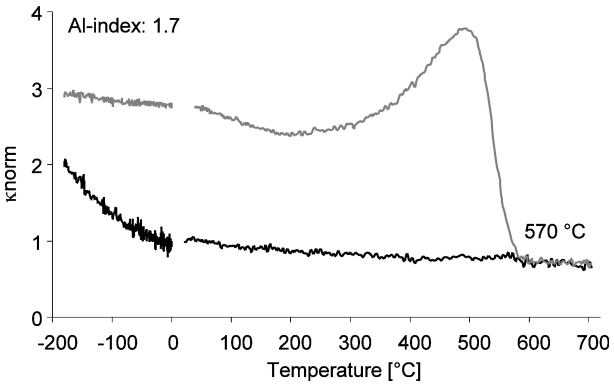

Fig. 3.17: *Normalized magnetic susceptibility (κnorm) of an IMT-2 illite as a function of temperature. Black curve represents the heating, grey curve the cooling run.*

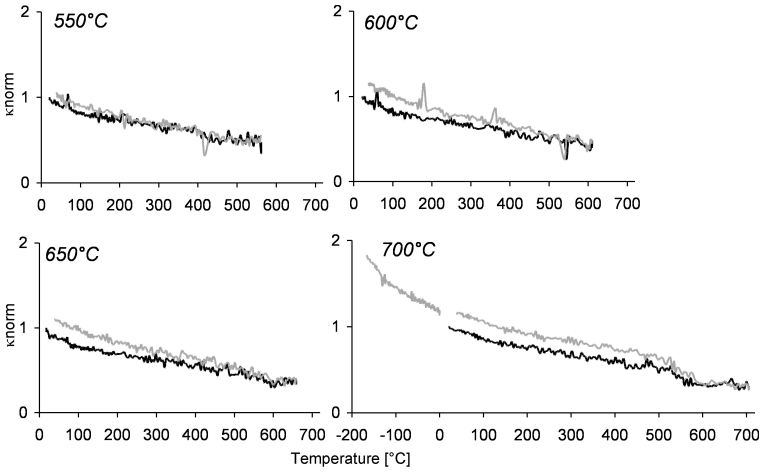

Fig. 3.18: *Normalized magnetic susceptibility (κnorm) of progressively and repeatedly heated and cooled IMT-2 illite as a function of temperature up to 700 °C. Black curve represents the heating run, grey curve the cooling run. A weak irreversibility starts during the 600 °C step. After heating to 700 °C a T_C of 580 °C indicates the formation of magnetite, although the low-temperature behavior of the cooling curve is still dominated by paramagnetic behavior.*

run up to 700 °C. In the cooling run however, the formation of a ferrimagnetic phase is indicated by a T_C of ~570 °C, slightly lower than a T_C typical for magnetite. The subsequent low-temperature run shows relatively constant κ-values, which is consistent with the formation of a ferrimagnetic phase. However, a Verwey transition is not observed. The low Al-index (1.7) indicates the formation of only small amounts of a ferrimagnetic phase.

In contrast to the first heating cycle to 700 °C, repeated heating and cooling of illite (Fig. 3.18) shows only a subordinate formation of magnetite with a distinct T_C at ~ 590 °C during the last 700 °C step. The subsequent low-temperature run, however, shows a hyperbola typical for paramagnetic minerals and only a very weak increase of κ is observed. This behavior implies that the paramagnetic illite still dominates the magnetic behavior, with only very small amounts of magnetite forming, probably with grain sizes in the SD threshold, thus suppressing the Verwey transition (Muxworthy 1999). This experiment data shows the possibility of some ferrimagnetic phase formation during heating of illite, which is in agreement with the heating of vein illite from the Soultz granite (Fig. 3.9 a). Normally, illite shows stable behavior during heating to 700 °C and no release of iron or other ions from the crystal lattice, which is essential for the magnetite formation. However, one possibility is that octahedral ions located at the crystal edges of the illite lattice can diffuse during heating and react to form minor quantities magnetite (Warr, pers. comm.). This type of reaction may explain why more magnetite is formed from the finer-grain sized illites of the Soultz granite.

Discussion

The magnetite-bearing Soultz granite underwent two principal stages of hydrothermal alteration as already reported in former studies (e.g., Traineau 1991, Jacquemont 2002), which however, mainly focused on the rift-related alteration history. The presented study herein led to a better understanding of the "old" (Middle Carboniferous to Permo-Triassic) alteration history using the combination of conventional petrology and thermomagnetic behavior of the different mineral assemblages. The different alteration events are displayed in Fig. 3.20. The stage I event took place under retrograde conditions during cooling and consolidation of the magma, and affected the fresh granite pervasively without any evidence of magnetite oxidation. But at the same time the oxidation of magnetite to martite locally occurred, which is confined to discrete zones. Thus, this stage I event is called localized. The subsequent stage II alteration events are also related to discrete zones, but these alteration events happened during post-emplacement tectonics, such as faulting due to the exhumation and unloading of the plutonic body. In the following, these alteration events are discussed in relation to the chronological alteration history.

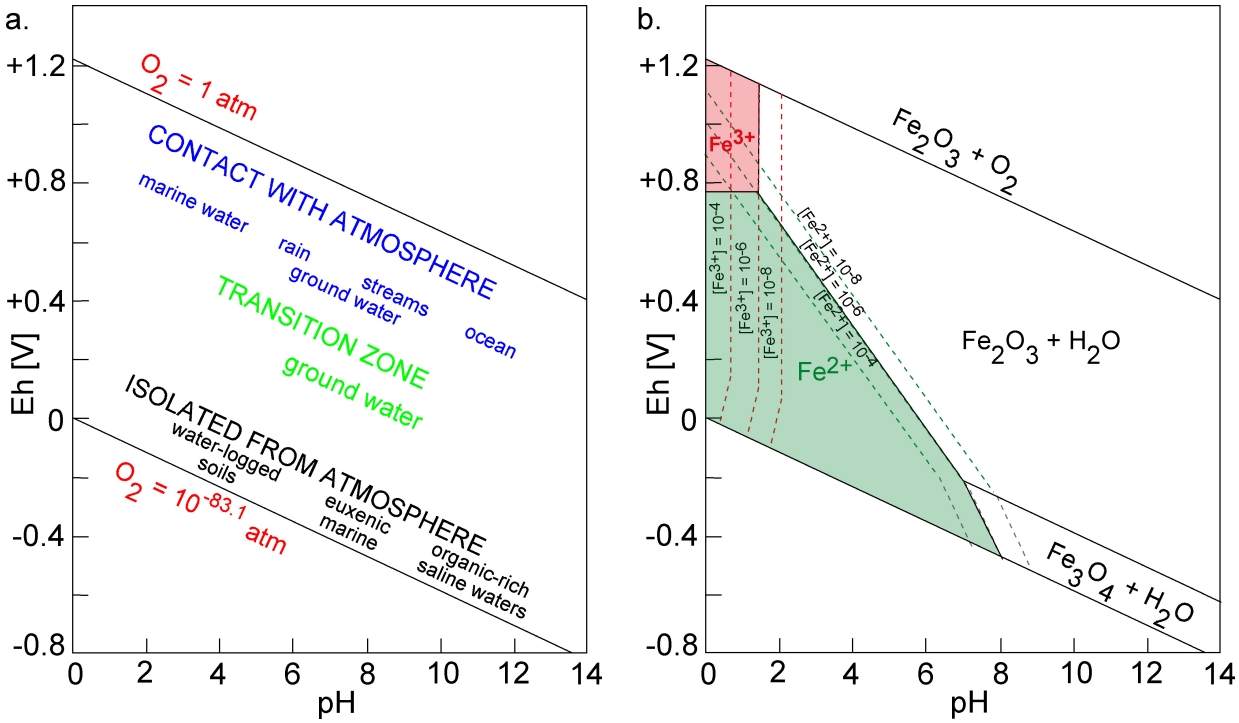

Fig. 3.19: *Eh-pH diagrams showing* ***a.*** *stability limits for natural waters at the earth's surface at 25 °C. The limits are based on partial pressures of oxygen at 1 and $10^{-83.1}$ atm. The range of Eh and pH conditions for various natural environments is modified after Garrels and Christ (1965).* ***b.*** *Eh-pH diagram showing the stability fields for hematite and magnetite. The boundary for the ionic species is drawn with activity = 10^{-6} molL^{-1}. In the field labeled Fe^{2+}, $[Fe^{2+}] > [Fe^{3+}]$. In the field labeled Fe^{3+}, $[Fe^{3+}] > [Fe^{2+}]$. Dashed lines represent variation in Fe^{3+} and $Fe2^{+}$ in molL^{-1}, for a solution coexisting with hematite or magnetite (modified from Garrels and Christ 1965). Only at very low pH values, Fe^{3+} has a significant activity.*

Stage I alteration: implications of the tectonics during magma cooling

The initial stage I event caused the alteration of the primary rock forming minerals, particularly plagioclase and biotite, but during this event the primary accessory mineral magnetite remained without any evidence of oxidation. Therefore this type of alteration is despite its widespread occurrence, without any consequence for the magnetic properties of the granite, and samples are referred to as "fresh" from the magnetic point of view. Because hematite was formed at the same time parallel to the biotite cleavage, the fO_2 during cooling of the magma is related to the hematite/magnetite (HM) buffer (Fig. 3.3). The granite is called "fresh" from the magnetic point of view. The κ(T) curves of such fresh granite show behavior typical for magnetite, which clearly constitutes the dominant magnetic mineral in this type of sample. The only other ferromagnetic (s.l.) mineral recognized microscopically was some hematite, which however, was not detected by the κ(T) curves.

In the depth interval between 1550 and 1580 m (central part of the borehole profile, Fig. 3.1) a granite, which shows the oxidation of magnetite, was related to the pervasive stage I alteration by e.g., Jacquemont (2002), Traineau et al. (1991) and Genter (1989). This study, however, clearly indicates that the oxidation of magnetite was caused by elevated fO_2 as indicated by the chlorite composition, when assuming a constant primary lithological composition before alteration. Such elevated fO_2 is associated with similar temperatures (~260 - 307 °C) from chlorite geothermometry, when comparing with the fresh granite, This can be explained by the formation of an adjacent permeable zone, where O_2-rich fluids could infiltrate and mix with residual fluids during the consolidation of the magma. At this stage the plutonic body was not completely cooled

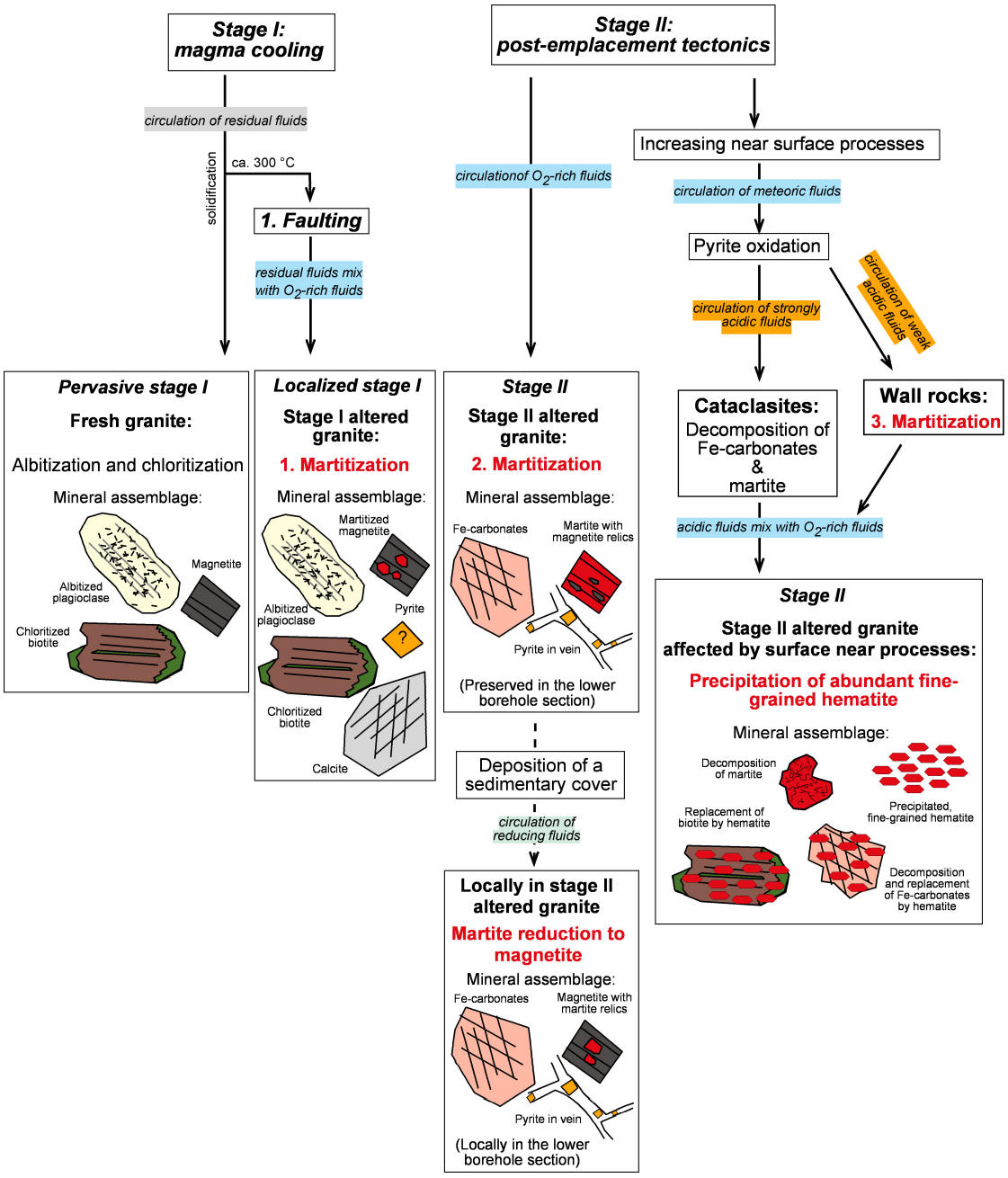

Fig. 3.20: *Schematic diagram of the "old" alteration history of the Soultz granite.* ***Stage I*** *alteration is related to the cooling of magma with pervasively and locally circulated fluids. The first faulting event occurred.* ***Stage II:*** *Next faulting event, probably due to unloading and exhumation, resulted in the infiltration of fluids that reacted with already altered granite (stage II granite). Thus, abundant Fe-rich carbonates were formed. Pyrite was formed at the latest during this event. The third alteration event occurred during the exhumation to a paleo-erosion surface. Circulation of meteoric fluids within the upper part of the plutonic body caused an oxidation of pyrite, which resulted in the circulation of strongly acidic fluids. At the paleo-erosion surface such acidic fluids mixed with meteoric fluids, for example rain water, and abundant fine-grained hematite precipitated. See text for discussion.*

down, which suggests the formation of fault zones already during the late stage of magma cooling. Thus, granites from this depth interval were not only affected by a pervasive (autosomatism) event but also by a fault-related event with infiltrating O_2-rich fluids. This scenario is also supported by the κ(T) measurements, where the thermomagnetic behavior of granite from the central part revealed the presence of pyrite (Fig. 3.5 e), which is a typical mineral in the fault zones from the lower borehole section. The appearance of traces of pyrite at this interval is interpreted as a relic. It is suggested that

the pyrite was more abundant before been removed by a later fluid event (stage II), which circulated through the upper borehole section (this event is explained further below).

The occurrence of pyrite, the relatively high temperatures indicated by the alteration minerals and elevated fO_2 imply that this fault zone was already active during the cooling of the pluton in Variscan times. This assumption is supported by the AMS (anisotropy of the magnetic susceptibility) study (Chapter II.1) as well as paleomagnetic investigations (Chapter II.2), which indicates both a Variscan stress regime and a Carboniferous paleopole position of the Soultz granite at this time. In contrast to the wall rocks of stage II that show abundant Fe-bearing carbonates, the wall rocks of this fault zone – namely the stage I granites – are characterized by the precipitation of just pure calcite. This feature may indicate that the central depth interval was not overprinted by the late stage II alteration events. Clues to the varying types of carbonates that formed in the altered granites are given by Komninou and Yardley (1997). They suggested that different mineralogical alteration assemblages depend both on the path the fluid follows and the extent of pre-existing alteration in the granite. According to their geochemical modeling, the precipitating sequence of minerals with an unaltered granite is 18.4% carbonates, 21.2% quartz, 40.0% K-feldspar, 18.3% hematite and 2.1% pyrite. The initial pure composition of calcite formed during a first alteration phase is related to the albitization of plagioclase. However, when the same fluid reacts with partially altered granite, carbonates strongly dominate and the precipitating sequence is 92.9% carbonates, 3.6% quartz, 3.1% muscovite and 0.4% pyrite and no hematite. In this case the carbonates incorporated more Fe because of the enhanced alteration of iron-bearing silicates, such as biotite and/or chlorite. Thus as the occurrence of Fe-bearing carbonates is characteristic for the alteration mineralogy of stage II altered granites in all other studied fault zones of the Soultz granite, it can be deduced that this type of fluid-rock interactions occurred already in altered granites. Such Fe-bearing carbonates of the stage II altered granite could be here routinely detected using the $\kappa(T)$ measurements.

Stage II alteration: implications of the post-emplacement tectonics

The $\kappa(T)$ curves of stage II altered granites are characterized by the reactions of Fe-carbonates during thermomagnetic measurements and the formation of ferrite phases, identified as Mg-Mn-ferrites with varying T_Cs between 400 and 600 °C. Furthermore, the presence of Fe-bearing carbonate is indicated by a high Al-index and has a strong influence on the thermomagnetic behavior of the $\kappa(T)$ measurements. The formation of highly magnetic (ferrimagnetic) phases blurs the thermomagnetic behavior of weakly magnetic (paramagnetic) minerals. For example, heating paramagnetic illite resulted in the formation of only small quantities of a ferrimagnetic phase, as indicated by a low Al-index. This was not detectable if Fe-bearing carbonates and/or magnetite was present. Cataclased granite from the upper part of the pluton (1417-1550 m) also yield low Al-index values because magnetite and the Fe-bearing carbonates are widely decomposed and replaced by fine-grained hematite, which shows only restricted reaction to magnetite. This latter aspect is important for paleomagnetic studies, because the alteration of primary minerals during thermal demagnetization is undesired. According to the paleomagnetic study of Chapter II.2 samples with decomposed martite and Fe-carbonates but abundant fine-grained hematite, are shown to behave stable during thermal demagnetization and carry stable paleomagnetic direction. For the fine-grained hematite, which replaced iron carbonates in cataclased granites from the upper part of the profile, Permo-Triassic directions were recorded. This alteration mineralogy and the related paleomagnetic results indicate that the Fe-carbonates characteristic of polyphase stage II alteration must have already formed at the latest during Permian times.

The discordantly overlying Permian sandstones and sedimentary breccia with granite pebbles on

top of the granite imply that during this period the granite was exposed to a paleo-erosion surface. Genter and Traineau (1996) described subhorizontal joints developed during unloading, which occur in the intensively fractured upper part of the borehole profile. The near surface position of this highly fractured zone allowed circulation of meteoric water into the upper part of the exposed granite. The pyrite reacted with ferric ions and water to produce ferrous ions, sulfate ions and an acidity of pH < 3 (Appelo and Postma 1999). The corresponding reactions were introduced (reaction 2-5). Such acidic fluids dissolved Fe^{2+}- and Fe^{3+}-ions (Fig. 3.19 b) causing a modification of magnetite to hematite (martite), as reported by Ohmoto (2002). He suggested a non-redox reaction, as been the principal mechanism for the reaction of magnetite to hematite in aqueous environment:

(16) $Fe_3O_4 + 2H^+ = Fe_2O_3 + Fe^{2+} + H_2O$

This reaction is an acid-base reaction and not a redox reaction because there is no change in the valence of Fe or other ions. Wesolowski et al. (2000a) have recognized that well-crystallized magnetite is readily converted to well crystallized hematite by reactions with acids, even at ambient temperatures. Under strongly acidic conditions Fe^{3+} is soluble, which causes a decomposition of martite, as it is also observed in the cataclased Soultz granite from the upper borehole section. With further distance from the cataclased granites martite survived in the wall rocks because of the fluid-wall rock interactions that neutralize the acidic fluids almost instantaneously (e.g., Marescotti et al. 2000). This observation implicates a spatial restriction of the activity of the strongly acidic fluids within the cataclased granite. Similar alteration conditions were described by Remolar et al. (2002), who reported about the Rio Tinto source area and the upward percolation of groundwater through sulfide bearing ore bodies emplaced during hydrothermal events. Such percolation resulted in highly acidic headwaters with pH = 0.8 - 2.3, that are able to transport ferrous and ferric iron in acid-sulfate waters. When these fluids mixed with rainwater the pH increases to ~3-4 and ferric iron begins to precipitate, forming for example goethite or hematite. In the Soultz granite, abundant hematite is present in the upper section of the borehole profile and probably formed under similar conditions.

The deposition of the overlying cover during Mesozoic or Tertiary times probably caused a change to a more neutral nature of the fluids. Such fluids did not affect the magnetic mineralogy of the Soultz granite and thus this episode is not detected using magnetic methods. First with the entry of an organic matter from the overlying sedimentary cover (Lédesert et al. 1999), again an affect on the magnetic mineralogy is observed. Now, such fluids caused the reduction of martite to magnetite. The thermomagnetic behavior shows relatively low Al-index values because of the presence of abundant magnetite and additional T_Cs typical for ferrimagnetic phases, which formed during the reaction of Fe-carbonate. Such a thermomagnetic behavior was observed for granites from the vicinity of a permeable fault zone in the depth of ~2170 m (Genter et al. 1995), where fluids still circulate through the Soultz granite.

Incipient thermomagnetic irreversibility as a new paleotemperature indicator?

The proposed hypotheses of a new paleotemperature indicator by Hrouda et al. (2003) using stepwise heating/cooling cycles of κ(T) curves could not be confirmed by the thermomagnetic studies of the Soultz granite. The authors proposed that the first sign of irreversibility in stepwise heated samples could be used to determine the maximum paleotemperature underwent by the rock in nature. In the stage I altered granite, irreversibility was observed at temperatures > 400 °C due to the formation of magnetite, by the thermal reaction of martite. In the stage I altered granite martite was formed by the oxidation of magnetite, which accompanied the chloritization of biotite. The chlorite geothermometer method of Cathelineau (1988) revealed temperatures

< 307 °C for the biotite chloritization, which is also correlated to the magnetite oxidation. If the above mentioned hypothesis is true, the beginning of the irreversible behavior of martite should start at similar temperatures. However this temperature significantly differs from the temperature (400-450 °C) detected during the repeated heating/cooling cycles of κ(T) measurements performed on the same sample material. Other investigations of the alteration mineral assemblage, such as the fluid inclusion studies of healed magmatic quartz (Dubois et al. 1996) indicate that the Soultz granite did not experience temperatures higher than 340 °C during the whole hydrothermal alteration history (stage I and II). These temperatures are significantly lower than temperatures predicted from the thermomagnetic irreversibility behavior. For the stage II altered granite, temperatures between 130 and 160 °C were detected from the fluid inclusion studies of Dubois et al. (1996). These granites contain abundant Fe-bearing carbonates. A weak irreversibility of the κ(T) measurements of ankerite and siderite started at temperatures > 300 °C show no correlation between the temperature underwent by the rock in nature and the temperature detected by the repeated heating/cooling cycles of κ(T) measurements. These results clearly indicate that repeated heating/cooling cycles of the κ(T) measurements cannot be used in a simple way for detecting paleotemperatures in hydrothermally altered granites. In addition to temperature, the stability field of a mineral phase strongly depends on other relevant parameters, particularly fO_2, pH, cation concentration, time factor, among others. Such parameters control significantly the thermomagnetic mineral reactions in a rock that occur during hydrothermal alteration. As these parameters are not considered during the κ(T) measurements, there is no correlation between the irreversibility temperature and the alteration temperature underwent by the rock in nature.

Conclusions

The identification of magnetic minerals using κ(T) measurements provides important constraints on the alteration mineralogy in the Soultz granite. Though paramagnetic minerals like Fe-bearing carbonates, pyrite, or the antiferromagnetic hematite could not be detected by their T_C or T_N, they could be identified by their characteristic reactions to ferrimagnetic phases during heating/cooling experiments. Therefore the combination of thermomagnetic methods along with optical studies, microprobe and XRD proved a useful approach in understanding the "old" succession of the Soultz granite. The deduced alteration history is summarized as follows:

(1) Pervasive stage I alteration led to the albitization and chloritization of the granite as reported by Traineau et al. (1991) but did not affected the magnetic mineralogy.

(2) Coexistent with the stage I alteration, initial faulting at high temperatures (~ 239 – 307 °C) induced the magnetite oxidation to martite under conditions of enhanced fO_2.

(3) Circulation of strongly acidic fluids, formed by the oxidation of pyrite, was restricted to the upper part of the profile (1417 – 1550 m). As a consequence, in the cataclastic granites martite was decomposed because of the dissolution of ferric iron in strongly acidic fluids. The fluid-rock interactions in the wall rock granites neutralized the strongly acidic fluids and magnetite reacted to martite. Deeper in the borehole profile these acidic fluids did not circulate, so the abundant pyrite was preserved.

(4) During the exposure to the Permian paleo-erosion surface strongly acidic fluids mixed with other fluids, for example rain water. The resulting pH increase promoted the precipitation of larger amounts of fine-grained hematite.

(5) At the depth of ~2210 m, the reduction of martite to magnetite was observed in a fault zone, which is correlated to the infiltration of organic matter from the overlying sedimentary cover. This alteration is assumed to represent the youngest event, which affected the magnetic mineral assemblage.

Chapter III:

Summary and discussion

Summary and discussion

Rock magnetic properties and petrological investigations of the Soultz granite provided a significant contribution for the understanding of the "old" (Middle Carboniferous to Permo-Triassic) hydrothermal alteration history considering in detail the chronology of magnetic mineral formation. This study clearly highlights the potential of combined magnetic and geological studies for the investigation of geological processes that are related to the modification of Fe-bearing (magnetic) minerals.

Former studies dealing with the Soultz granite (e.g., Jacquemont 2002, Traineau et al. 1991) subdivided the hydrothermal history into two main stages (stage I and II). Stage I was related to a pervasive alteration under retrograde conditions during magma cooling (stage I: pervasive alteration) and affected the whole plutonic body. Stage II was related to hydrothermal alteration caused by the circulation of fluids within veins in fault zones (stage II: vein alteration), which caused an alteration halo in their wall rocks. In earlier studies (e.g., Dezayes et al. 1995, Genter and Traineau 1995, Traineau et al. 1991) this stage II alteration was mainly related to the fracturation of the Soultz granite during the subsidence of the Upper Rhine Graben since Mid-Miocene. The integrated approach presented in this study allows a different insight into these two hydrothermal alteration stages. In the following chapter the history from the emplacement and solidification of the magmatic body during cooling (stage I) and the subsequent post-emplacement processes (stage II), such as exhumation of the plutonic body to a paleo-erosion surface and the influence of the Mesozoic sedimentary cover will be discussed. Moreover clues on the nature of the circulating paleo-fluids, considering physico-chemical factors such as the pH and fO_2, are drawn.

The results of AMS fabric, remanent magnetization and thermomagnetic behavior during $\kappa(T)$ measurements of the fresh and altered Soultz granite have been discussed in more detail in the related chapters (Chapter II.1, II.2, II.3). In conclusion attention will be paid on the two main scopes: (i) chronological succession of the "old" (Middle Carboniferous to Permo-Triassic) alteration history of the Soultz granite, and (ii) modification of the magnetic properties during different geological processes.

Stage I: cooling and solidification of the plutonic body

Magma emplacement

The emplacement of the Soultz granite was dated at 331 ± 9 Ma (U/Pb ages of zircon by Alexandrov et al. 2001). During the cooling of the magma, the primary minerals, mainly biotite and plagioclase, were altered by pervasively circulating residual fluids, which affected the whole plutonic body under retrograde conditions (e.g., Jacquemont 2002). In contrast to the main rock forming minerals, the accessory mineral magnetite remained stable without any evidence of alteration. Thus, this type of alteration is without any consequence for the magnetic properties of the Soultz granite. Such granite is called "fresh" from the magnetic point of view. In the fresh granite, MD magnetite is the carrier of the magnetic properties, which reveals the emplacement history of the magma as follows.

The fresh granite is characterized by magnetic susceptibilities (κ) > 10 x 10^{-3} SI indicating 0.1-2 vol% of magnetite (Clark 1999). Magnetite-bearing granitoids with such a high magnetic susceptibility are called ferrimagnetic granites and are typical for subduction-related I-type granites, which are defined as magnetite-series (Ishihara 1977). In contrast to these series, ilmenite-series show low, paramagnetic susceptibilities (< 1 x 10^{-3} SI), which are interpreted to represent S-type granites. The AMS fabric (Chapter II.1) of the fresh

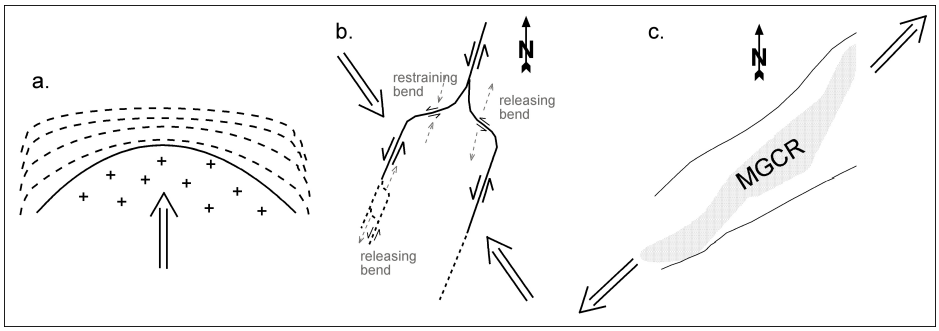

Fig. E: Schematic sketches of possible settings of magma emplacement. ***a.*** *Internal vertical stresses during the two-stage crystallization (Stussi et al. 2002),* ***b.*** *emplacement within a local extensional regime at releasing bands (modified after Greiling and Verma 2001) and,* ***c.*** *emplacement during the initiation of increasing extensional regime.*

Soultz granite provides directional data for the magmatic fabric, which can be interpreted in terms of the emplacement mechanism of the magma. The magnetic fabric is carried by magnetite, which is associated with biotite and hornblende. Petrofabric studies by Genter and Traineau (1996) revealed a weak alignment of biotite, which was interpreted to reflect the magmatic foliation plane. Own AMS and microscopic studies, revealed that the magnetic fabric correlates well with the magmatic fabric. Moreover, it was observed that the weak magmatic fabric is reflected by a relatively strong magnetic fabric (P`> 1.1) and oblate shapes of the magnetic ellipsoid (T > 1). These features are related to magnetite, which is interpreted to mimic the biotite alignment and thus acts as an amplification factor of magmatic fabric anisotropy. The orientation of the magnetic fabric is flat and planar (Fig. 1.8), which probably indicates a magma emplacement in the center of a batholith within a deceleration flow regime and horizontal spreading out of magma (Cruden 1990). Such subhorizontal magmatic fabric of the Soultz granite does not correlate with other magmatic fabrics of adjacent intrusions in the eastern (Odenwald Crystalline Complex; Greiling and Verma 2001) and western (Windstein, Kaiserbach; Flöttman and Oncken 1992) prolongation of the Mid-German Crystalline Rise. These intrusions show magmatic fabrics, which reflect the NW-SE-oriented shortening direction of the transtensional-transpressional Variscan stress regime (Ziegler 1996). The abnormal subhorizontal magmatic fabric of the Soultz granite can be explained by the following explanations. (i) Internal vertical stresses (Fig. E a) during the two-stage crystallization of the Soultz granite (Stussi et al. 2002) were stronger than the external Variscan stresses. (ii) The emplacement took place within local extensional stress regime along a left-lateral shear zone at releasing bends (Fig. E b), as suggested for some intrusions in the Odenwald by Greiling and Verma (2001). (iii) The emplacement took place during the initiation of increasing extensional setting (Fig. E c), as it is given for some magmatic rocks of the Odenwald by Altherr et al. (1999).

Cooling and solidification of the magma

During the cooling and solidification external stresses were absorbed by the plutonic body, which caused the formation of microcracks in the primary minerals, also in magnetite. The combination of optical microscopy and AMS studies in the stage I altered granite from the central depth interval (1550-1580 m) revealed that the microcracks in magnetite are preferentially NW-SE-oriented, which indicates a maximum horizontal stress direction of NW-SE. Fluid circulation initialized a microcrack-controlled oxidation of magnetite, which resulted in elongated magnetite relics with a preferentially NW-SE-oriented magnetic lineation (κ_{max}) in the host martite grains (Fig. 1.4). Along with this oxidation, the primary horizontal magnetic fabric of the fresh granite, evolved to a secondary NW-SE trending and relatively steeply dipping secondary magnetic

fabric in the stage I altered granite (Fig. 1.8). The oxidation of magnetite is recorded by decreased magnetic susceptibilities ($\kappa < 1 \times 10^{-3}$ SI), which correlates well with fault zones and hydrothermally altered Soultz granite. Such susceptibilities and anisotropies ($P` < 1.1$) are typical for paramagnetic granitoids (Ferré and Améglio 2000, Bouchez et al. 1987). The fact that hydrothermal alteration can cause the change from ferri- to paramagnetic behavior has to be considered when using the magnetic susceptibility for a discrimination of different granitoid intrusions. The development of the secondary magnetic fabric in the stage I altered Soultz granite probably indicates a compressional setting due to the Variscan stress regime (Ziegler 1996), or due to an incipient extensional regime as already mentioned above. A regionally extensional regime implies solidification of the Soultz granite during the late phase of the Variscan orogeny, probably passing into a post-orogenic stage.

Chemical analysis of chlorites from fresh and stage I altered granites revealed elevated fO_2 in the stage I altered granites, based on the Fe/(Fe+Mg) ratio (Deer et al. 1991), but similar temperatures of ~300 °C, based on the geothermometer after Cathelineau (1988). Such conditions in the fresh and stage I altered granites indicate an infiltration of O_2-rich fluids along faults into discrete and permeable zones during the cooling of the magma, implying a first brittle stage of the Soultz granite already during Variscan times. Because this event was confined to discrete zones during cooling of the magma, it is called localized stage I alteration. In the fault zones, the pervasively circulating residual fluids mixed with infiltrating O_2-rich fluids, which resulted in increased fO_2 able to oxidize magnetite into martite. The stage I granites probably represents the wall rocks of the Variscan fault zones.

The hypothesis of Variscan faulting is also supported by $\kappa(T)$ measurements (Chapter II.1). Pyrite, which is a typical mineral in the fault zones from the lower part (stage II), was identified in the central borehole interval. The presence of pyrite in the stage I altered granite indicates that pyrite might have been abundant mineral also in the upper fault zones before it was decomposed by near surface processes, as it is proposed in Chapter II.3 (equation 2-5). The formation of fault zones in the Soultz granite during Variscan times is proofed by paleomagnetic studies (Chapter II.2). The separated vectors in the stage I altered granite show directions (compare Fig. 2.11 a) typical for the paleo-position of the Saxothuringian terrane in Middle Carboniferous times (Edel 2001). This time frame correlates well with the dating of the Soultz granite at 331 ± 9 Ma (Alexandrov et al. 2001) and indicates that the plutonic body was faulted during its solidification. Similar paleo-vectors were also observed in wall rocks and cataclasites of stage II. Unblocking temperatures between 400 and 575 °C (Fig. 2.11 c) indicate magnetite as the main carrier of the remanent magnetization. Coercivities higher than 160 mT indicate that this magnetite has small grain sizes and an irregular shape (Tauxe et al. 2004). Such magnetite grains are able to carry stable remanent magnetization. This magnetization was neither overprinted during later hydrothermal events, nor during the drilling of the EPS-1 borehole. Small grain sizes and irregular shapes are characteristic for progressively oxidized magnetite relics. The progressive oxidation even led to grain sizes within the SD threshold for magnetite, which seems to be indicated by the magnetic fabric of progressively altered granites from the upper borehole section (Fig. 2.8). This magnetic fabric revealed NE-SW-oriented magnetic foliation planes, which is inverse relation to the NW-SE-oriented foliation planes of the central part (Fig. 1.10). Inverse magnetic fabrics are typical for SD magnetite (Rochette et al. 1999).

Stage II: post-emplacement tectonics

Polyphase faulting

A progressive grain size reduction of magnetite relics in stage I altered granites from the upper part of the borehole profile indicates that these granites are situated closer to a fault zones, where fluid-rock interactions caused a more intense alteration of the granite and a more intense oxidation of magnetite. Grain size reduction of magnetite relics up to SD magnetite grain sizes in the stage II altered granites is related to a polyphase hydrothermal alteration, which was probably triggered by the reactivation of Variscan fault zones. Each time, when O_2-rich fluids were able to infiltrate the granite, they caused a further grain size reduction of the magnetite relics. Repeated hydrothermal alteration events in the stage II granites are indicated by $\kappa(T)$ measurements, which revealed a complex behavior related to the occurrence of Fe-bearing carbonates. Fe-bearing carbonates are typical for polyphase hydrothermal events in the Soultz granite as it is also reported by Komninou and Yardley (1997). During the polyphase hydrothermal alteration abundant pyrite was formed in veins. In the EPS-1 borehole, pyrite is commonly observed in the lower fault zones only, which will be explained further below.

Paleomagnetic investigations of the stage I and stage II altered granites revealed that these polyphase hydrothermal overprints and the associated grain size reduction of magnetite did not changed the remanent magnetization acquired during Middle Carboniferous. This can be explained by different coercivity forces of magnetite grains. While the magnetic moments of the large, MD magnetite grains are able to align within the prevailing geomagnetic field, magnetic moments of small magnetite grains with irregular shapes remain unaffected. The prevailing temperatures in the range between 130 and 160 °C (Dubois et al. 1996) during the subsequent hydrothermal overprints were not high enough to affect the alignment of these magnetic moments and cause a remagnetization.

Beside the acquisition of a Middle Carboniferous direction, paleomagnetic investigations also indicate the acquisition of a Late Carboniferous direction (Edel 2001). This direction (B in Fig. 2.11) is carried by both magnetite and hematite, which is indicated by unblocking temperatures between 425 and 670 °C. The acquisition of this direction is very limited and only ascertained in two specimens from the cataclastic granites. The acquisition of the B direction is interpreted to reflect a second alteration event with infiltration of O_2-rich fluids in the Late Carboniferous, which is carried by both magnetite and hematite. During this time it can be assumed that temperatures were not as high as during the stage I event, which indicates that magnetite was also oxidized at lower temperatures. This repeated fluid infiltration was probably triggered by a reactivation of the Middle Carboniferous fault zones during the Late Carboniferous. Such a polyphase faulting and brittle deformation of the granites caused the destruction of the magnetic fabric evolved during Middle Carboniferous. As a consequence, polyphase cataclased granites show randomly distributed AMS fabrics (Fig. 1. 10). In contrast to the cataclasites, the AMS fabric was not affected in their wall rocks, which show magnetic fabrics similar to stage I altered granites from the central part. Unfortunately, the stage II altered granites are characterized by the presence of Fe-carbonates. Thermomagnetic investigations of Fe-carbonates revealed unstable behavior and reaction to strongly magnetic ferrite phases during heating. The formation of ferrimagnetic phases during heating is undesired in paleomagnetic investigations because it blurs the natural remanent magnetization during thermal demagnetization.

Exhumation and unloading of the plutonic body

The discordantly overlying Permian sandstones and sedimentary breccia with granite pebbles on top of the Soultz granite core imply that during this period the granite was exposed to a paleo-erosion surface. During unloading and exhumation to a paleo-surface an intensively faulted and fractured upper part of the plutonic body was developed (Genter and Traineau 1996). Now, high amounts of meteoric fluids were able to infiltrate, which led to the oxidation of pyrite (reaction 2-5, Chapter II.3). The oxidation of pyrite caused the formation of strongly acidic fluids (pH < 3, e.g., Remolar et al. 2002), which were able to dissolve Fe-carbonates and even martite. Such martite and Fe-carbonate decomposition is restricted to the cataclasites, because fluid-wall rock interactions neutralized the acidic fluids (e.g., Marescotti et al. 2000). Thus, wall rocks of the cataclasites were not affected by such highly acidic fluids and martite and Fe-carbonates remained. The abundant occurrence of Fe-carbonates and martite however, causes unstable behavior during thermal demagnetization of paleomagnetic investigations. The unstable behavior of wall rocks of stage II mineral assemblage was documented by thermomagnetic investigations, which showed reactions to ferrimagnetic ferrite phases (Chapter II.3) for Fe-carbonates and magnetite for martite. Thus, the most stable behavior during thermal demagnetization was obtained for the cataclasites from the upper part of the borehole profile, where Fe-carbonates and even old martite were decomposed.

Paleo-erosion surface

When the granite was exposed to a paleo-surface, the acidic fluids mixed with infiltrating meteoric fluids, which caused the neutralization of the acidic fluids. As a consequence, ferric iron from the oxidation and decomposition of Fe-bearing minerals, such as Fe-carbonates, biotite, chlorite and martite, could no longer exist in a fluid phase. Thus, abundant fine-grained hematite precipitated in the upper part of the plutonic body, which caused there a widespread hematitization. The fine-grained hematite replaced minerals, such as Fe-carbonates and chloritized biotite, or precipitated within veins in cataclasites. Because small magnetite relics are still present in these rocks, the AMS study revealed no information about the hematite fabric. Magnetite still dominates the magnetic behavior as long as it is present in the rock. On the other hand, granite samples containing abundant fine-grained hematite in the upper borehole section revealed stable behavior during thermal demagnetization. Permo-Triassic directions of these granites (Fig. 2.11 c) imply a preferential hematite precipitation during this time. The stable remanent magnetization of fine-grained hematite was not overprinted during subsequent hydrothermal events, because such hematite has a high crystalline anisotropy and thus relatively high coercivity. The alteration mineral assemblage of the granites from the upper borehole section indicates that pyrite and Fe-carbonates were already formed before Permo-Triassic times, which in turn confirms a polyphase hydrothermal alteration during Late Carboniferous.

Effect of the sedimentary cover

Polyphase hydrothermal alteration events and reactivations of the Variscan fault zones during Mesozoic and Cenozoic times, as reported from K/Ar dating on illites by Schleicher et al. 2004, are not recorded by magnetic properties in the Soultz granite. The only indication of younger fluid activity on the magnetic mineralogy was found in granites in the vicinity of a permeable fault zone in the depth of ~2170 m. Here, fluids migrate along a still open fault zone into the granite indicating ongoing circulation of fluids (Pribnow and Clauser 2000, Genter et al. 1995). Lédesert et al. (1999) have reported that the active fluids in this zone originated from the overlying sedimentary cover and transport organic matter into the granite. This entry of

organic matter is reflected by the reduction of martite back to magnetite (reaction 6 in Chapter II.3). Such a reduction of martite back to magnetite caused a grain size increase of the small magnetite relics. This grain size increase caused in turn a decrease of the coercivity of magnetite erasing relevant paleomagnetic information. AMS data from these granites also showed the "old" magnetic fabric acquired during Middle Carboniferous.

Implications of reactivation of the Variscan fault zones

An overprint of the magnetic properties during the Upper Rhine Graben was not observed in this study although numerous works (e.g., Dubois et al. 1996, Pauwels et al. 1992, Smith et al. 1998) reported on the Tertiary alteration history of the Soultz granite. An explanation for this lack could be the reducing nature of the modern fluids as mentioned above. On the other hand, the activity of such fluids in other parts of the borehole profile would be indicated by reduced martite. Therefore, it is more likely that the reactivation of Variscan fault zones is the reason for the absence of younger magnetic overprints. During Variscan times magnetite was oxidized for the first time, which caused stable magnetic properties in the stage I altered granite and in the wall rocks of stage II, as well. It was shown that the initial alteration of the stage I granite took place under relatively high temperatures (~300 °C). Remanence acquisition during a hydrothermal alteration at such high temperatures cause stable magnetization of the rock that could not be overprinted during subsequent hydrothermal (stage II alteration) events at temperatures between 130-180 °C (Dubois et al. 1996). Wall rocks of stage II, which carry similar paleo-field direction and similar AMS fabric as the stage I altered granites, confirm the hypothesis of stable Variscan remanence. During the reactivation of the Variscan fault zones by Tertiary graben formation, the "young" hydrothermal fluids infiltrated into already altered granites, where the Variscan hydrothermal alteration caused stable magnetic properties. This indicates that post Permo-Triassic hydrothermal overprints had nearly no consequence for the magnetic properties of the Soultz granite. If during the formation of the Upper Rhine Graben new fault zones (Mohr-Coulomb faulting) were developed in this part of the Rhinegraben, O_2-rich fluids would have infiltrated and oxidized the magnetite in the "magnetically fresh" Soultz granite, in spite of relative low temperatures, as it is indicated by the Late Carboniferous direction carried by hematite and magnetite. The infiltration of O_2-rich fluids during the formation of the Upper Rhine Graben, however, is not indicated by the magnetic properties.

References

Ade-Hall, J.M. 1971. Magnetic evidence for the hydrothermal alteration of basalts. Eos, Transactions, American Geophysical Union, 52, 4, pp.191.

Akimoto, S., Katsura, T. and Yoshida, M. 1957. Magnetic properties of the Fe_2TiO_4-Fe_3O_4 system and their change with oxidation. J. Geomagn. Geoelectr., 9, 165-178.

Alexandrov, P., Royer, J.-J. and Deloule, E. 2001. 331 ± 9 Ma emplacement age of the Soultz monzogranite (Rhine Graben basement) by U/Pb ion-probe zircon dating of samples from 5 km depth. Earth and Planetary Sciences, 332, 747-754.

Altherr, R., Henes-Klaiber, U., Hegner, E., Satir, M. and Langer, C. 1999. Plutonism in the Variscan Odenwald (Germany): from subduction to collision. International Journal of Earth Science, 88, 3, 422-443.

Appelo, C.A.J. and Postma, D. 1999. Geochemistry, groundwater and pollution. A.A. Balkema, Rotterdam, Netherlands.

Archanjo, C.J., Launeau, P. and Bouchez, J.L. 1995. Magnetic fabric vs. Magnetite and biotite shape fabrics of the magnetite-bearing granite pluton of Gameleiras (Northeast Brazil). Physics of the Earth and Planetary Interiors, 89, 63-75.

Audunsson, H. and Levi, S. 1989. Drilling-induced remanent magnetization in basalt drill cores. Geophys.J.Int., 98, 613-622.

Bando, Y., Kiyama, M., Yamamoto, N., Takada, T., Shinjo, T. and Takaki, H. 1965. The magnetic properties of α-Fe_2O_3 fine particles,. J. Phys. Soc. Japan, 20, 2086.

Baria, R., Baumgärtner, J., Gérard, A. and Garnish, J. 2000. The European HDR programme: main targets and results of the deeping of the well GPK2 to 5000 m. Proceeding World Geothermal Congress 2000, Kyushu – Tohoku, Japan, May 28 – June 10, 2000.

Bergmüller, F., Bärlocher, C., Gexer, B., Grieder, M., Heller, F. and Zweifel, P. 1994. A torque magnetometer for measurements of the high-field anisotropy of rocks and crystals. Meas. Sci. Technol., 5, 1466-1470.

Bloemendal, J. and de Menocal, P. 1989. Evidence for a change in the periodicity of tropical climate at 2.4 Myr from whole-core magnetic susceptibility measurements. Nature (London), 342, 6252, 897-900.

Borradaile, G.J. and Henry, B. 1997. Tectonic applications of magnetic susceptibility and its anisotropy. Earth-Science Reviews, 42, 1-2, 49-93.

Bouchez, J.L. 1997. Granite is never isotropic: an introduction to aMS studies of granitic rocks. In: Bouchez, J.L., Hutton, D. and Stephens, W.E. (eds) Granite: from Segregation of Melt to Emplacement Fabrics. Dordrecht: Kluwer Academic, 95-112.

Bouchez, J.L. and Gleizes, G. 1995, Two-stage deformation of the Mount-Louis-Andorra granite pluton (Variscan Pyrenees) inferred from magnetic susceptibility anisotropy. Journal of the Geological Society of London, 152, 4, 669-679.

Bouchez, J.L., Gleizes, G., Djouadi, T. and Rochette, P. 1990. Microstructure and magnetic susceptibility applied to emplacement kinematics of granites: the example of the Foix pluton (French Pyrenees). Tectonophysics, 184, 157-171.

Bouchez, J.L., Bernier, S., Rochette, P. and Guineberteau, B. 1987. Log des susceptibilités magnétiques et anisotropies de susceptibilités dans le granite de Beauvoir: conséquences pour sa mise an place. Géologie de la France, 2-3, 223-232.

Bücker, C.J., Cashman, K.V. and Planke, S. 1999. Data report: physical and magnetic characterization of aa and pahoehoe flows: hole 990A. Proc. ODP, Sci. Res., 163, 41-49.

Burt, D.M. 1972. The system Fe-Si-C-O-H: A model for metamorphosed iron formations: Carnegie Institute Washington Year Book 1971-1972, 435-443.

Butler, R.F. 1998. Paleomagnetism: Magnetic Domains to Geologic Terranes. Electronic Edition, www.geo.arizona.edu/Paleomag/book/.

Cañon-Tapia, E. 1996. Single-grain versus distribution anisotropy: a simple three-dimensional model. Physics of the Earth and

Planetary Interiors, 94, 1-2, 149-158.

Cathelineau, M. 1988. Cation site occupancy in chlorites and illites as a function of temperature. Clay Minerals, 23, 471-485.

Cathelineau, M. and Nieva, D. 1985. A chlorite solid solution geothermometer; the Los Azufres (Mexico) geothermal system. Contribution to Mineralogy and Petrology, 91, 3, 235-244.

Cautru, J.P. 1987. Coupe géologique passant par le forage GPK1 câlée sur la sismique réflexion. BRGM/IRMG document.

Clark, D. 1999. Magnetic petrology of igneous intrusions: implications for exploration and magnetic interpretation. Exploration Geophysics, 30, 2-26.

Clemens, J.D. and Mawer, C.K. 1992. Granitic magma transport by fracture propagation. Tectonophysics, 204, 339-360.

Cruden, A.R. 1990. Flow and fabric development during the diapiric rise of magma. Journal of Geology, 98, 681-698.

de Boer, C.B. and Dekkers, M.J. 2001. Unusual thermomagnetic behaviour of haematites: neoformation of a highly magnetic spinel phase on heating in air. Geophys. J. Int., 144, 481-494.

de Boer, C.B., Mullender, T.A.T. and Dekkers, M.J. 2001. Low-temperature behaviour of heamatite: Susceptibility and magnetization increase on cycling through the Morin transition. Geophys. J. Int., 146, 201-216.

Deer, W.A., Howie, R.A. and Zussman, J. 1991. An introduction to the Rock-Forming Minerals. – 2nd edition, 696 p., New York (Longman Scientific & Technical).

Dekkers, M.J., 1997. Environmental magnetism; an introduction. Geologie en Mijnbouw, 76, 1-2, 163-182.

de Wall, H., Kontny, A. and Vahle, C. 2004. Magnetic susceptibility zonation a melilitic dyke complex (Riedheim dyke, Hegau volcanic field, Germany) evidence for multiple magma pulses? J. Volcan. Geotherm. Res., 131, 143-163.

de Wall, H. and Worm, H.-U. 2001. Recognition of drilling-induced remanent magnetization by Q-factor analysis: a case study from the KTB-drillholes. J. Appl.Geophys. 46, 55-64.

de Wall, H., Karl, A., Nano, L., Rieger, M. and Schmitt, T. 2000. Magnetische Suszeptibilitätsmessungen zur petrographischen Charakterisierung von Granitoiden – Vergleich von Feld- und Labormessungen (Saghro-Gebiet, Anti-Atlas, Marokko). Z. angew. Geol., 46, 4, 223-230.

Dezayes, Ch., Villemin T., Genter, A., Traineau, H. and Angelier, J. 1995. Analysis of fractures in boreholes of the Hot Dry Rock project at Soultz-sous-Forêts (Rhine graben, France). Scientific Drilling, 5, 31-41.

Dietl, C. (submitted to "Zeitschrift der DGG"). Die magnetische Susceptibilität – eine wertvolle Materialeigenschaft zur Charakterisierung von Granitintrusionen.

Dietl, C. and Stein, E. 2001. The diapiric emplacement and related magmatic fabrics of the porphyritic Ludwigshöhe granite, Central Odenwald (Germany). Mineralogy and Petrology, 72, 145-164.

Dubois, M., Ayt Ougougdal, M., Meere, P., Royer, J.-J., Boiron, M.-Ch. and Cathelineau, M. 1996. Temperature of paleo- to modern self-sealing within a continental rift basin: The fluid inclusion data (Soultz-sous-Forêts, Rhine graben, France). Eur. J. Mineral., 8, 1065-1080.

Dunlop, D.J. and Özdemir, Ö. 1997. Rock Magnetism: Fundamentals and frontiers. Cambridge University Press, Cambridge.

Edel, J.B., Schulmann, K. and Holub, F.V. 2003. Anticlockwise and clockwise rotations of the Eastern Variscides accommodated by dextral lithospheric wrenching: paleomagnetic and structural evidence. Journal of the Geological Society, 160, 209-218.

Edel, J.B. 2001. The rotations of the Variscides during the Carboniferous collision: paleomagnetic constrains from the Vosges and the Massif Central (France). Tectonophysics, 332, 69-92.

Edel, J.B. and Wickert, F. 1991. Paleopositions of the Saxothuringian (Northern Vosges, Pfalz, Odenwald, Spessart) in Variscan times: paleomagnetic investigation. Earth and Planetary Science Letters, 103, 10-26.

Elwood, B.B., Burkart, B., Rajeshwar, K. and Darwin, R. 1989. Are the iron carbonate minerals, ankerite and ferroan dolomite, like siderite, important in paleomagnetism? Journal of Geophysical research, 94, B6, 7321-7331.

Elmore, R.D., London, D., Bagley, D. and Gao, G. 1993. Evidence for paleomagnetic dating of diagenesis by basinal fluids, Ordovician carbonates, Arbuckle Mountains, Southern Oklahoma. Applications of Paleomagnetism to Sedimentary Geology, SEPM, Special Publication No. 49, 115-128.

Elsass, P., Aquilina, L., Beauce, A., Benderitter, Y., Fabriol, H., Genter, G. and Pauwels, H. 1995. Deep structures of the Soultz-sous-Forêts HDR site. Proc. World Geothermal Congress, Florence, Italy, 2543-2647.

Ferré, E. 2002. Granite magnetic types; a review and implications for AMS studies. Abstracts with Programs - Geological Society of America, 34, 6, 52, Oct 2002.

Ferré, E. 2002. Theoretical models of intermediate and inverse AMS fabrics. Geophysical Research Letters, 29, 7, 31/1-31/4.

Ferré, E.C. and Améglio, L. 2000. Preserved magnetic fabrics vs. Annealed microstructures in the syntectonic recrystallised George granite, South Africa. Journal of Structural Geology, 22, 1199-1219.

Ferré, E.C., Wilson, J. and Gleizes, G. 1999. Magnetic susceptibility and AMS of the Bushveld alkaline granites, South Africa. Tectonophysics, 307, 113-133.

Fisher, R., Orsi, G., Ort, M. and Heiken, G. 1993. Mobility of a large-volume pyroclastic flow – emplacement of the Campanian ignimbrite, Italy. Journal of Volcanology and Geothermal Research, 56, 3, 205-220.

Flöttmann, T. and Oncken, O. 1992. Contraints on the evolution of the Mid Crystalline Rise – a study of outcrops west of the river Rhine. Geologische Rundschau, 81/2, 515-543.

Franke, W., Dallmeyer, R.D. and Weber, K. 1995. Geodynamik evolution. Springer Verlag, Berlin, Federal Republic of Germany (DEU).

Frederichs, T., von Dobeneck, T., Bleil, U. and Dekkers, M.J. 2003. Towards the identification of siderite, rhodochrosite, and vivianite in sediments by their low-temperature magnetic properties. Physics and Chemistry of the Earth, 28, 669-679.

Frost, B.R. 1991b. Introduction to oxidation fugacity and its petrologic importance. In Lindsley, D.H., Ed., Oxide Minerals: petrologic and magnetic significance, Reviews in Mineralogy, 25, 1-9.

Fuller, M., Hastedt, M. and Herr, B. 1998. Coring-induced magnetization of recovered sediment. Proceedings of the Ocean Drilling Program, Scientific Results, 157, 47-56.

Genter, A., Traineau, H., Lédesrt, B., Bourgine, B. and Sylvie Gentier 2000. Over 10 years of geological investigations within the HDR Soultz project, France. Proceedings World Geothermal Congress 2000, Kyushu – Tohoku, Japan, May 28 – June 10, 2000.

Genter, A., Homeier, G., Chèvremont, P. and Tenzer H. 1999. Deeping of GPK-2 HDR borehole, 3 880-5 090 m (Soultz-sous-Forêts, France), Geological Monitoring. Rapport BRGM R 40685, Orléans, 80.

Genter, A. and Traineau, H. 1996. Analysis of macroscopic fractures in granite in the HDR geothermal well EPS-1, Soultz-sous-Forêts, France. Journal of Volcanology and Geothermal Research, 72, 121-141.

Genter, A. Castaing, C; Brosse, J M; Ouillon, G and Traineau, H. 1995. Multiscale organization of fractures in a deep granite reservoir. Terra Abstracts, 7, 1, pp.189

Genter, A. and Traineau, H. 1991. Geological survey of the HDR borehole EPS1, Soultz-sous-Forêts, Alsace – France. BRGM, R 32433.

Genter, A. 1989. Géothermie roche chaude sèche : le granite de Soultz-sous-Forêts (Bas-Rhin, France) : fracturation naturelle ;

altérations hydrothermales, interactions eau–roches, thèse, université d'Orléans, 201 p.

Gleizes, G., Nedelec, A., Bouchez, J.L., Autran, A. and Rochette, P. 1993. Magnetic susceptibility of the Mont-Louis Andorra ilmenite-type granite (Pyrenees); a new tool for the petrographic characterization and regional mapping of zoned granite plutones. Journal of Geophysical Research, B, Solid Earth and Planets, 98, 3, 4317-4331.

Graham, J.W. 1954. Magnetic susceptibility anisotropy, an unexploited petrofabric element. Geological Society of Americs Bulletin, 65, 12, 2, 1257-1258.

Grégoire, V., Darrozes, J., Gaillot, P. and Nédélec, A. 1998. Magnetite grain shape fabric and distribution anisotropy vs rock magnetic fabric: a three-dimensional case study. Journal of Structural Geology, 20, 7, 937-944.

Greiling, R.O. and Verma, P.K. 2001. Strike-slip tectonics and granitoid emplacement: an AMS fabric study from the Odenwald Crystalline Complex, SW Germany. Mineralogy and Petrology, 72, 165-184.

Günther, A. 2003. Magnetische Anisotropie gebänderter Eisenerze und deren Beziehung zu kristallographischen Vorzugsorientierungen. GKSS-Forschungszentrum Geesthacht GmbH, Geesthacht, GKSS 2003/35.

Hading, K.L., Morris, W.A., Balch, S.J., Lapointe, P. and Latham, A.G. 1988. A comparison of magnetic character and alteration in three granite drill cores from eastern Canada. Canadian Journal of Earth Sciences, 25 (8), 1141-1150.

Hargraves, R.B., Johnson, D. and Chan, C.Y. 1991. Distribution anisotropy; the cause of AMS in igneous rocks? Geophysical Research Letters, 18, 12, 2193-2196.

Hedley, I.G. 1968. Chemical remanent magnetization of the FeOOH, Fe_2O_3 system. Phys. Earth Planet. Inter., I, 103-121.

Herrero-Bervera, E., Walker, G.P.L., Canon-Tapia, E. and Garcia, M.O. 2001. Magnetic fabric and inferred direction of dikes, conesheets and sill swarms, Isle of Skye, Scotland. Journal of Volcanology and Geothermal Research, 106, 3-4, 195-210.

Hirt, A.M., Lowrie, W., Julivert, M. and Arboleya, M.L. 1992. Paleomagnetic results in support of a model for the origin of the Asturian Arc. Tectonophysics, 213, 3-4, 321-339.

Hoare, I.C., Hurst, H.J., Stuart, W.I. and White, T.J. 1988. Thermal decomposition of pyrite. J. Chem. Soc. Faraday Trans., 1(84), 3071-3077.

Hrouda, F., Mueller, P. and Hanak, J. 2003. Repeated progressive heating in susceptibility vs. temperature investigation; a new palaeotemperature indicator? Physics and Chemistry of the Earth. 28, 16-19, 653-657

Hrouda, F., Putis, M. and Madaras, J. 2002. The Alpine overprints of the magnetic fabrics in the basement and cover rocks of the Veporic Unit (Western Carpathians, Slovakia). Tectonophysics, 359, 3-4, 271-288.

Hrouda, F., Jelinek, V. and Zapletal, K. 1997. Refined technique for susceptibility resolution into ferromagnetic and paramagnetic components based on susceptibility temperature-variation measurement. Geophysical Journal International, 129, 3, 715-719.

Hrouda, F. 1994. A technique for the measurement of thermal changes of magnetic susceptibility of weakly magnetic rocks by the CS-2 apparatus and KLY-2 Kappabridge. Geophysical Journal International, 118, 3, 604-612.

Hrouda, F. 1982. Magnetic anisotropy of rocks and its application in geology and geophysica. Geophysical Serveys, 5, 1, 37-82.

Hunt, Ch.P. and Moskowitz, B.M., Banerjee, S.K. 1995. Magnetic Properties of Rocks and Minerals.

Hutton, D.H., Dempster, T.J., Brown, P.E. and Decker, S.D. 1990. A new mechanism of granite emplacement: intrusion in active extensional shear zones. Nature, 343, 452-455.

Isambert, A. and Valet, J.-P. 2003. Stable Mn-magnetite derived from Mn-siderite by heating in air. Journal of Geophysical research, 108, B6, EPM 2.

Ishihara, S. 1977. The magnetite series and ilmenite series granitic rocks. Mining Geol., 27 (5), 145, 293-305.

Ising, G. 1942. Den varviga lerans magnetiska egenskaper. Geologiska Foereningen I Stockholm Foerhandlingar, 64, 2, 126-142.

Jacquemont, B. 2002. Etude des interactions eaux-roches dans le granite de Soultz-sous-Forêts. Quantification et modélisation des transferts de matiére par les fluides. Ecole et Observatoire des Sciences de la Terre, Centre de Géochemie de la France (UMR 7517).

Jelinek, V. 1977. Statistical processing of magnetic susceptibility measured in groups of specimens. Stud. Geoph. Geod., 22, 50-62.

Just, J., Kontny, A., de Wall, H. and Hirt, A. and Martín-Hernández, F. 2004. Development of magnetic fabrics during hydrothermal alteration in the Soultz-sous-Forêts granite from the EPS-1 borehole, Upper Rhine Graben. In Magnetic Fabric: Methods and Applications, 238, 509-526, eds Martín-Hernández, F., Lüneburg, C. M., Aubourg, C. and Jackson, M., Geological Society, London, Special Publications.

Kanamatsu, T. and Niitsuma, N. 2004. Rock magnetism and paleomagnetic stratigraphy of forearc sediments of the Japan Trench, ODP Sites 1150 and 1151. The Island Arc, 13, 1, 180-190(11).

Katinas, V. 1999. Apatinio triaso feromagnetiniu mineralu tyrimai Zvelsenu-8 grezinyje. Identification of ferromagnetic minerals of the Lower Triassic in the Zvelsenai-8 Borehole. Geologija – Vilniaus Universitetas, 27, 5-9.

King, E.L., Haflidason, H., Sejrup, H.P. and Lovlie, R. 1998. Glacigenic debris flows on the North Sea Trough mouth fan during ice stream maxima. Marine Geology, 152, 1-3, 217-246.

Kirschvink, J.L. 1980. The least-squares line and plane and the analysis of paleomagnetic data. Geophysical Journal of the Royal Astronomical Society, 62, 3, 699-718.

Kletetschka, G and Wasilewski, P. 2001: Grain size limit for SD hematite. Physics of Earth and Planetary Interiors, 129, 1-2, 173-179.

Kletetschka, G and Wasilewski, P, Taylor, P.T. 2000: Hematite vs. Magnetite as the signature for planetary magnetic anomalies? Physics of the Earth and Planetary Interiors, 119, 259-267.

Kligfield, R., Lowrie, W. and Pfiffinger, O.A. 1982. Magnetic properties of deformed oolitic limestones from the Swiss Alps; the correlation of magnetic anisotropy and strain. Eclogae Geologicae Helvetiae, 75, 1, 127-157.

Komninou, A. and Yardley, B.W.D. 1997. Fluid-rock interactions in the Rhine Graben: A thermodynamic model of the hydrothermal alteration observed in deep drilling. Geochemica et Cosmochimica Acta, 61, 3, 515-531.

Konrad, H.J. and Nairn, A.E.M.. 1972. The paleomagnetism of the Permian rocks of the Black Forest, Germany. Geophys. J. Roy. Astron. Soc., 27, 369-382.

Kontny, A., Woodland, A.B. and Koch, M. 2004. Temperature dependent magnetic susceptibility behaviour of spinelloid and spinel solid solutions in the system Fe_2SiO_4-Fe_3O_4 and $(Fe,Mg)_2SiO_4$-Fe_3O_4. Phys. Chem. Minerals, 31, 28-40.

Kontny, A., Vahle, C. and de Wall, H. 2003. Characteristic magnetic behavior of subaerial and submarine lava units from the Hawaiian Scientific Drilling Project (HSDP-2). Geochemistry, Geophysics, Geosystems – G (super 3), 4, 2, 31pp.

Kontny, A. and de Wall, H. 2000. Case studies on the use of temperature-dependent susceptibility for the characterisation of magneto-mineralogical changes during metamorphism. Physics and Chemistry of the Earth, A25/5, 421-429.

Kontny, A., Friedrich, G., Behr, H.J., de Wall, H., Horn, E.E., Möller, P. and Zulauf, G. 1997. Formation of ore minerals in metamorphic rocks of the German continental deep drilling site (KTB). Journal of Geophysical Research, 102, B8, 18.323-18.336.

Kravchinsky, V.A., Krainov, M.A., Evans, M.E., Peck, J.A., King, J.W., Kuzmin, M.I., Hideo, S., Kawai, T. and William, D.F. 2003. Magnetic record of Lake Baikal sediments; chronological and paleoclimatic implication for the last 6.7 Myr. Paleogeography, Paleoclimatology, Paleoecology, 195, 3-4, 281-298.

Kukla, G., Friedrich, H., Ming, L.X., Chum, X.T., Tungsheng, L. and Sheng, A.Z. 1988. Pleistocene climates in China dated by magnetic susceptibility. Geology (Bolder) , 16, 9, 811-814.

Laubscher, H. 1987. Die tektonische Entwicklung der Nordschweiz. Eclogae Geologicae Helvetiae, 80, 2, 287-303.

Lédesert, B., Berger, G., Meunier, A., Genter, A. and Bouchet, A. 1999. Diagenetic-type reactions related to hydrothermal alteration in the Soultz-sous-Forets Granite, France. European Journal of Mineralogy, 11, 4, 731-741.

Leonhard, W., de Wall H., Stein, E. and Greiling, R.O. 2001. AMS-Messungen am Leuchtenberger Granit/Oberpfalz.- Exkursionsführer und Veröffentlichungen der GGW, 212, 64 - 66.

Loizeau, J.L., Pardos, M., Monna, F., Peytremann, Ch., Haller, L. and Dominik, J. 2004. The impact of sewage treatment plant`s effluent on sediment quality in a small bya in Lake Geneva (Switzerland-France). Part2: Temporal evolution of heavy metals. Lakes & Reservoirs: Research and Management, volume 9, issue 1, page 53.

Lowrie, W. 1990. Identification of ferromagnetic minerals in a rock by coercivity and unblocking temperature properties. Geophysical Research Letters, 17, 2, 159-162.

Lowrie, W. 1980. Geologie des chaines alpines issues de la Tethys--Geology of the Alpine chains born of the Tethys. Memoires du B.R.G.M., 115, 316-330.

Lowrie, W. and Opdyke, N.D., 1973. Paleomagnetism of igneous and sedimentary samples. Initial Reports of the Deep Sea Drilling Project. 15, 1017-1022.

Martín-Hernández, F. and Hirt, A.M. 2003. The anisotropy of magnetic susceptibility in biotite, muscovite and chlorite single crystals. Tectonophysics, 367, 13– 28.

Martín-Hernández, F. and Hirt, A.M. 2001. Separation of ferrimagnetic and paramagnetic anisotropies using a high-field torsion magnetometer. Tectonophysics, 337, 209-221.

Mason, B. and Moore, C.B. 1982. Principles of geochemistry. John Wiley & Sons, New York, NY, United States.

Marescotti, P., Vanko, A. and Cabella, R. 2000. From oxidizing to reducing alteration: mineralogical variations in pillow basalts from the east flank, Juan de Fuca Ridge. Proceedings of the Ocean Drilling Program, Scientific Results, 168, 119-135.

Mix, A.C., Tiedemann, R., Blum, et al., 2003. Observations on the effect of a nonmagnetic core barrel on shipboard paleomagnetic data: results from ODP Leg 202. Proceedings of the Ocean Drilling Program, Initial Reports, Volume 202

Morin, J. 1950. Magnetic susceptibility of α-Fe_2O_3 and Fe_2O_3 with added titanium. Phys. Rev., 78, 819-820.

Morris, R.C. 1993. Genetic modeling for banded iron-formation of the Hamersley Group, Pilbara craton, Western Australia: Precambrian Research, 60, 243-286.

Morrish, A.H. 1994. Canted Antiferromagnetism: Hematite. World Scientific, London.

Murad, E. 1996. Magnetic properties of microcrystalline iron (III) oxides and related materials as reflected in their Mössbauer spectra. Phys. Chem. Minerals, 23, 248-262.

Muxworthy, A.R. and McClelland, E. 2000. Review of the low-temperature magnetic properties of magnetite from a rock magnetic perspective. Geophys. J. Int., 140, 101-114.

Muxworthy, A.R. 1999. Low-temperature susceptibility and hysteresis of magnetite. Earth and Planetary Science Letters, 169, 51-58.

Nador, A., Lantos, M., Toth-Makk, A. and Thambo-Bozso, E. 2003. Milankovitsch-scale multi-proxy records from fluvial sediments of the last 2.6 Ma, Pannonian Basin, Hungary. Quaternary Science Reviews, 22, 20, 2157-2175.

Nagata, T. 1961. Rock Magnetism. Maruzen, Tokyo, 96-99.

Nairn, A.E.M. 1960. Paleomagnetic results from Europe. Journal of Geology, 68, 3, 285-306.

Nakamura, N. and Nagahama, H. 2001. Changes in magnetic and fractal properties of fractured granites near the Nojima Fault, Japan. The Island Arc, 10, 486-494.

Nourgaliev, D.K., Borisov, A.D., Heller, F., Yasonov, P.G., Burov, B.V., Khasanov, D.I., Ibragimov, Sh.Z. and Chernova, I.Yu. 2003. Geomagnetic field variations in Central Europe over the last 12,000 years from Lake Naroch (Belarus) sediments. Izvestiya – Russian Academy of Sciences. Physics of the Solid Earth, 39, 3, 247-256.

Ohmoto, H. 2003. Nonredox transformations of magnetite-hematite in hydrothermal systems. Economic Geology, 98, 157-161.

Ohmoto, H. 2002. Banded iron formations as guides for the history of the lithosphere, atmosphere, and hydrosphere. Abstracts with programs – Geological Society of America, 34, 6, 283-284.

Oliver, R., 1986. Fluids expelled tectonically from orogenic belts: Their role in hydrocarbon migration and other geologic phenomena. Geology, 14, 99-102.

O`Reilley, W. 1984. Rock and Mineral Magnetism. Glasgow: Blackie.

Ort, M., Rosi, M. and Anderson, Ch. 1999. Correlation of deposits and vent locations of the proximal Campanian Ignimbrite deposits, Campi Flegrei, Italy, based on natural remanent magnetization and anisotropy of magnetic susceptibility characteristics. Journal of Volcanology and Geothermal Research, 91, 2-4, 167-178.

Ort, M. H., Coira, B.L. and Mazzoni, M.M. 1996. Generation of a crust-mantle magma mixture; magma sources and contamination at Cerro Panizos, central Andes. Contributions to Mineralogy and Petrology, 123, 3, 308-322.

Özdemir, Ö. and Dunlop, D.J. 2000. Earth and Planetary Science Letters. 177, 1-2, 59-67.

Özdemir, Ö., Dunlop, D.J. and Muskowitz, B.M. 1993. The effect of oxidation on the Verwey transition in magnetite. Geophys. Res. Let., 20, 16, 1671-1674.

Palmer, H.C. and MacDonald, W.D. 1999. Anisotropy of the magnetic susceptibility in relation to source vents of ignimbrites; empirical observations. Tectonophysics, 307, 1-2, 207-218.

Parry, L.G. 1967. Magnetic properties of dispersed magnetite powders. Phil.Magn., 303-312.; F.D. Stacy, The Koenigsberger ratio and the nature of thermoremanence in igneous rocks. Earth Planet Sci Lett., 2, 67-68.

Pauwels, H., Fouillac, Ch. And Fouillac, A.M. 1993. Chemistry and isotopes of deep geothermal saline fluids in the Upper Rhine Graben: Origin of compounds and water-rock interactions. Geochimica et Cosmochimica Acta, 57, 2737-2749.

Pauwels, H., Fouillac, C. and Criaud, A. 1992. Water-rock interactions during experiments within the geotheramal Hot Dry Rock borehole GPK1, Soultz-sous-Forêts, Alsace, France. Applied Geochemistry, 7, 243-255.

Peck, J.A., King, J.W., Colman, S.M. and Kravchinsky, V.A. 1994. A rock-magnetic record from Lake Baikal, Siberia; evidence for late Quaternary climate change. Earth and Planetary Science Letters, 122, 1-2, 221-238.

Petrovsky, E., Kapicka, A., Pérez-Maqueda, L.A., Criado, J.M. Subrt, J. and Grygar, T. 2004. Effect of microstructure on magnetic properties of maghemite. Geophysical Research Abstracts, 6, 02449.

Pfleiderer, S. and Halls, H.C. 1990. Magnetic anisotropy of rocks saturated with ferrofluid; a new method to study pore fabric? Physics of the Earth and Planetary Interiors, 65, 1-2, 158-164.

Port, G. 2001. Climatic signals recorded in rockmagnetic properties of Pleistocene Mediterranean sediments. Edition Wissenschaft, Reihe Geowissenschaften, 71, 109pp.

Potter, D. and Stephenson, A. 1988. Single-domain particles in rocks and magnetic fabric analysis. Geophysical Research Letters,

15, 10, 1097-1100.

Pouchou, J.L. and Pichoir, F. 1984. A new model for quantitative X-ray microanalysis: Part I. Application to the analysis of homogeneous samples: La Recherche Aérospatiale, 3, 167-192.

Pribnow, D. and Clauser, C. 2000. Heat and fluid flow at the Soultz Hot Dry Rock System in the Rhine Graben. Proceedings World Geothermal Congress 2000, 3835-3840.

Ramsay, J.G. and Huber, M.I. 1983a. The Techniques of Modern Structural Geology, Vol. I, Strain analysis. Academic press, London, 1-307.

Reisinger. J., Edel, J.B. and Mauritsch, H.J. 1994. Late Carboniferous-Late Permian peleomagnetic overprinting of Carboniferous granitoids in southern Bohemian Massif (Austria). Physics of the Earth and Planetary Interiors, 85, 1-2, 53-65.

Remolar, D.F, Amils R., Morris, R.V. and Knoll, A.H. 2002. The Tinto river basin: an analog for meridiani hematite formation on mars? Lunar and Planetary Science XXXIII (2002).

Roche, A., Saucier, H., Lacaze, J. 1962. Etude paleomagnetique des roches volcaniques permiennes de la region Nideck-Donou. Bull. Serv. Carte Geol. Alsace Lorraine.

Rochette, P., Aubourg, Ch. and Perrin, M. 1999. Is this magnetic fabric normal? A review and case studies in volcanics formations. Tectonophysics, 307, 219-234.

Rolf, Ch. 2000. Das Kryogenmagnetometer im Magnetiklabor Grubenhagen. Geol. Jb. E52, 161-188.

Rummel, F. 1991. Physical properties of the rock in the granitic section of borehole GPK1, Soultz-sous-Forêts. Geothermal Science and Technology. 3, 199-216.

Rummel, F. and König, E. 1991. Physical properties of core samples, borehole EPS-1, Soultz-sous-Forêts, Velocity-, densitya and magnetic susceptibility-logs, depth interval 933-2227 m. Interner Bericht, Ruhr-Universität Bochum.

Schellschmidt, R. and Clauser, C. 1996. The Thermal Regime of the Upper Rhine Graben and the Anomaly at Soultz. Z. angew. Geol., 42, 40-46.

Scherbakov,V. P., McClelland, E. and Scherbakova, V.V. 1993. A model of multidomain thermoremanent magnetization incorporating temperature-variable domain structure. Journal of Geophysical Research, 98/II, No. B4, 6201-6216.

Schild, M., Vollbrecht, A., Siegesmund, S. and Reutel, Chr. 1998. Microcracks in granite cores from the EPS-1 geothermal borehole, Soultz-sous-Forêts (France): paleostress directions, paleofluids and crack-related Vp-anisotropies. Geologische Rundschau, 86, 775-785.

Schleicher, A., Warr, L., Kober, B., Laverret, E. and Clauer, N. 2004. The nature of Mesozoic hydrothermal illites in the Soultz-sous-Forêts granite, Upper Rhine Graben. Continental Extension, an International Earth Science Meeting of Société Géologique de France (SGF) and Geologische Vereinigung (GV) in collaboration with EUCOR-Urgent, Strasbourg – France, 20 - 26 September 2004.

Schumacher, M.E. 2002. Upper Rhine Graben: Role of preexisting structures during rift evolution. Tectonics, 21/1, 6.

Shunshan, X., Ganguo, W., Jianshe, W. and Bailin Ch. 2003. Hydrothermal alteration of magnetic fabrics of rocks in the Xiaoban gold-bearing shear belt, Fujian Province, China. Geofisica Internacional, 42, 1, 83-94.

Smith, M.P., Savary, V., Yardley, B.W.D., Valley, J.W., Royer, J.J. and Dubois, M. 1998. The evolution of the deep flow regime at Soultz-sous-Forêts, Rhine Graben, eastern France: Evidence from a composite quartz vein. Journal of Geophysical Research, 103, B11, 27,223-27,237.

Soffel, H.C. and Harzer, F. 1991. An Upper Carboniferous-Lower Permian (280 Ma) palaeomagnetic pole from the western margin of the Bohemian Massif. Geophysical Journal International. 105, 2, 547-551.

Stacy, F.D. 1967. The Koenigsberger ratio and the nature of thermoremanence in igneous rocks. EarthPlanet. Sci. Lett., 2, 67-68.

Stage, M. 2001. Recognition of cyclicity in the petrophysical properties of a Maastrichtian pelagic chalk oil field reservoir from the Danish North Sea. AAPG Bulletin, 85, 11, 2003-2015.

Stephenson, A. 1994. Distribution anisotropy: two simple models for magnetic lineation and foliation. Physics of the Earth and Planetary Interiors, 82, 49-53.

Studemeister, P.A. 1983. The redox state of iron: a powerful indicator of hydrothermal alteration. Geoscience Canada, 10, 189-194.

Stumm, W. and Morgan, J.J. 1996. Aquatic Chemistry. An introduction emphasizing chemical equilibria in natural waters. 3. Auflage. John Willey and Sons. New York.

Stussi, L.M., Cheilletz, A., Royer, J.J., Chèvremont, P. and Féraud, G. 2002. The hidden monzogranite of Soultz-sous-Forêts (Rhine Graben, France). Mineralogy, petrology and genesis. Géologie de la France, 45-64.

Tait, J.A., Bachtadse, V., Franke, W. and Soffel, H.C. 1997. Geodynamic evolution of the European Variscan fold belt: paleomagnetic and geological constraints. Geol. Rundschau, 86, 585-598.

Tarling, D.H. and Hrouda, F. 1993. The Magnetic Anisotropy of Rocks. Chapman and Hall, London.

Tauxe, L., Luskin, C. and Selkin, P. 2004. Paleomagnetic results from the Snake River Plain; contribution to the time-avaraged field global database. Geochemistry, Geophysics, Geosystem – G (super 3), 5, 18, 19 pp.

Tauxe, L., Bertram, H.N. and Seberino, Ch. 2002. Physical interpretation of hysteresis loops: Micromagnetic modeling of fine particle magnetite. Geochemistry Geophysics Geosystems, 3, 10.

Traineau, H., Genter, A., Cautru, J.P., Fabriol, H. and Chenremont, P. 1991. Petrography of the granite massif from drill cutting analysis and well log interpretation in the geothermal HDR borehole GPK1 (Soultz, Alsace, France). Geotherm. Sci. & Tech., 3(1-4), 1-29.

Turunen, P.O. 2000. The effect of hydrothermal alteration on petrophysical parameters of rocks at Kuusamo, Finland. International Geological Congress, Abstracts, Congres Geologique International, Resumes, 3, unpaginated.

van Wees, J.-D., McCann, T., Dadlez, R., Gaupp, R., Narkiewicz, M., Bitzer, F., Scheck, M. 2000. On the origin of the Southern Permian Basin, central Europe. Mar. Pet. Geol., 17, 43-59.

Varekamp, J.C. 2004. Copahue Volcano: A Modern Terrestrial Analog for the Opportunity Landing Site? EOS, Transactions, American Geophysical Union, 85, 41, p.401 cont. on page 407.

Watari, F., Delavignette, P., van Landuyt, V. and Amelinckx, S. 1983. Electron microscopic study of dehydration transformation. Part III: High resolution observation of the reaction process $FeOOH \rightarrow Fe_2O_3$. Solid State Chem., 48, 49-64.

Wesolowski, D.J., Machesky, M.L., Palmer, D.A. and Anovitz, L.M. 2000a. Magnetite surface charge studies to 290 °C from in situ pH titrations. Chemical Geology, 167, 193-229.

Williams, P.F., Goodwin, L.B. and Ralser, S. (1994). Ductile deformation processes. In: Hancock (Hrsg), Continental deformation. Pergamon Press, Oxford, 1-27.

Wooldridge, A.L., Haggerty, S.E. Rona, P.A. and Harrison, Ch.G.A. 1990. Magnetic properties and opaque mineralogy of rocks from selected seafloor hydrothermal sites at oceanic ridges. Journal of Geophysical Research, B, Solid Earth and Planets, 95, 8, 12,351-12,374.

Worm, H.-U. and Rolf, C. 1994. Remanent magnetization of KTB drill cores. Sci.Drill. 4, 185-196.

Ziegler, P.A. 1996. Geodynamic processes governing development of rifted basins, in Geoodynamic Evolution of Sedimentary Basins. Edited by F. Roure, et al., pp. 19-127, Inst Fr. du Pét./Tech., Paris, 1996.

Ziegler, P.A. 1986. Geodynamic model for the Paleozoic Crustal Consolidation of Western and Central Europe. Tectonophysics, 126, 303-328.

Zolk, J. 2004. Kartierung der Eastern Rift Zone des Kilauea-Vulkans im SE Pahoa-District, Hawaii. Unveröffentlichte Diplomkartierung, Ruprecht-Karls-Universität Heidelberg, 133 pp.

Zwing, A. and Bachtadse, V. 2000. Paleoposition of the northern margin of Armorica in Late Devonian times: Paleomagnetic and rock magnetic results from the Frankenstein Intrusive Complex (Mid-German Crystalline Rise). Journal of Geophysical research, 105, B9, 445-456.